2008

Layer by layer self-assembly of star polymers using coordination chemistry

Lilian Chang
San Jose State University

LAYER BY LAYER SELF-ASSEMBLY OF STAR POLYMERS USING COORDINATION CHEMISTRY

A Thesis

Presented to

The Faculty of the Department of Chemical and Materials Engineering

San Jose State University

In Partial Fulfillment

of the Requirements for the Degree

Master of Science

by

Lilian Chang

May 2008

APPROVED FOR THE DEPARTMENT OF CHEMICAL AND MATERIALS ENGINEERING

Dr. Melanie McNeil

Dr. Richard Chung

Dr. Roger Terrill

Dr. Robert Miller, IBM Almaden Research Center

Dr. Joseph Sly, IBM Almaden Research Center

APPROVED FOR THE UNIVERSITY

ABSTRACT
LAYER BY LAYER SELF-ASSEMBLY
OF STAR POLYMERS USING COORDINATION CHEMISTRY

by Lilian Chang

Molecular self-assembly is a low cost approach using "bottom-up" (small scale to large scale) approach in nanostructure construction which allows for a precise arrangement of molecules. In this work, thin polymer film multilayers that alternate between amino-functionalized star polymers (PS-NH_2) and zinc porphyrin (pigment) functionalized star polymers (PS-ZP) were successfully generated via layer-by-layer self-assembly on silicon dioxide surfaces. Combined analysis of SPR and QCM results shows that the PS-NH_2 and PS-ZP layers have equal thicknesses but the PS-ZP layer has a different refractive index compared to the PS-NH_2 layer. AFM confirms that the multilayer thin film is stable with uniform and complete polymer coverage while UV-Vis spectroscopy proves the organometallic coordination interactions between the PS-NH_2 layer and the PS-ZP layer. The ability to order pigment-arrays within thin film structures through layer-by-layer self-assembly presents a simple way to generate energy-cascade material for application in photovoltaics.

ACKNOWLEDGMENTS

I would like to express my heartfelt gratitude to my research advisor, Dr. Melanie McNeil, for her mentoring, guidance, and support throughout the period of my research. Her counsel, patience, and enthusiasm have greatly enhanced the quality of my graduate research and enriched my experience. I would also like to thank Dr. Robert Miller and Dr. Joseph Sly, my technical advisors in IBM Almaden Research Center, without whom this research would not have been possible. My sincere appreciation goes to Dr. Robert Miller for the opportunity to work under his leadership and be a part of his team in IBM Almaden Research Center and to Dr. Joseph Sly for the brilliant ideas, invaluable advice and the insights into the field of molecular self-assembly. I would also like to acknowledge the immense help given by Victor Lee from IBM Almaden Research Center. Both Dr. Joseph Sly and Victor Lee (IBM) worked tirelessly to ensure that my research was adequately supplied with star polymers.

My special thanks also go to the following dedicated researchers in IBM Almaden Research Center, namely Dr. Michael Jefferson, Dr. William Risk, Dr. Jane Frommer, and Dr. William Hinsberg who have offered tremendous help in understanding and analyzing the data obtained from the various characterization techniques used in this research. I am also extremely grateful to them for their patience and guidance in helping me to acquire the skills in using the characterization tools. I am very fortunate to be able to work with talented individuals who regarded me as their peer instead of a novice. I would also like to especially thank Dr. Kay Kanazawa for his invaluable help in investigating the properties of the resulting film through analysis of QCM data, Dr. Roger

Terrill from the Chemistry Department of San Jose State University, and Dr. Richard Chung from the Chemical and Materials Engineering Department of San Jose State University for their helpful suggestions and assistance during the course of the research. I would like to record my gratitude and thanks to the Department of Chemical and Materials Engineering Department of SJSU and Defense Microelectronics Activity, DMEA Grant # H94003-07-2-0705-SJSU, for making this research possible.

My immense gratitude to the editors, namely Dr. Robert Miller, Dr. Joseph Sly, Dr. Jane Frommer, Dr. William Risk, Dr. William Hinsberg, and my dad, Chang Chong Weng, who have helped to fine-tune the thesis so as to ensure the research work is presented in the highest quality possible. My sincere thanks to all the staff of IBM Almaden Research Center who have made my stay in IBM an enriching and unforgettable experience and to my colleague Cecile Bonifacio for the helpful conversations that most often times yielded useful insights into my research. Last but not least, I must thank my husband and best friend, John Ngoi, without whose love, patience, and encouragement, the thesis would not have been completed.

I dedicate this thesis to my loving parents Chang Chong Weng and Sow Siew Lee who raised me to believe I can achieve whatever I set my heart on.

TABLE OF CONTENTS

LIST OF FIGURES

LIST OF TABLES

CHAPTER ONE
INTRODUCTION

1.1 Self-Assembly

For several decades, molecular self-assembly has been an exciting area of focus. Self-assembly is defined as a mechanism in which molecules spontaneously assemble into ordered configurations without external assistance, usually through reversible non-covalent type interactions [1]. Reversibility provides opportunities for the molecules to readjust their relative positions to form defect-free aggregates [1]. Non-covalent interactions that are widely used in self-assembly are Van der Waals, hydrogen bonding and electrostatic interaction.

Molecular self-assembly is a core concept in supramolecular chemistry which refers to the chemistry behind non-covalent type interactions between molecules. Supramolecular chemistry is defined by pioneers in the field as "chemistry beyond the molecule" [2]. This field of chemistry focuses on the use of reversible and weak non-covalent type interactions such as Van der Waals, hydrogen bonding, electrostatic forces, π-π interactions, hydrophobic forces, and metal coordination to assemble molecules into a multi-molecular structure [2]. Another key concept introduced by supramolecular chemistry is the host-guest chemistry which gives rise to the idea of molecular recognition. Host-guest chemistry describes the interaction between a molecule (host) with its target complementary molecule (guest) to produce a host-guest complex. It is important to develop detailed understanding of the mechanism and driving forces of supramolecular chemistry in order to allow sensible control over the phenomenon. Due to the non-covalent nature of the interactions involved in supramolecular chemistry, the

effect of the medium and solvent interactions can play a major role in the association process of the molecules and influence the entire self-assembly system [3].

The prevailing interest in self-assembly was fueled by the vital importance of this mechanism in biological systems. A typical example of self-assembly in nature is the folding of protein molecule chains into functional three-dimensional structures through non-covalent interactions such as hydrogen bonding and Van der Waals. Also, self-assembly is a practical way of making a nanostructure, making the technique an essential part of nanotechnology. Nanotechnology is the branch of engineering that is sometimes known as molecular manufacturing, which deals with the design, manufacturing, and characterization of materials in the nano scale level, *i.e.*, 10^{-9} m [4]. Self-assembly facilitates bottom-up (from smaller scale to larger scale) approach in constructing nanostructures rather than the conventional top-down (from larger scale to smaller scale) approach [5].

The use of self-assembly in the generation of multilayer thin films attached to a solid substrate has gained increasing attention due to the wide range of applications of these films such as in optical coatings, anticorrosion coatings, drug-entrapment and release, catalyst-encapsulation, and dye-sensitized solar cells (DSSC). The greatest advantage of self-assembly in the generation of multilayer thin films is that it allows the autonomous organization of small components into an ordered structure in an efficient manner. Also, with specific tailoring of the components and interactions, one can retain exquisite control over the assembly and position the structures with nanometer (10^{-9} m) resolution [5]. Depending on the type of application of the multilayer thin film

structures, different characteristics of the film will need to be controlled, *e.g.*, the control of mass transport in multilayer films for drug-release in the biomedical field. Hence, a high level of control over the orientation and organization of the film components at nano-dimensions is highly desirable.

Of all the multilayer thin film assembly techniques, layer-by-layer (LBL) film deposition is employed extensively in the construction of functional materials because it is versatile, simple, and economical. Electrostatic LBL was one of the earliest LBL techniques and was first introduced by Decher and co-workers [6, 7]. The basic principle behind electrostatic self-assembly is that two oppositely charged moieties will be attracted to each other when suspended in a fluid [7]. In essence, fabrication of electrostatic LBL films only requires three beakers with two containing aqueous solutions of oppositely charged poly-ions and one containing the washing solution (a new washing solution is used for each wash). Figure 1 illustrates the complete cycle of the LBL deposition technique for a bilayer formation using a polycation as the first layer on a hydrophilic substrate [7]. A bilayer denotes two monolayers of different absorbing species. The substrate is first dipped into the polycation solution for adsorption of the first layer and then into a washing solution to remove any polycations that are non-physically adsorbed. The polycation-coated substrate is subsequently dipped into a polyanion solution, completing the bilayer formation with adsorption of the oppositely charged polyelectrolyte. The entire system is rinsed again with the washing solution. The number of desired bilayers is obtained by repeating the entire dipping cycle [7].

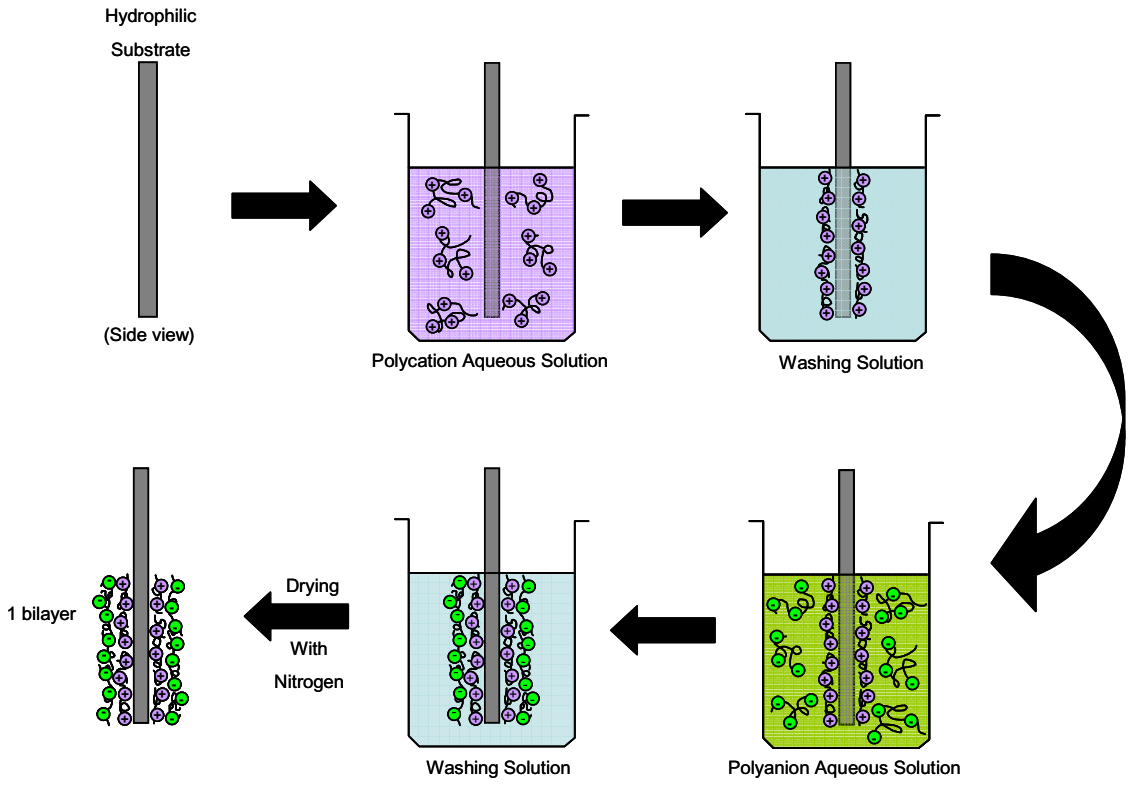

Figure 1. Layer-by-layer (LBL) deposition technique for one bilayer formation.

Experimental parameters that need to be considered for effective LBL multilayer formation include substrate type, pH, solution concentration, ionic strength of the solutions, and immersion time. Although electrostatically assembled films are still predominant in literature [7-17], there have been examples of films assembled using other adsorption mechanisms with secondary interactions such as hydrogen bonds [18-20] or via very specific interactions, *e.g.*, avidin-biotin affinity binding [7].

Polyvalent interactions are the most common of the major types of interactions mentioned for LBL assembly and may play a part in strengthening the interactions between alternating layers in LBL. Polyvalent interactions (also known as multivalent

interactions) occur throughout biological systems and can be defined as interactions through multiple simultaneous contacts resulting in a cumulative effect [21, 22]. Valency can be described as the number of separated but similar interactions that can be formed through host-guest interactions [22]. Hence, interactions that involve more than one host-guest interaction are known as polyvalent. An example of polyvalency is the binding of multiple antibodies to a macrophage. A single antibody is unable to ingest a pathogen while more antibodies strengthen the interactions between the pathogen and the macrophage through polyvalency, increasing the chances of the pathogen being recognized and ingested [21]. Similarly, high densities of electrostatic interactions between two polymer layers will result in high multiple concurrent contacts at any point in time, increasing the attraction between the two layers. This type of interaction is especially important in the use of hyperbranched polymers to grow multilayer thin films since the interactions between the peripheries of the hyperbranched polymer exist at an equilibrium and are usually individually non-covalent, weak interactions. Collective effects from polyvalent interactions will amplify the existing interaction and increase the strength of association between the layers [21]. Figure 2 illustrates the concept of polyvalency.

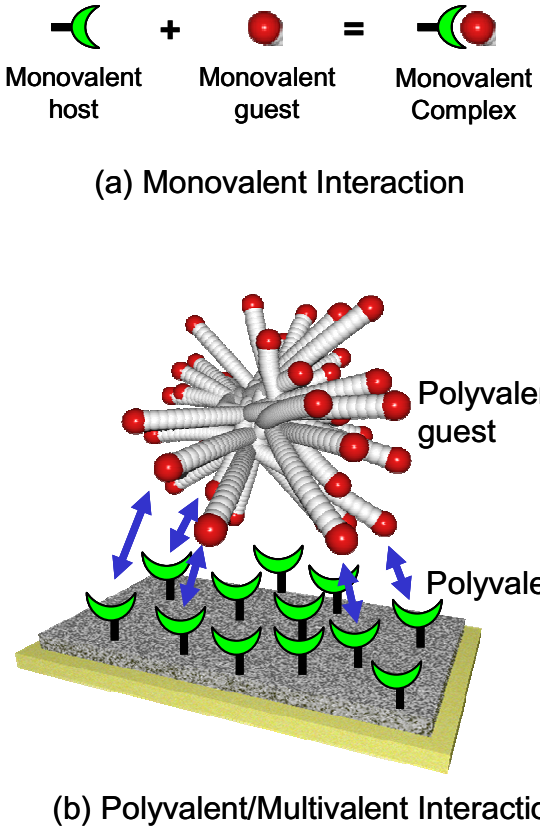

Figure 2. (a) Monovalent interaction versus (b) polyvalent (multivalent) interaction.

1.2 Hyperbranched Polymers

The evolution of polymer architectures from linear polymers in the 1930s to cross-linked and branched polymers in the 1950s fueled an increased attention to molecular thin films. Today, highly branched globular structures such as dendrimers are receiving much attention. Dendrimers are a unique class of materials that can be distinguished by their treelike architecture with branched and sub-branched tendrils reaching out from a central core [23]. The well-defined geometry and surface functionality of dendrimers allow this class of polymers to be identified as promising

candidates for use as molecular building blocks involving self-assembly [24]. The synthesis of dendrimers begins with a simple core unit with new "generation" of branching introduced at every successive reaction. Every subsequent addition of branches to the existing structure is labeled with increasing generation number as depicted in Figure 3(a) for a 4^{th}-generation dendrimer. The growth of the periphery of the dendrimers will eventually lead to steric hindrance, extending the reaction time and complicating the synthesis [23]. In the production of light-harvesting films with dendrimers, the light-harvesting ability increases with dendrimer generations due to the increase of peripheral chromophores (*i.e.*, light absorbing chemical group). The requirement of higher generation dendrimers in producing functional thin films contributes to the high cost of manufacturing such films [23].

The era of branched polymers also saw the birth of another category of polymer architecture known as the star polymers. Due to several early problems in star polymer synthesis, these structures were left in the shadow of the dendritic polymers. However, there have been mounting efforts in reviving this polymer architecture since star polymers share the same necessary topological attributes that give dendrimers their capability. Star polymers are also much cheaper to make without complicated multi-step organic synthesis and self-imposed structural restrictions due to steric hindrances (as in the case of high dendrimer generations) [25]. Three of the most prominent features shared by both polymer architectures are branches stemming from a single point, functional end points on the branches, and void spaces between branches [25, 26]. Figure

3 illustrates the structural representations of a 4th-generation dendrimer and a star polymer.

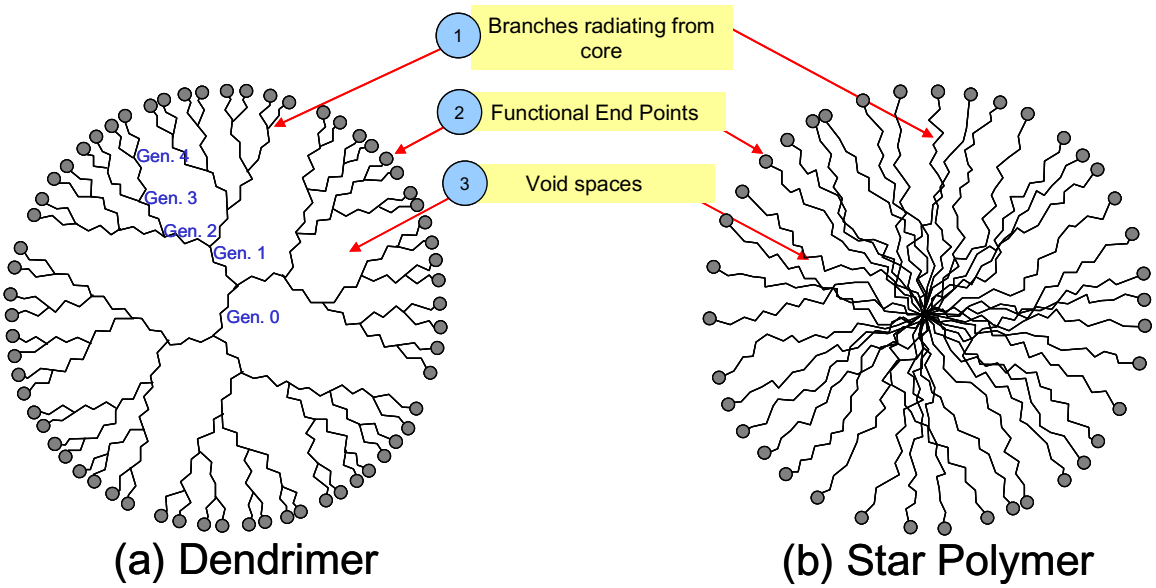

Figure 3. General topology of (a) dendrimer and (b) star polymer.

The ability to functionalize the end points on the branches of star polymers and dendrimers open a vault of opportunities for self-assembly. Through the functionalized groups on the periphery of the globular polymers, different types of interaction can be explored for film fabrication through the LBL technique. One particular application of interest is functionalizing the periphery of star polymers with porphyrin dyes to resemble light-harvesting antenna.

Although LBL deposition of polyelectrolytes is the more general route pursued in self-assembly, such assemblies are found to present irregular structures, causing inter-diffusion between layers, or an increase of film permeability as the number of layers increases [12]. Other defects that limit the applicability of LBL self-assembly are

adsorbed impurities, pinholes, grain boundaries, and surface roughness which leads to an accumulation of defects as each new layer is added [27]. Hyperbranched polymers represent a possible solution to alleviate the problem of defects accumulating within the film due to the possibility of bridging over defects [27].

1.3 Porphyrins and Coordination Chemistry in Self-Assembly

Porphyrins are chemical compounds found naturally in living cells of animal and plants. They combine with metals such as iron to produce hemes in the animal world and magnesium to produce chlorophyll in the plant world. Porphyrins are useful materials for both electron and energy transfer. Figure 4 shows the structure of a porphyrin.

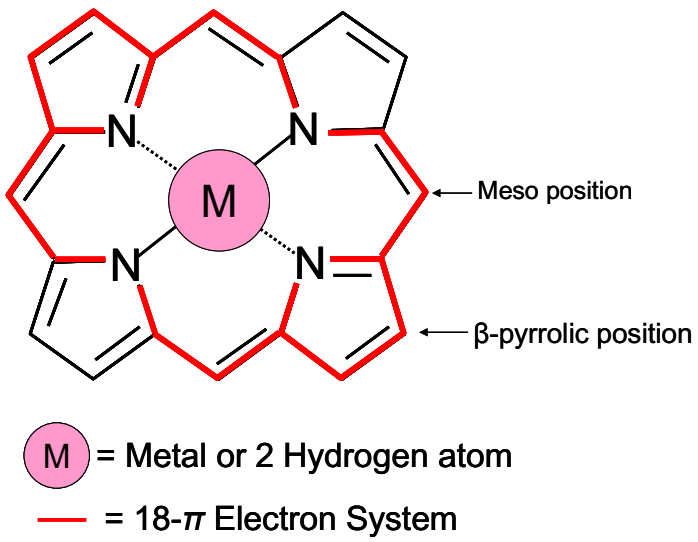

Figure 4. Porphyrin structure.

Porphyrins are unique due to their long-lived intermediate electronic state that is accessible when irradiated by visible light. This photo-excited state allows electron transfer to occur in the chloroplast. This electron transport mechanism in nature can be imitated using porphyrin and a complementary species that accepts electrons.

Metalloporphyrins are porphyrins with a metal center. The 18-π electron system as highlighted in Figure 4 makes the porphyrin a stable aromatic. Substituents to the meso position promote solubility while substitutents at the β-pyrrolic position are used for chemical attachment [28].

The assembly of porphyrin multilayer systems using ligand coordination properties of metalloporphyrin appears to be promising [29]. Zinc-porphyrins are frequently used in stable systems due to the capability of the zinc (Zn) central ion to form penta-coordinated complexes. The Zn^{2+} ion has empty d^{10} orbitals and interacts with an electron donor species that has an unshared electron pair through a "keyhole" principle known as a coordination bond [2, 29]. Figure 5 shows the interaction between the zinc central ion in porphyrin with an amino group which is an electron donor species. By functionalizing the arms of the star polymer with Zn-porphyrin, the polymers can be assembled on surfaces or polymer layers containing electron donor species through coordination chemistry. The introduction of coordination chemistry in self-assembly opens up a tremendous array of building blocks with different kinds of metal ions and ligands. The wide selection of materials enables further tuning of film properties through careful combination of the different components.

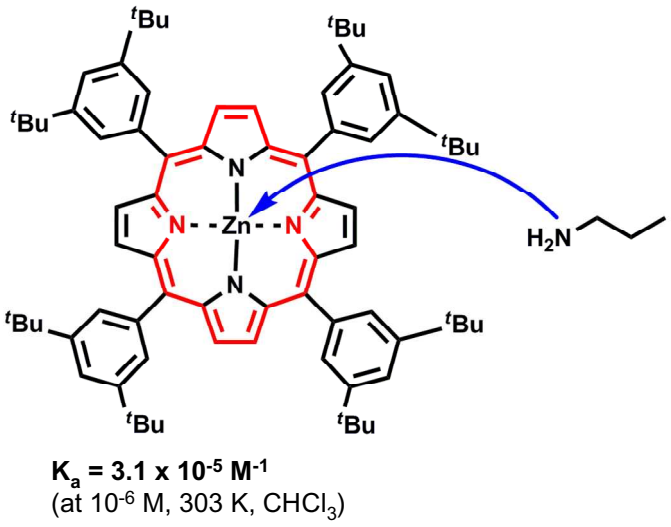

Figure 5. Coordination chemistry between zinc-center in porphyrin with an amino group.

Interest was sparked in organic artificial photosynthetic devices ever since Michael Gratzel reported the dye-sensitized solar cell (DSSC) which is currently under limited production for military use by Konarka, a company based in Lowell, MA [30]. The idea of using a dye for charge transfer was the catalyst for studies using porphyrin functionalized dendrimers. This idea seems very feasible due to resemblance of the morphology and photochemical features of porphyrin dendrimers to light-harvesting antenna [31]. Since star polymers share most of the important features of the dendrimers [25], it seems plausible that porphyrin functionalized star polymers may be used to produce low-cost and efficient organic photovoltaic (PV) devices by exploiting the electron excitation characteristics of porphyrins.

1.4 Characterization Techniques

An abundance of characterization techniques have been used to study the structural, chemical, optical and electrical properties of LBL films. One of the most common methods used is ultraviolet-visible (UV-Vis) spectroscopy to monitor the adsorption process. UV-Vis is used in the study of interaction between light in the visible and near ultraviolet ranges and matter. This technique is especially useful in the study of dyes due to the strong and obvious peaks in the absorption spectrum in the visible region.

Atomic force microscopy (AFM) is also widely used to assess film quality, film morphology, and film thickness. The AFM is a scanning probe used primarily to obtain high resolution images of the topography of surfaces. In an AFM's simplest embodiment, the sample is scanned by a probe mounted onto a cantilever spring. Deflection of the cantilever by forces between the probe and the sample is monitored. An image of the sample topography is created by plotting the cantilever deflection at each position on the sample's surface. In the intermittent contact (tapping) mode used in this study, an oscillating cantilever scans the sample surface. The amplitude of the oscillation is used as the feedback for sensing the surface; changes in amplitude are plotted as topography. Phase images are produced by plotting changes in the phase of the oscillating cantilever as it scans over the sample surface. Contrast in the phase image reflect changes in sample-tip interaction that arise from the viscoelastic nature of the material under study [32].

Recent developments in sensing devices have provided capability for *in-situ* monitoring of the layer formation using a flow cell. Two such devices are the surface plasmon resonance (SPR) detector and the quartz crystal microbalance (QCM).

The quartz crystal microbalance (QCM) is an ultra-sensitive mass sensing device, capable of measuring mass changes in the nanogram (10^{-9}) range. The QCM is commonly used in thin film technology to monitor film growth. It measures the mass of each layer as it is deposited by measuring the change in oscillation frequency of the quartz crystal. The QCM substrate is a piezoelectric quartz crystal that is sandwiched between two electrodes connected to an oscillator. The quartz crystal oscillates at its resonance frequency as AC voltage is applied across the electrodes. Mass uptake or removal on the surface changes the resonance frequency of the quartz crystal. The mass of the applied film can be correlated to the change in frequency through the Sauerbrey equation shown as Equation 1 [33].

$$\Delta f = -2 f_0^2 \frac{\Delta m}{A\left(\mu_q \rho_q\right)^{1/2}} \qquad \text{Equation 1}$$

where Δf is the frequency change resulting from the mass change, Δm, on the quartz crystal, f_0 is the fundamental frequency of the crystal, A is the piezoelectric-active area, μ_q is the shear modulus, and ρ_q is the quartz density.

The SPR detector is a relatively new instrument that has shown great promise in measuring the thickness and index of thin film layers. The most widely used SPR detector is the prism-based SPR system. Other types of SPR detectors include grating coupled systems and optical waveguide systems. The prism-based SPR detector can be

arranged in different configurations. The typical SPR configuration consists of a prism, a noble metal film, and a flow cell arranged as shown in Figure 6 together with a light source and a photodetector.

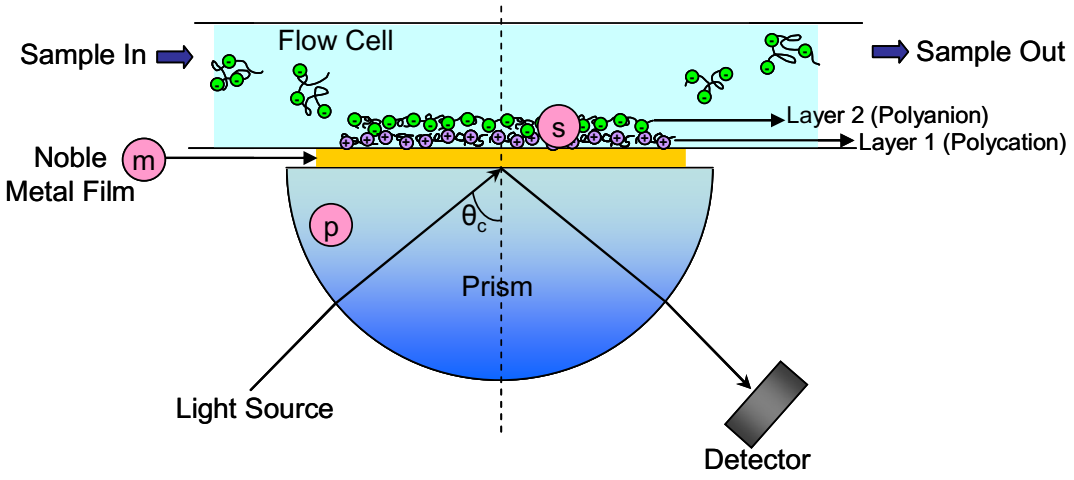

Figure 6. Typical SPR set-up. The sensing layer, glass prism, and metallic film are labeled s, p, and m, respectively while θ_c is the critical angle for TIR to occur.

Surface plasmon resonance takes place when a plane-polarized light hits a metal film under very exact conditions of total internal reflection (TIR). As the light beam travels through the prism towards the plane of interface, total internal reflection occurs above the critical angle, at the point where all the incident light is reflected within the prism. The reflecting plane of the prism is coated with a thin layer of noble metal such as gold [34]. Surface plasmons are free electrons oscillating parallel along the surface of the metal film when the film is in contact with a dielectric interface (*i.e.*, the fluid medium to be analyzed in the flow cell) and can be excited with plane-polarized light [34, 35]. Under TIR conditions, the light arriving at the metal surface excites the free surface

electrons (plasmons) on the metal and causes them to generate an evanescent field, part of which penetrates into the flow cell. Resonance occurs when the momentum of the plasmons is equal to the momentum of the incoming light, resulting in energy being transferred to the surface plasmons. Surface plasmon resonance results in a decrease in the intensity of reflected light. The angle where complete attenuation of the reflected light occurs is known as the resonance angle [34-36]. This type of arrangement is the angular SPR that is widely used. Another configuration that is less widely used is the spectral SPR where the SPR too is set up at a fixed angle of incident light while varying the wavelength until resonance is observed.

In the angular SPR, the velocity and momentum of the plasmons change when the refractive index of the medium in the flow cell changes since light travels at different velocity in different media [34]. The change in the momentum of plasmons causes the light angle of incident at which surface plasmon resonance occurs to change. The sequential deposition of thin film layers as shown in Figure 6 results in changes in refractive index and causes the resonance to occur at a different angle of incidence. Sequential shifts in the resonance angle can be correlated to the thickness of each layer using the three-layer Fresnel equation for p-polarized light, as shown in Equation 2 [36]. The derivative of Equation 2 can also be expanded upon to account for different SPR set-up for higher accuracy as discussed by Kurihara *et al.* [37].

$$R = \left| \frac{r_{pm} + r_{ms} \exp(2ik_{mz}d)}{1 + r_{pm} r_{ms} \exp(2ik_{mz}d)} \right|^2 \qquad \text{Equation 2}$$

where subscripts *p*, *m*, and *s* represent the glass prism, the metallic film, and the sensing layer accordingly, shown in Figure 6. R denotes the reflectance of the light while amplitude reflectance for the metal-sensing layer and prism-metal interfaces are given by r_{pm} and r_{ms}. The thickness of the metallic film is denoted by d while the wave-vector component perpendicular to the interface at the metallic film is represented by k_{mz}.

1.5 Overall Significance

Light-harvesting is the primary step in photosynthesis. The high efficiency of which plants and some bacteria harness solar energy to power their metabolic needs makes them obvious candidates for emulation. The light-harvesting antenna architectures in natural systems are exquisitely intricate with the pigment molecules (light-harvesting component) held together in a structured assembly by protein molecules [38]. The interaction involved between the protein molecule and the pigment molecule (*e.g.*, a metalloporphyrin) is organometallic coordination chemistry as shown in Figure 7. Multilayer thin films using metalloporphyrins are a close mimic of the photosynthetic pathway of a plant.

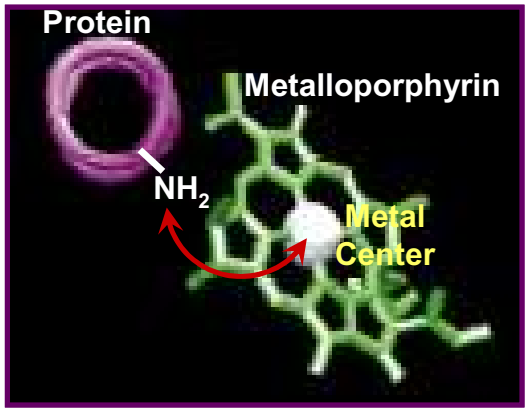

Figure 7. Interaction between protein molecule and pigment molecule (metalloporphyrin) in natural light-harvesting systems.

This artificial photosynthetic system has tremendous potential in regard to the photovoltaics (PV) industry. In 2003, the photovoltaic (PV) industry became a US 4.5 billion-dollar business [39]. The current thin film modules in PV applications are typically manufactured using amorphous silicon (136 Watt/module). According to an article by Renewable Energy Access, the current supply of silicon is not enough to meet the demand of the solar industry [40]. The current PV market is dominated by silicon-based thin film solar cells costing USD 126 for a 42 Watt module ($3.00/Watt). Silicon prices have escalated to USD 200/kg in 2006 from USD 25/kg in 2004 [41].

Fabrication of organic solar panels using LBL assembly with polymer constituents lowers manufacturing cost compared to the state-of-the art silicon wafer manufacturing technology required for silicon films. The simplest process design for LBL requires separate tanks containing dye-functionalized polymers and a rinsing agent. The LBL process can be fully automated to minimize human intervention and preserve

consistency in film quality. The LBL technique is a fast and reliable technique that can shorten the time-to-market cycle.

A competitive advantage of star polymer thin films versus dendrimer thin films is the price of the materials. A fourth generation dendrimer costs approximately USD 1,500 per kg [23] as opposed to the star polymers that is only approximately USD 87.40 per kg. Dendrimers are expensive due to the multi-step synthesis required in order to achieve high generations. In comparison, star polymers are much simpler to synthesize and functionalize [25].

CHAPTER TWO
LITERATURE REVIEW

2.1 Overview of Layer-by-Layer Self-Assembly

Early efforts in artificial self-assembly techniques required chemical adsorption of functionalized molecules, restricting the choice of molecules that can be used. In the 1990s, Decher and co-workers introduced a more versatile technique for multilayer film production, known as the layer-by-layer (LBL) technique. In their study, they used oppositely charged species for each alternating film. Prior to the introduction of LBL, the Langmuir-Blodgett (LB) technique was the predominant method used in fabrication of nano-structured films through molecular control [6, 7, 42]. In the LB technique, lipids or water insoluble polymers and molecules can form organized monolayers at the surface of the water which can be transferred onto a solid support. The monolayer is formed due to strong anisotropic interaction of the molecules with water which causes the molecules to organize on the water surface. Multilayer thin films can then be prepared through successive dipping of a solid substrate up and down through the monolayer as shown in Figure 8.

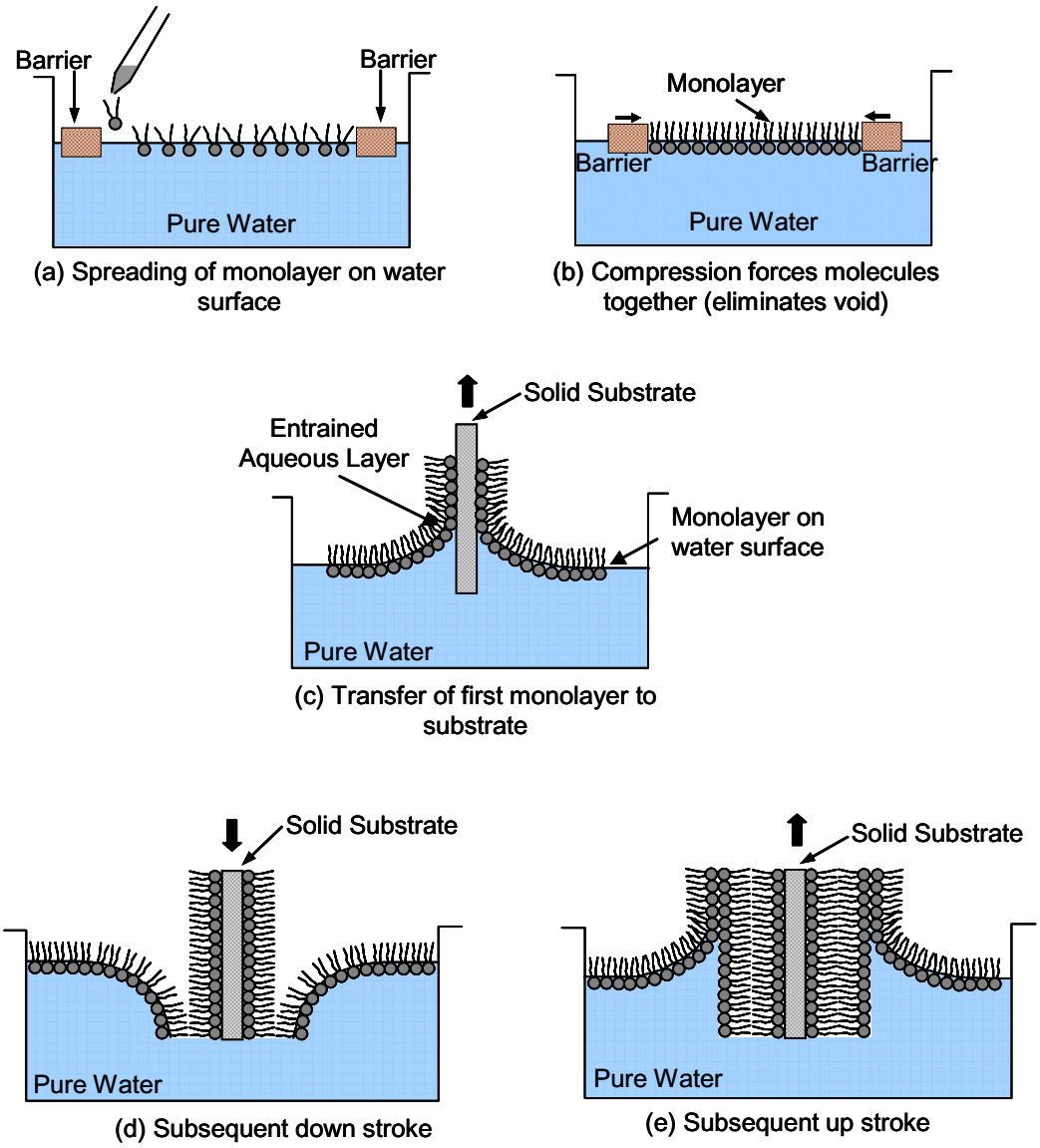

Figure 8. Langmuir-Blodgett (LB) film deposition.

The LB technique has several limitations including restrictions on the types of molecules suitable for the employment of LB technique due to the requirement for strong anisotropic interaction between the molecule and the liquid, the mechanical softness of the film, limited temperature range, and typically very slow deposition rate that is easily disturbed by very small degrees of contamination.

The LBL method was first employed on polyelectrolytes of opposite charges but has been extended to other types of charged materials such as dendrimers [16, 17], and nanoparticles [43]. Several experimental parameters have been identified by Oliveira *et al.* [7] to significantly affect multilayer buildups using LBL. The parameters are substrate type, polymer concentration, pH and ionic strength of the solution, and immersion time. Yoo *et al.* [10] used linear polymers and demonstrated that the characteristics of a bilayer produced from electrostatic interaction, such as bilayer composition, surface wettability, and amount of layer interdigitation (*i.e.*, the degree one layer diffuses into the other layers) can be varied systemically through pH control of the solutions.

Oliveira *et al.* [7] categorized the LBL films into four main categories according to the adsorption mechanism: electrostatic assembly from highly-charged polyelectrolytes, electrostatic assembly from partially-charged polyelectrolytes, assembly through secondary interactions such as hydrogen bonds, and assembly through very specific interaction such as the biotin-avidin interaction. Although a majority of the research on LBL assembly is still focused on electrostatic interactions [8-17], there have been many other studies exploring other means for self-assembly, *e.g.*, hydrogen bonding interactions [18-20] or coordination chemistry [27, 43-48].

2.2 Dynamic Layer Deposition Technique

Traditionally, LBL assembly has been carried out via dipping method, where the substrate is immersed into alternating complementary LBL solutions with an intermediate rinsing step. Recent development by Kim *et al.* [49] suggests that multilayer film fabrication can unite the advantages of LBL assembly and a fluidic system to allow dynamic deposition on a specific region of a substrate. Kim and his colleagues [49] studied the effects of flow rate, residence time and polyelectrolytes concentration to optimize the dynamic LBL assembly technique. Using the dynamic LBL assembly technique, they reproduced the poly(diallyldimethylammonium chloride) (PDDA) and poly(ethyleneimine) (PEI) system studied by Dante *et al.* [50] with conventional dipping. Kim *et al.* [49] used ellipsometry, UV-Vis spectroscopy, and AFM to compare thickness and UV-Vis absorption maxima of films fabricated using dynamic deposition with the reported results by Dante *et al.* [50] and found that the resulting film quality of dynamic deposition was comparable to dipped films. The dynamic LBL assembly technique offers the capability for region-selective coating by allowing only a selected region to be in contact with the flow channel and supports *in-situ* characterization techniques such as Surface Plasmon Resonance (SPR) and Quartz Crystal Microbalance (QCM).

2.3 Coordination Chemistry

In recent years, researchers have begun to explore coordination chemistry in an attempt to find other approaches for self-assembly. This effort was also fueled by the fact that a study done by Klitzing *et al.* [12] concluded that electrostatic assemblies from

polyelectrolyte present irregular morphologies and results in interpenetration of layers, where one layer diffuses into another layer. The study also reveals that a complex combination of factors such as solvent effects and type of polyion significantly affects the structure of a multilayer film. The conclusions made by Klitzing *et al.* [12] were built upon results of a detailed study conducted by Loshe and co-workers on the structure of molecular thin polyelectrolyte multilayer films using neutron reflectometry [14, 15]. Loshe *et al.* [14] found that roughening of successive deposited layers of poly(styrenesulfonate) (PSS) and poly(allylamine hydrochloride) (PAH) leads to progressively increasing layer thickness. This is due to the increase in the number of adsorption sites for the consecutive deposition and interpenetration of the alternating species before the film settles into an equilibrium thickness. Their previous study [15] established the length scale of interdigitation as approximately 12 Å. The Bragg peaks observed in Figure 9 below provide evidence that the deposited PSS and PAH films consist of well-defined layers [15]. The thin broken line in the inset in Figure 9 illustrates the profile without surface roughness while the thick line shows the profile with surface roughness. Comparing the thick line in the inset to the thin broken line, they postulated that the surface roughness was due to chain-to-chain interdigitation [15].

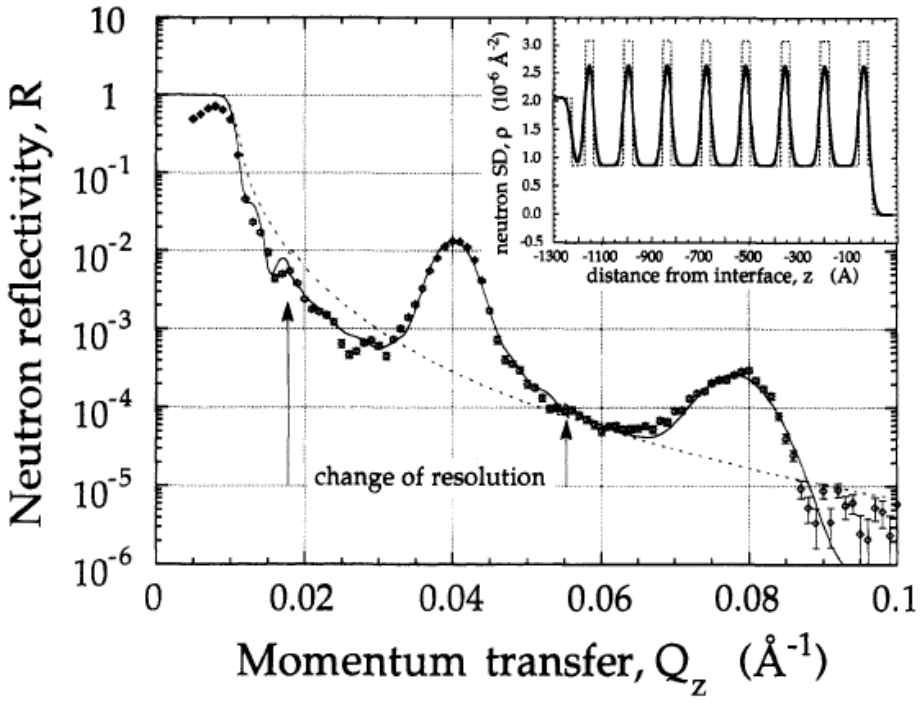

Figure 9. Fitting of neutron reflectivity data of sample (thick black line). The arrows indicate change of instrument resolution at two points [15] (reprinted with permission from American Chemical Society).

Metal-ion coordination has been shown to have utility in the construction of multilayer films [27, 29, 43-48]. Besides simplicity, coordination chemistry provides stable bonding with high ligand-metal specificity. Wanunu *et al.* [43] were able to fabricate highly controlled nanostructures, comprising of nanoparticle components using coordination chemistry type interactions. In another study, Wanunu and colleagues [27] demonstrated that LBL growth of multilayers is possible through the use of metal-organic coordination of Zr^{4+} ions and adding one molecular layer in each step. They first functionalized the gold (Au) surface with molecules containing hydroxamate functionality and then introduced tetravalent ions (Zr^{4+}), followed by a ligand providing the first branched layer of interest. The result of their study is show in Figure 10. The

film thickness values obtained by 4 different methods, *i.e.*, ellipsometry, transmission spectroscopy, AFM, and X-ray photoelectron spectroscopy (XPS), are almost identical, denoting highly regular film growth [27]. The first point is the thickness of the initial layer reacted to functionalize the Au surface.

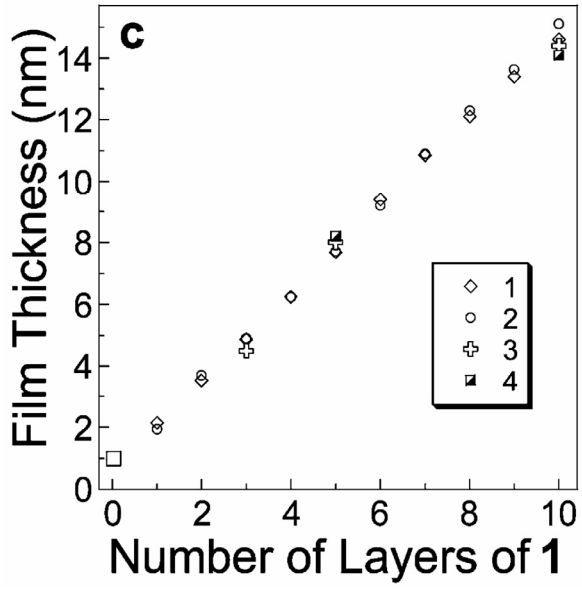

Figure 10. Film thickness values of self assembled monolayer of branched molecule with alternate binding of metal ion and the branched molecule obtained by (1) ellipsometry, (2) transmission spectroscopy, (3) AFM, and (4) XPS. The first point (square) denotes the hydroxamate groups for surface functionalization [27] (reprinted with permission from American Chemical Society).

Kohli and Blanchard [44] were able to successfully incorporate coordination chemistry with covalent bonding to grow layered molecular assemblies on silicon substrates and gold substrates. They were able to demonstrate the compatibility of interaction chemistry whereby one layer can interact via coordination chemistry and the other layer via covalent bonding. The versatility introduced by coordination chemistry presents opportunities in tuning film properties through uniquely designed ligands.

2.4 Hyperbranched Polymers

Dendritic architecture is prevalent in biological systems and is speculated to have evolved over billions of years into structures with optimized interfaces for different biological functions. Synthetic mimics of the architecture known as dendrimers were the brainchild of both Flory, who conceptualized it and Tomalia, who developed the synthesis of such molecules [51]. Tomalia then co-founded Dendritech, Inc. bringing dendrimer production to the commercial scene. Table 1 shows four major classes of macromolecular architectures [51]. Class I and Class II type architecture define the origins of conventional polymer science while Class III is still a candidate for tremendous growth since it is associated to new polyolefins topologies. Class IV is currently receiving a lot of scrutiny due to the possibility of mimicking important biological systems.

Table 1. Major classes of macromolecular architecture [51].

Era	Class	Architecture	Examples
1930s	I	Linear	Plexiglass, Nylon
1940s	II	Cross-linked	Rubbers, Epoxies
1960s	III	Branched	Low Density Polyethylene, Metallocene-Based Polyolefins
Present	IV	Dendritic	Nano-drugs, Light-harvesting, Biological sensors

The star polymer architecture was born somewhere in the transition between the branched and dendritic era. Dendrimers overtook star polymers in term of popularity due to several problems encountered with star polymers associated with controlling and functionalizing the structures [25]. From the literature regarding dendrimer applications [23, 24, 26], the basic features of dendrimers that were most utilized were the branched

architecture originating from one point, the ability to functionalize the ends of the branches and the void spaces between the branches [25]. These traits are all shared by the star polymer architecture. Although star polymer architecture presents a wealth of potential, it is still overshadowed by the dendrimers due to limited research in using star polymers.

There are several ways to synthesize the star polymers. Hadjichristidis *et al.* [52] outlined three general anionic synthetic routes to obtain star polymers and discussed the pitfalls of each of the synthesis methods. The most useful method of star polymer synthesis is through linking reaction of living polymers with electrophilic reagents under certain conditions. Hadjichristidis and colleagues [52] also discussed the introduction of different types of functional groups at the end or along the polymer chain, *i.e.*, functionalized initiator and terminal functionalizing agents. The use of functionalized initiators ensures complete functionalization of the arms while the use of functionalized terminating agents is more problematic [52]. Beil and Zimmerman [53] demonstrated that star polymers can be prepared in many fewer steps compared to dendrimers and both types of polymer share similar structures. They also reported a synthetic approach to fabricate nanosized cross-linked and "cored" star polymers. In their study, Beil *et al.* [53] hypothesized that a very flexible structure that does not retain shape can be produced if a high degree of inter-arm cross-linking is not obtained.

Tsukruk *et al.* [17] fabricated multilayers of dendritic films via self-assembly of dendrimers with amine groups and dendrimers with carboxylic group using electrostatic interaction. They concluded that the average thickness of a molecular layer in the

multilayer films were smaller than the ideal diameter of the dendrimers. This conclusion leads to the assumption of a compressed state of the dendritic macromolecules within the multilayer structure as illustrated in Figure 11.

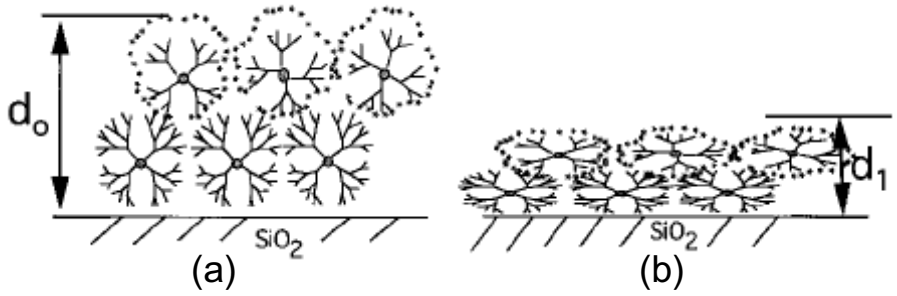

Figure 11. The (a) ideal globular shaped, and (b) actual compressed state, of the organization of the dendritic molecules within the self-assembled molecular films [17] (reprinted with permission from American Chemical Society).

2.5 Porphyrins and Coordination Chemistry

Functionalized polymers with porphyrins are examples of new materials designed for LBL assemblies. The interest in porphyrins is due to their photophysical properties, making them strong contenders for use in nanostructured photovoltaics devices [31]. The awareness of the functionality of porphyrins was fueled by the dye-sensitized solar cells (DSSC) introduced by Gratzel. In 1991, O'Regan and Gratzel [54] presented the concept behind the DSSC using low to medium-purity materials and low cost processes that exhibits energy conversion efficiency, making it commercially viable. In their model, a monolayer of charge transfer dye was attached to a titanium dioxide electrode (TiO_2). Photoexcitation of the dye causes the infusion of electrons into the TiO_2 electrode. The flow of electrons which generates the photocurrent is maintained through a redox system with electron donation from the electrolyte and a counter-electrode such as platinum (Pt).

Expanding on his previous work, Gratzel [55] then introduced the use of transition metal complexes together with oxide films of nanocrystalline morphology for increased conversion efficiency, allowing harvesting of a larger fraction of sunlight.

There have been studies on porphyrin dendrimers with porphyrin molecules attached to the arms of the dendrimers [31, 56-60]. Metals can be incorporated in either the core or the periphery [60]. Zenkevich and von Borczyskowski [29] discussed the "keyhole" principle for non-covalent self-assembly using metalloporphyrins. The basic principle for such self-assembly is related to molecular recognition. The porphyrin central metal ion may specifically interact via coordination bond with another recognition site [29]. The multiporphyrin arrays formed through coordination chemistry possess efficient light-harvesting properties. Harth and colleagues [56] compared porphyrin-cored dendrimers and their exact linear analogues and found that the dendrimers have unique properties compared to other architectures and exhibited more efficient energy transfer. The study concluded that the dendritic architecture is superior in encapsulating the porphyrin core. Kaschak *et al.* [61] aimed to fabricate an inorganic "leaf" and proposed a possible structure for energy transfer and electron transfer processes using alternating porphyrin layers and inorganic polyanions spacer layers through LBL assembly. This study is interesting as it brings us closer to being able to mimic the exquisite level of control nature has over molecular orientations and distances.

Da Cruz and fellow researchers [46] studied the self-assembly of porphyrin monolayers via metal complexation (coordination chemistry) on ligand layers. Da Cruz *et al.* [46] were able to clearly demonstrate the role of metal in film assembly with

control experiments as shown in Figure 12. No adsorption of hydrogen-tetraphenyl porphyrin (H_2TPP) is observed on the SiPy treated substrate as shown by curve (c) in Figure 12, compared to the strong adsorption of cobolt cobolt-tetraphenyl porphyrin (CoTPP) denoted by curve (a).

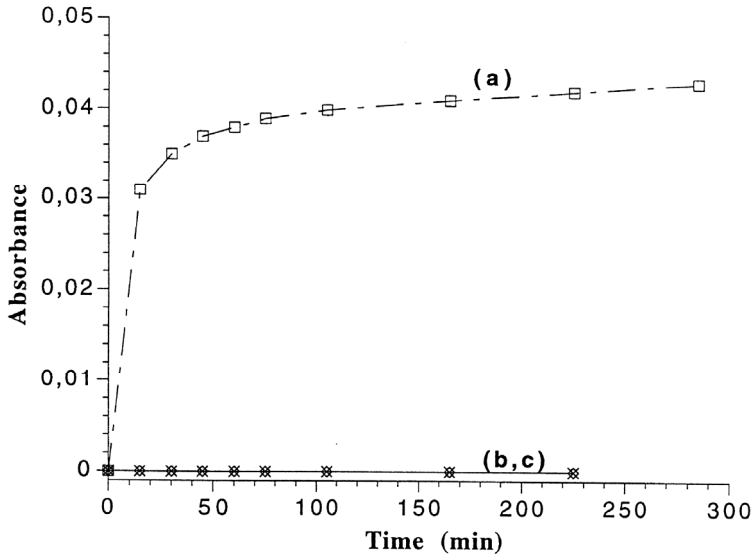

Figure 12. Kinetics of absorption of cobolt-tetraphenyl porphyrin (CoTPP) in chloroform on a (a) 1-(3-(triethoxysilyl)propyl)-3-(pyridine-4-methyl)-urea (SiPy) coated surface, and (b) untreated substrate. Kinetics of absorption of hydrogen-tetraphenyl porphyrin (H_2TPP) on SiPy treated substrate is presented in (c) as control experiment [46] (reprinted with permission from Elsevier Limited).

2.6 Role of Solvent in LBL Self-Assembly

Solution conditions are found to affect certain self-assembly systems. For example, in the self-assembly of polyelectrolytes where the growth and architecture of the resultant multilayer structure can be extensively controlled by changing the solution conditions [10, 13, 62]. Yoo *et al.* [10] were able to change the layer thickness and degree of interlayer penetration of polyelectrolyte multilayers through control of the pH of the dipping solution used in the LBL self-assembly process. Yoo and fellow researchers

varied the pH of the poly(allyamine hydrochloride), PAH, and poly(acrylic acid), PAA, solution and the thickness of the resultant layers were measured using profilometry and ellipsometry. The thickness versus number of deposited bilayers (combined PAH and PAA layer thickness) for certain pH combinations are shown in Figure 13, from which the authors concluded that the LBL deposition process for the PAH/PAA self-assembly system follows a linear trend and produced reproducible results. Ellipsometry measurements were collected for the films deposited on silicon wafer to better profile the change in layer thickness with respect to pH as shown in Figure 14. Yoo *et al.* concluded from Figure 14 that the PAA layer thickness decreases as the pH of the PAA solution increases while the layer thickness of the PAH layer increases when the pH of the PAH dipping solution increases.

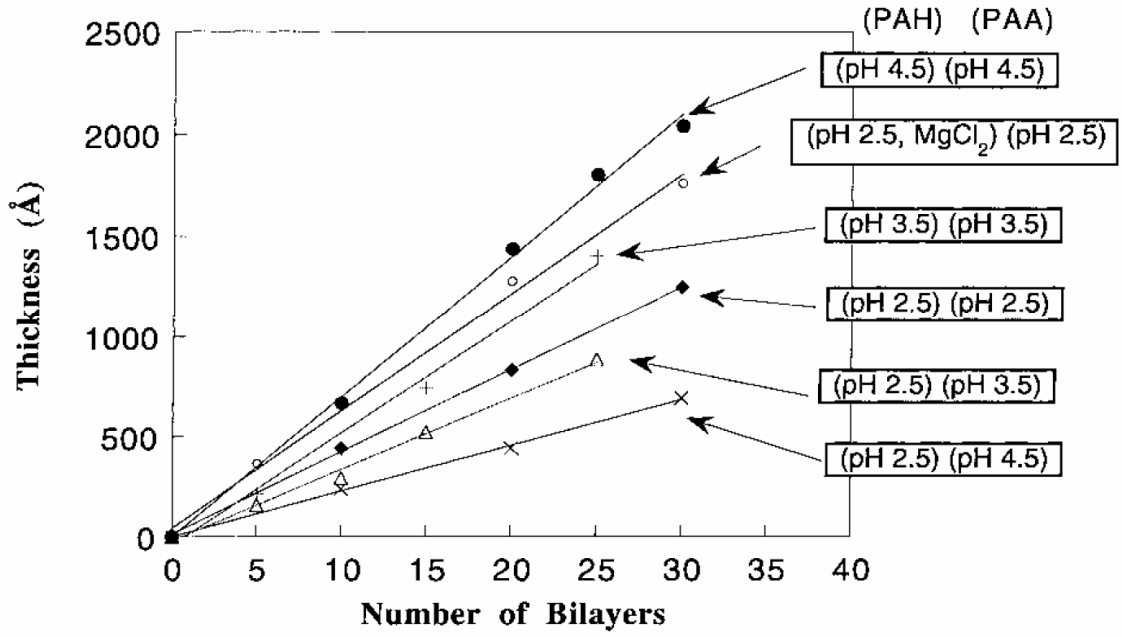

Figure 13. Plots of thickness with respect to number of deposited bilayer, PAH/PAA films deposited from solutions with different pH adjustments [10] (reprinted with permission from American Chemical Society).

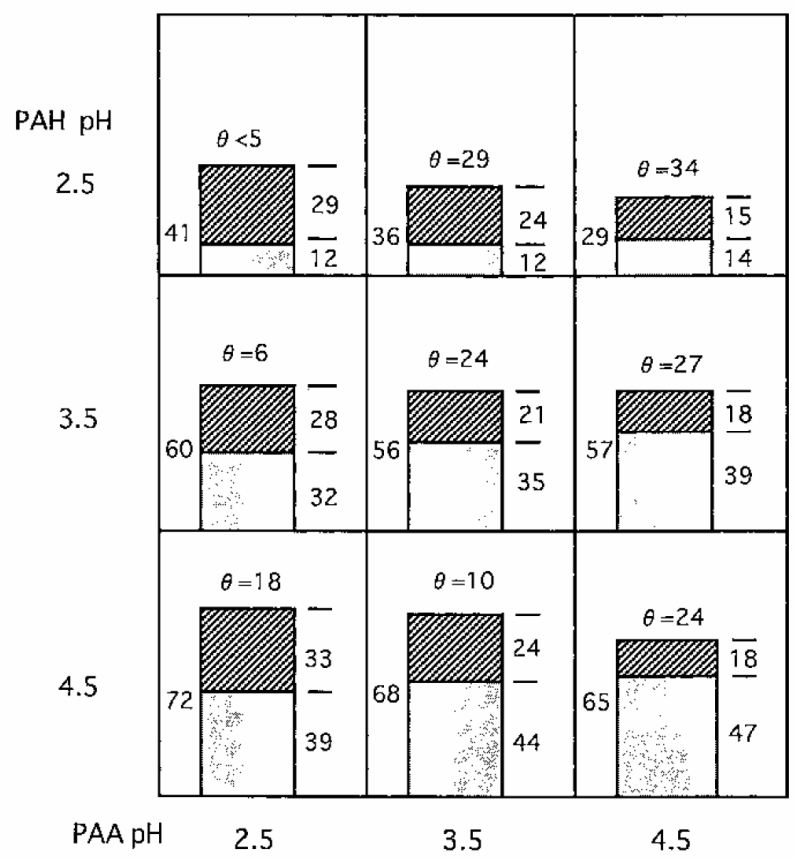

Figure 14. Average thickness increase of PAH and PAA layer within a bilayer deposited using dipping solutions of different pH. The lighter regions represent the PAH layer while darker regions represent the PAA layer [10] (reprinted with permission from American Chemical Society).

Tang *et al.* [13] conducted a study on the influence of solvent conditions on self-assembly of hyperbranched polyanion and linear polycation into multilayer films and concluded that the pH and tetrahydrofuran (THF) to water volume ratio affects the absorption behavior of the hyperbranched polyester and also the surface morphology and hydrophobicity of the films. At a higher THF to water volume ratio or at a lower pH, the adsorption rate for the hyperbranched polyester was higher and produced a rougher and less hydrophilic surface [13].

Mizutani *et al.* [63] conducted a study on the solvent effects and binding mechanism of amines and amino esters to zinc porphyrin through molecular recognition. They found that the binding affinity was high in both non-polar (dichloromethane) and polar (water) solvents, whereby low binding affinity was observed in a solvent of intermediate polarity (water-methanol mixture). Mizutani *et al.* concluded that there were two competitive driving forces operating, *i.e.*, the host-guest coordination interaction between the zinc atom and the amino group in organic solvents and the desolvation-driven binding in water. This study underscores the importance of the correct choice of solvent in LBL self-assembly to ensure desired intermolecular interaction is achieved and the specificity of the interaction is not compromised.

Together with the effect of solvents on the interaction between complementary molecules for LBL self-assembly, efforts have been directed into the study of solvent effect within a hyperbranched polymer molecule [64, 65]. Stechemesser and his colleague Eimer [64], concluded in their study of the swelling of poly(amido amine) starburst dendrimers that there is significant swelling of large dendrimers molecules (more than 4 generations) which may imply that molecules can be trapped and released from the dendritic structure by changing the solvent quality. Murat and Grest [65] presented molecular dynamics simulation of a coarse-grained model of dendrimers in different solvent quality. They concluded that the solvent quality affects the amount of overlapping dendrons within the dendrimers, *i.e.*, amount of dendron overlaps increases as the solvent quality decreases. The study of solvent effects on hyperbranched polymer molecule may be valuable in aiding the understanding of the contribution of trapped

solvents within the molecule to the film thickness as the hyperbranched molecules self-assemble into a film.

2.7 Characterization Techniques

Oliveira *et al.* [7] summarized the characterization techniques commonly used to evaluate optical, structural and electrical properties of the LBL assembled films. The adsorption process of each layer is usually monitored using UV-Vis spectroscopy while Quartz Crystal Microbalance (QCM) is used to measure the amount of material absorbed on each layer. Film thickness is measured using Atomic Force Microscopy (AFM), X-ray diffraction, and ellipsometry. Other methods of evaluation that are not as common include Surface Plasmon Resonance (SPR), fluorescence measurements, and contact angle measurements. UV-Vis spectroscopy and QCM are common techniques used in examination of LBL assembly as shown by several group of researchers [66-68].

Tuo *et al.* [67] successfully monitored the growth of water-insoluble azo-containing polyelectrolyte multilayer film fabricated using LBL adsorption in anhydrous N, N-dimethylformamide (DMF) with UV-Vis spectroscopy. The resultant multilayer surface was imaged with AFM. From the UV-Vis absorption spectra shown in Figure 15, it can be concluded that the thickness of the multilayer film can grow linearly up to tens of bilayers. Tuo and his colleagues concluded from the AFM image in Figure 16 that the multilayer surface was rather smooth which led to the assumption that hydrophobic aggregates were eliminated with the use of anhydrous DMF instead of aqueous solution.

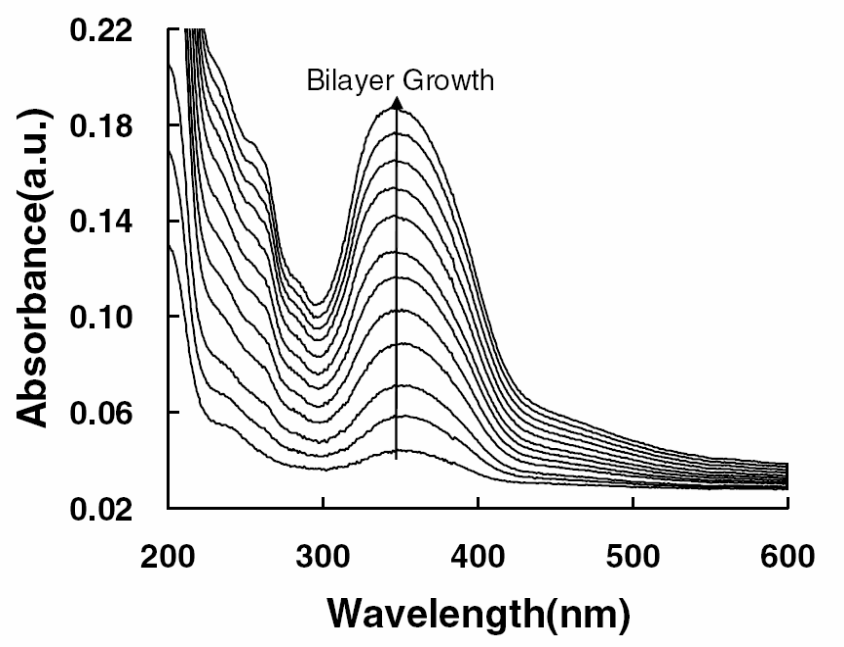

Figure 15. The UV-Vis absorption spectra of azo-containing polyelectrolyte multilayers with respect to the number of bilayer [67] (reprinted with permission from Springer).

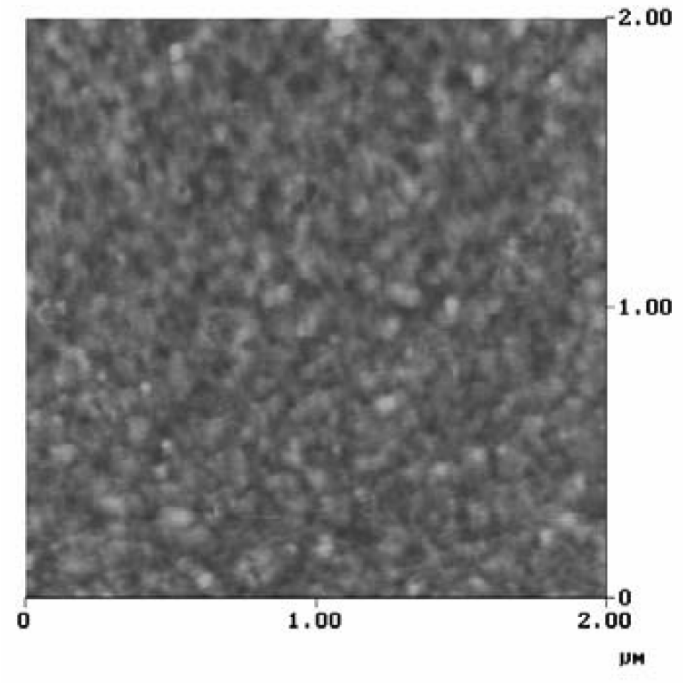

Figure 16. The AFM surface morphology of the azo-containing polyelectrolyte multilayers with 12 bilayers [67] (reprinted with permission from Springer).

Xu *et al.* [69] studied the layer-by-layer self-assembly of chitosan and glucose oxidase (GO_x) using QCM. The QCM result in Figure 17 shows a linear relationship between the frequency shifts and the number of bilayer of the chitosan/GO_x films. Xu and colleagues concluded from the QCM results that each bilayer has approximately the same thickness and structure. They were able to elucidate the thickness of the chitosan and GO_x layers through mathematical modeling under certain assumptions (*e.g.*, a densely packed layer).

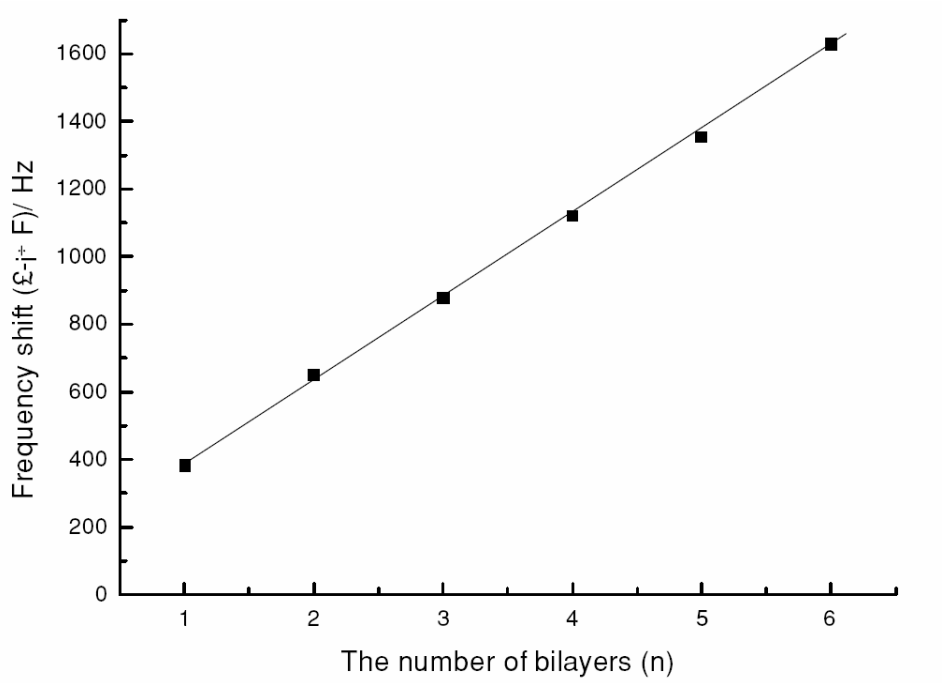

Figure 17. Frequency shifts with respect to number of bilayers of chitosan/glucose oxidase deposited onto quartz crystal with platinum surface obtained from QCM [69] (reprinted with permission from Springer).

Although highly accurate and sensitive, the SPR technique is not as widely applied in layer-by-layer deposition. In a survey of 2005 literature for commercial optical biosensor, Rich and Myszka [70] pointed out that some improvements needed to

be made as how the SPR data are processed and reported. They emphasized in their review the importance of reporting data together with the computational model used for the fitting and not just the results of the computation. They also provided hints on how to produce high quality data and well-performed analysis by the careful design of experiments with the aid of control experiments.

Theoretically, as each layer of film is deposited on the gold surface, the index of refraction increases, shifting the resonance minimum to higher angle. These sequential shifts in the resonance angle can be associated with the thickness of each layer through the Fresnel equation. This is a powerful tool in detection and characterization of each polymer layer. Since recent studies [49] support the use of flow cells in layer-by-layer deposition, SPR can be used as a tool for layer-by-layer thickness analysis. Lately, there has been growing realization of the potential of SPR in monitoring LBL assembly [71-76]. Ray and Nabok [71] successfully monitored self-assembly of three layers of PSS/PAA films and the curves exhibited consistent increase of resonance curves with increase in number of polymer layers shown in Figure 18.

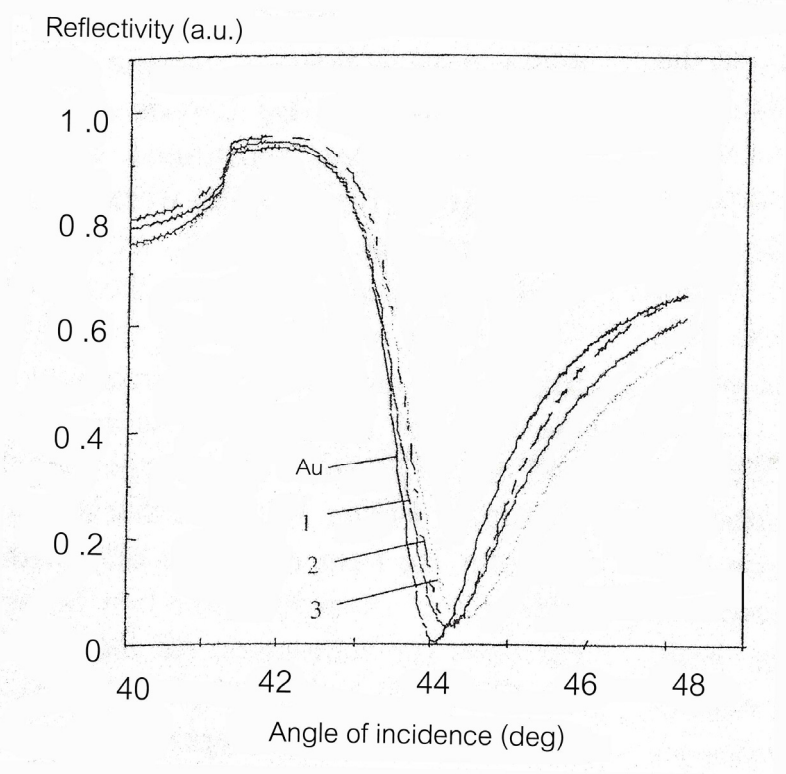

Figure 18. SPR curves for bare gold (Au) and deposited layers of PAA/PSS films of (1) one, (2) two, and (3) three layers [71] (reprinted with permission from American Scientific Publishers).

Crespo-Biel *et al.* [42] used SPR to investigate self-assembly of guest-functionalized dendrimers and host-modified gold nanoparticles in the construction of a self-assembled organic/inorganic multilayer structure. Crespo-Biel concluded from the SPR time study shown in Figure 19 that the adsorption behavior was similar for different concentrations of dendrimers and gold nanoparticles. They concluded from the slope of the reflectivity change as a function of the number of bilayers, shown in Figure 19(c) and Figure 19(d) that a ten-fold increase in the concentrations for both the dendrimers and the nanoparticles results in only 1.5 times more adsorption which confirms the specificity of the interaction involved.

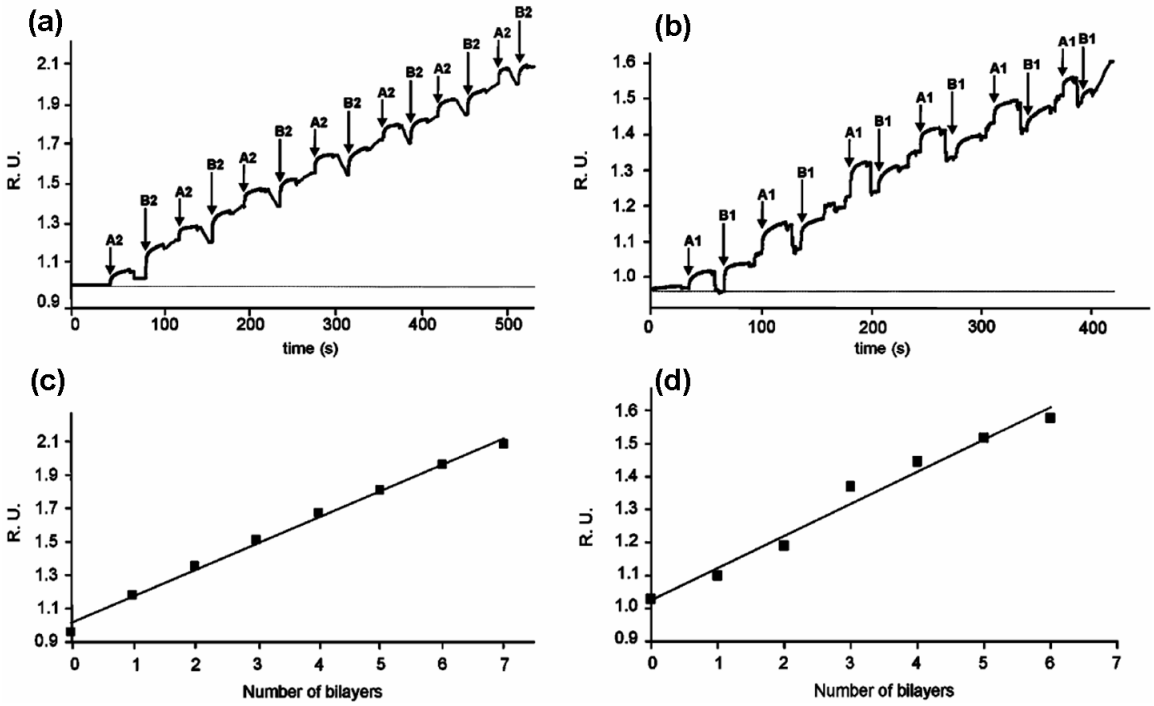

Figure 19. SPR time traces for LBL self assembly of dendrimers and gold nanoparticles using solutions of (a) 0.1 mM dendrimer and 58 μM nanoparticles, and (b) 0.01 mM dendrimers and 5.8 μM nanoparticles. SPR reflectivity changes as a function of number o bilayers of self-assembly using solutions of (c) 0.1 mM dendrimer and 58 μM nanoparticles, and (d) 0.01 mM dendrimers and 5.8 μM nanoparticles [42] (reprinted with permission from American Chemical Society).

Baba and fellow researchers [74] were able to elucidate electrochemical and optical properties of LBL assembled polymer films using a combination of SPR and cyclic voltammetry. Szekeres *et al.* [75] grew multilayers alternating between MgAl-layered double hydroxide (LDH) and a polyelectrolyte and used shifts in the SPR angle to evaluate the LBL process. Zhang *et al.* [72] also employed SPR technique to study LBL films and found that the polyaniline-sulfonated polyaniline films become more compact as hydrostatic pressure increases and this phenomenon can be observed from the surface plasmon spectra.

2.8 Summary

The literature survey section aims to provide a background on the various technology and development that has led to their integration into this research. The extensive literature available on LBL and coordination chemistry supports the assimilation of both concepts in the fabrication of a multilayer system using hyperbranched polymers such as star polymers. The ability to build such system using coordination chemistry will require modifications to the periphery of the star polymers. Due to the attributes of the star polymers as previously mentioned, success in the construction of a multilayer assembly of these materials will catalyze efforts in incorporating them into a wide range of applications such as solar cells and even as bio-reactors.

Process parameters that have been found to be important are the substrate type, polymer concentration, pH and ionic strength of the solution, and immersion time. UV-Vis is widely employed for dye-containing LBL systems due to strong absorption of light in the visible region. SPR and QCM offer real time measurement of layer thickness and layer uniformity while AFM is widely used to evaluate film morphology and film quality, *i.e.*, to see if the films maintain their properties over a period of time.

CHAPTER THREE
HYPOTHESIS AND OBJECTIVES

3.1 Hypothesis

The hypothesis of this study was that multilayers of thin films that alternate between an amino-functionalized star polymer (PS-NH_2) and a zinc-porphyrin-functionalized star polymer (PS-ZP) can be formed on silicon dioxide surfaces via layer-by-layer deposition. The initial film formation occurs due to electrostatic interaction on silicon dioxide surfaces. The subsequent alternating layer depositions are held together by coordination chemistry between the amino groups and the zinc-porphyrin groups at the periphery of the star polymers. The driving force for film formation is the strong interaction between the two different types of star polymer and their relatively weak self-affinity. Each layer assembly process was postulated to be self-limiting due to these interactions, *i.e.*, the imposition of factors such as geometrical constraints from the first layer formation restricts the layer to a monolayer. Figure 20 illustrates the stated hypothesis.

The main objectives of this research were to use self-assembly to produce multilayers of ordered, molecularly thin layers containing dye materials, and to characterize the multilayer assembly to determine uniformity and coverage of each polymer layer. Film stability was also investigated in terms of dewetting over time. Dewetting is generally described as the detachment of thin film from the substrate and the formation of droplets. The process conditions required for complete coverage for each polymer layer were determined.

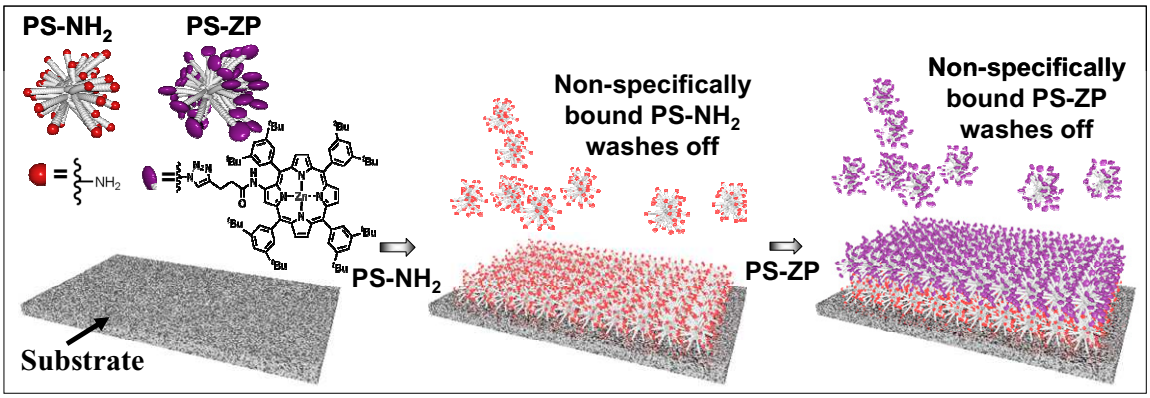

Figure 20. LBL assembly of functionalized star polymers [77].

3.2 Justification

Hyper-branched polymers are interesting materials for self-assembly due to their molecular topologies [25, 26] and the functionality leading to polyvalency [21]. The hyperbranched polymers of interest in this research are star polymers. They are cheaper to synthesize compared to dendrimers since they require fewer synthesis steps [52, 53]. However, efforts in functionalizing star polymers and using them in LBL assembly are still rare. Many of the LBL assembly studies reported in the literature exploit electrostatic interactions as a mechanism for multilayer film assembly [8-17]. Two groups of researchers, Wanunu *et al.* [27, 43] and Mor *et al.* [47] agreed that systems employing small molecule coordination chemistry show regular growth of multilayer structures. Wanunu and fellow researchers [27, 43] demonstrated that coordination chemistry offers high specificity, simplicity and stability. Porphyrins have been identified as important candidates in the fabrication of photovoltaics devices [57-61] and thus, are interesting for other reasons. The PS-ZP star polymer mimics the light-harvesting function of the pigment molecule in natural systems while the PS-NH_2 star

polymer mimics the support function mentioned in Section 1.5. Applying the concept introduced by Gratzel [54, 55], multilayers of porphyrin-star polymers can be grown on titanium dioxide (TiO_2) electrodes with spacer layers. The porphyrin layers can be of different types and assembled into films, each with a longer absorption wavelength from top to bottom, allowing the excitons to move from the top layer and accumulate at the bottom layer closest to the electrode for injection into the electrode. The ability to fabricate a multilayer system of porphyrin-star polymers with alternating spacing layers is therefore a valuable area of research.

CHAPTER FOUR
MATERIALS AND METHODS

Amino-terminated polystyrene star polymers (PS-NH_2) and zinc-porphyrin-terminated polystyrene star polymers (PS-ZP) were prepared by the Miller group at IBM Almaden Research Center and used to study LBL assembly on silicon dioxide (SiO_2) substrates. Characterization tools such as SPR and QCM were used to determine uniformity of layer thickness as each polymer layer was deposited. AFM was employed to study the surface coverage of polymers on substrates, the surface coverage of polymer on polymer-coated surfaces, and to monitor film stability over time. Film stability studies involved investigating surface topography over time to observe if dewetting occurs. UV-Vis spectroscopy was used to monitor the film formation on silicon dioxide to obtain information on the role of star polymer morphology and coordination chemistry in building up layers. Processing conditions to obtain complete layer coverage without compromising film quality were also investigated. Results provide information on layer uniformity, film coverage, film stability and whether coordination chemistry can be used for multilayer growth. Table 2 is an experimental matrix showing the framework of the main experiments designed to achieve the stated objectives. Experiments 1 to 3 in Table 2 were carried out with dynamic deposition using a flow cell. Table 3 shows the supporting experiments designed to provide additional information on the system. The samples for studies outlined in experiment 4 to 6 in Table 3 were prepared using a flow system while the samples used in experiment 7 were prepared using the dipping method.

Table 2. Main experimental matrix to achieve objectives.

Surface	Exp.	Layer Combination	No. of Layers	No. of Runs	Experimental Goal
Sputtered Silicon Dioxide	1	PS-NH_2/PS-NH_2	2	3	• Effect of double deposition (QCM, SPR)
	2	PS-NH_2/PS-ZP/PS-ZP	3	3	
	3	Alternating PS-NH_2/PS-ZP*	10	3	• Thickness uniformity (SPR) • Mass uniformity (QCM) • Layer homogeneity and coverage of final layer (AFM) • Dewetting (AFM**)

*Layer deposition of stated combinations until desired number of layers is achieved
**AFM images are collected after 12 hrs, 24 hrs, 36 hrs, and 1 week.
Note: Experiments are carried out using dichloromethane (CH_2Cl_2) or tetrahydrofuran (THF) as the solvent under constant temperature, residence time, and concentration.

Table 3. Supporting experiments for additional information on system.

Surface (Substrate)	Exp.	Layer Combination	No. of Layers	No. of Runs	Experimental Goal
Silicon Dioxide (Silicon wafer)	4	PS-NH_2	1	3	• Surface coverage and homogeneity of base layer (AFM)
	5	PS-ZP	1	3	• Surface coverage and homogeneity of base layer (AFM)
	6	Alternating PS-NH_2/PS-ZP*	4	3	• Surface coverage and homogeneity of final layer (AFM) • Dewetting (AFM**)
Silicon Dioxide (Quartz wafer)	7	Alternating PS-NH_2/PS-ZP*	9	3	• % arm interaction after each layer deposition (UV-Vis) • Uniformity of PS-ZP layer.

*Layer deposition of stated combinations until desired number of layers is achieved
**AFM images are collected after 12 hrs, 24 hrs, 36 hrs, and 1 week.
Note: Experiments are carried out using dichloromethane (CH_2Cl_2) or tetrahydrofuran (THF) as the solvent under constant temperature, residence time, and concentration.

4.1 Materials

Using (*p*-toluenesulfonate)-terminated polystyrene star polymers, the arms of the polymers were functionalized with amino and zinc-porphyrin groups, respectively. The (*p*-toluenesulfonate)-terminated polystyrene star polymers have approximately 23 arms with an estimated 30 repeat units and an average hydrodynamic radius (R_h) of 4.5 nm [78]. The amino-terminated polystyrene star polymer (PS-NH_2) and the zinc (II) triazole peripherally functionalized polystyrene star polymers (PS-ZP) were synthesized using IBM proprietary synthetic procedures [78]. After the final drying step, the final product of the PS-NH_2 and PS-ZP are colorless and light crimson, respectively. The PS-NH_2 is represented by Figure 21(a) while Figure 21(b) illustrates the PS-ZP.

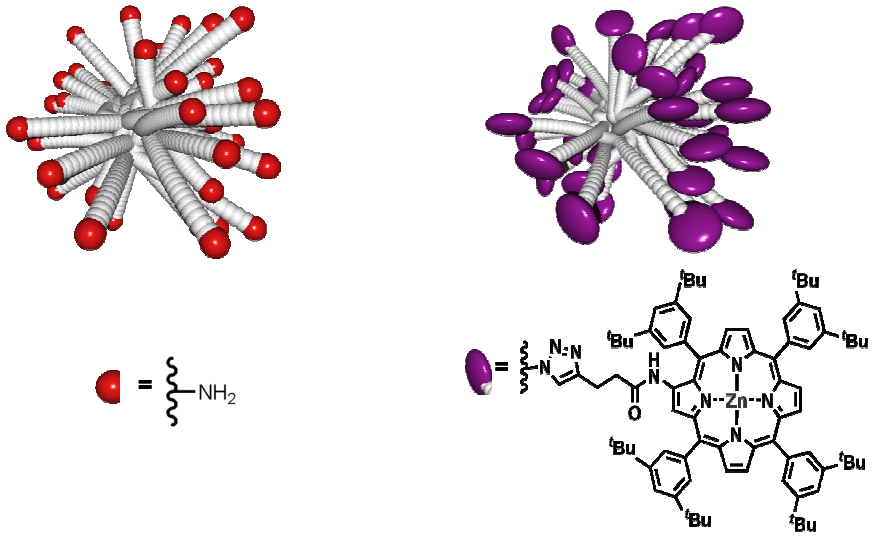

Figure 21. Structural representation of (a) amino-functionalized star polymer and (b) zinc-porphyrin-functionalized star polymer [77].

Solvents used were obtained from a Pure Solv solvent dispensing system purchased from Innovative Technology Incorporated. Other supplementary reagents and solvents were purchased from the Aldrich Chemical Company. The solvents were either used as received or purified before use by standard literature procedures to remove impurities. Acids and bases were purchased from J.T. Baker and used as received.

Schott SF11 wafers were used in the SPR apparatus to match the refractive index of the prism which was also made from SF11. SF11 is a dense alkaline silicate glass with less than 47 wt. % of lead oxide (PbO) and has an index of refraction (n) of 1.76196 at 854 nm at 25 °C [79]. Commercial grade SF11 wafers were purchased from Stefan Sydor Optics. The SF11 substrates are 1 mm thick and 1.0 inch in diameter with a root

mean square (RMS) surface roughness of less than 10 Å. Prior to changing to SF11, initial SPR experiments were conducted using BK7 (*i.e.*, BK7 wafer and BK7 prism). BK7 is a borosilicate crown optical glass with a refractive index (n) of 1.50978 at 854 nm wavelength and 25 °C [79]. The BK7 wafers were purchased from Esco Products and measured 0.5 mm in thickness and 1 inch in diameter. The SPR instrument was migrated to the SF11 optical system after initial experiments using BK7 showed that surface plasmon resonance was occurring almost at the limits of the instrument's angular scan. Since SF11 has a higher refractive index compared to BK7 at a given wavelength and temperature, the use of SF11 prisms and wafers enabled surface plasmons to be excited at an angle nearer to the center of the scan range of the SPR instrument. One side of the SPR substrates (both the SF11 and BK7 wafers) was coated using an in-house procedure with 3 nm chromium (Cr), followed by 50 nm gold (Au) and subsequently 4 nm silicon dioxide (SiO_2) as the final surface layer, as explained in the substrate preparation section (Section 4.2.1).

Substrates used for the QCM were 5 MHz quartz crystals pre-deposited with gold and silicon dioxide. The quartz crystals that were bought from Maxtec Incorporated have a polished SiO_2 surface with titanium (Ti) as the adhesion layer.

The silicon wafers used in the dipping experiments are single-side polished wafers purchased from Virginia Semiconductor Incorporated, measuring 0.25 mm in thickness and 1.0 inch in diameter. The polished side of the silicon wafer offers a flat surface for a more accurate analysis of the topography by the AFM.

Quartz substrates for UV-Vis measurements were 1.0 inch in diameter and 0.5 mm thick substrates polished on both sides, obtained from Boston Piezo-Optics, Incorporated. Quartz substrates provide transparency in the UV-Vis for absorption studies.

4.2 Methods

4.2.1 Substrate Preparation

The choice of substrate for polymer deposition is of obvious importance. The choice of substrates is determined by the type of interaction under study and the analytical methods envisaged. Silicon dioxide was the principal surface of interest in this research. A layer of silanol groups is present on silicon dioxide (SiO_2) surfaces. The layer of acidic silanol groups on the SiO_2 surface results in an overall negative surface charge. This is the predominant force in anchoring the first layer of amino-functionalized star polymer through electrostatic interaction.

The substrates used for SPR studies, *i.e.*, SF11 glass coated with gold (Au) followed by silicon dioxide (SiO_2) as the top layer, were the only substrates prepared in-house. Prior to metal deposition, the SF11 glass is cleaned. According to literature [80], soft manual cleaning for commercial grade polished substrates led to better surface uniformity compared to ultrasonic automatic cleaning or the combination of both. Each of the substrates was gently wiped with acetone using lens paper before being treated with UV ozone and Millipore water. The cleaned SF11 substrates were coated with thermally evaporated 3 nm Cr as the adhesion layer and 50 nm Au before being sputter-coated with a 4 nm top layer of SiO_2 immediately after thermal evaporation. The thermal

evaporation of Cr/Au and SiO_2 sputtering was done under vacuum using a well-maintained thermal evaporator and sputterer and produce a contaminant-free surface. SiO_2 target was used in the sputterer. The gold layer on the SF11 substrate is vital to support surface plasmon generation while the SiO_2 layer is necessary for the adsorption of the first polymer layer, PS-NH_2. QCM substrates were purchased pre-sputtered with SiO_2. Silicon wafers have a layer of native SiO_2 on the surface and were used for AFM studies while quartz wafers were used for UV-Vis studies.

Prior to using any of the substrates for preparation of AFM samples or for analysis by SPR or QCM (with exception of quartz wafers), substrates were treated with UV ozone for 20 minutes to remove organic contaminants. After UV ozone treatment, the substrates were briefly rinsed with Millipore water and dried under a gentle flow of filtered nitrogen. The substrates were then subjected to a brief rinse with pure ethanol to remove any water residue before being once again dried under a gentle flow of filtered nitrogen.

Quartz wafers were used in the UV-Vis analysis due to their transparency. The surface is first treated with acidic piranha etch and then a basic version of the piranha recipe with an intermittent rinse with water and a final rinse with pure ethanol. (*Caution: the piranha solution is extremely corrosive and should be handled with great care*). This treatment removes organic residues from the substrates and hydroxylates (the addition of –OH groups) the surface to produce a dense layer of silanols. The acidic piranha etch is prepared with aqueous hydrogen peroxide, H_2O_2 (30% w/w), and sulfuric acid, H_2SO_4 (17.8 M) in a 1: 4 volume ratio. In the basic version of piranha etch, the sulfuric acid is

replaced with concentrated ammonium hydroxide (NH_4OH), *i.e.*, 20% aqueous hydrogen peroxide (30% w/w) and 80% ammonium hydroxide (28.0% – 30.0% w/w). After a final rinse with pure ethanol, the substrates were dried under a gentle flow of filtered nitrogen.

Substrates that were not used immediately after the preparation steps discussed above were stored in wafer containers and wrapped in aluminum foil to prevent contamination.

4.2.2 Solution Preparation

The PS-NH_2 solution was prepared by weighing 25 mg of the powdered form into 25 mL of solvent to obtain a 1 mg/mL concentration of clear solution. The PS-NH_2 solution was then filtered through a 0.2 μm filter before use. Similarly, the PS-ZP solution was prepared by dissolving 25 mg of the light crimson polymer powder into 25 mL of solvent. The crimson PS-ZP solution was then filtered with a 0.2 μm filter.

Depending on the solvent system of interest, the polymer solutions were prepared in the appropriate solvent. Pure, anhydrous and inhibitor-free tetrahydrofuran, THF was used from the Pure Solv solvent dispenser. Pure dichloromethane, CH_2Cl_2 (*Caution: dichloromethane is a known carcinogen*) and toluene (*Caution: toluene is a known reproductive toxicant*) was also obtained via the Pure Solv solvent dispenser. Pure chloroform, $CHCl_3$ was distilled to remove traces of ethanol.

4.2.3 LBL Deposition Method

LBL can be carried out using two deposition methods: the conventional dipping or a dynamic deposition technique using a fluidic device. The dynamic deposition

technique supports *in-situ* characterization techniques such as SPR and QCM that used flow cells. The dipping technique was used to generate samples for the UV-Vis experiments outlined in Table 3. As described in the substrate preparation section, the substrates were treated accordingly prior to deposition with either method.

The ability to deposit films continuously allows *in-situ* measurement of the layer growth using SPR and QCM. In the dynamic deposition method, solutions are continuously injected into the flow cell. This procedure is based on a study done by Kim *et al.* [49] using dynamic LBL deposition in which they were able to build well-defined multilayers using continuous flow of solution without a soak time. The dynamic deposition was carried out in a flow cell that is either an independent flow system, shown in Figure 22, or a flow cell built into the SPR and QCM instrument, as explained in the next section (Section 4.3). In the flow system shown in Figure 22, the silicon wafer was placed with the polished side of the wafer facing upwards onto the cell base with the sides of the wafer pushed against the guiding pin to align the wafer to the flow cell. The vacuum system for the cell base was then turned on to hold the silicon wafer in place before the flow cell was lowered onto the base. The vacuum system for the flow cell was turned on to lock the flow cell onto the base prior to introduction of solution into the flow cell.

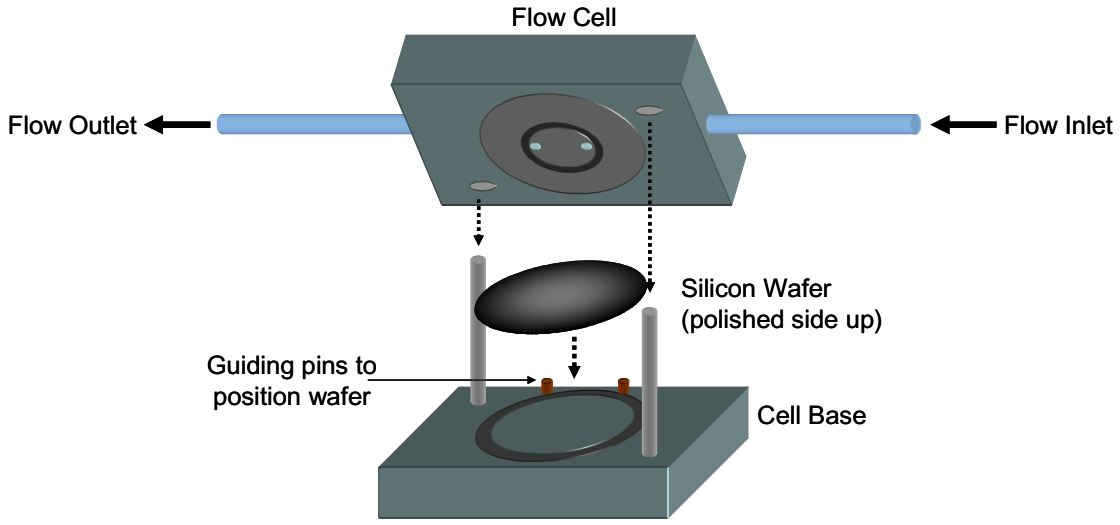

Figure 22. Flow System for dynamic deposition of polymers.

Identical procedures were used for dynamic deposition of the star-polymer using an independent flow system or using the SPR and QCM instruments. The solutions were injected into the flow cell using a syringe pump at a fixed flow rate of 1 mL/min. The choice of the first solution depends on which star polymer is desired as the base layer. The desired star polymer solution is injected into the flow cell at 1 mL/min until 2 mL has been injected. This is followed immediately by a rinsing step with 6 mL of the same solvent used in preparation of the polymer solution at the same flow conditions of 1 mL/min. Similarly, the second layer was deposited with injection of 2 mL at 1 mL/min of the second type of functionalized star polymer and subsequently with 6 mL at 1 mL/min of solvent as the rinse. In the case where a solvent exchange is necessary to expose the polymeric film to a stabilizing solvent, *i.e.*, deposition of star polymer in dichloromethane followed by a final THF rinse, the polymer deposition was carried out similarly with 2 mL of polymer solution in dichloromethane injected into the flow cell at

1 mL/min but the rinsing step consisted of 6 mL of dichloromethane rinse at 1 mL/min followed by 3 mL THF rinse at 1 mL/min. After attaining the desired number of layers, the substrate was dried under a gentle flow of filtered nitrogen for approximately 2 minutes before AFM characterization.

Using the dipping method, the substrate was dipped for 2 minutes into the functionalized star polymer solution desired for the base layer. The subsequent processing involved 3 rinsing steps in 3 separate beakers containing the same solvent used for polymer solution preparation. In order to form the second layer of thin film, the substrate containing the first layer was then dipped into the other functionalized star polymer solution (the complement of the first layer) followed by 3 rinses in 3 different beakers of the solvent. In the case of dichloromethane deposition with a final THF wash, the rinsing step consisted of 3 rinses with dichloromethane followed by an additional THF rinse. After the desired number of layers had been achieved, the substrate was dried under a gentle flow of filtered nitrogen for 2 minutes before being characterized using UV-Vis.

If substrates were not immediately analyzed on the AFM or UV-Vis after preparation using the methods mentioned, the substrates were stored in wafer holders and wrapped in aluminum foil to prevent contamination and photo-degradation of the polymers.

4.3 Instrumentation

4.3.1 Surface Plasmon Resonance (SPR)

Surface plasmon resonance (SPR) angular detection was used to determine if the deposited layers formed uniform monolayers. There are two modes of operation available for the SPR, *i.e.*, the kinetic mode (intensity versus time mode) and the angular scan mode (intensity versus angle mode). An analysis of the resonance angle shift (from the angular scans done after each deposition) indicates the relative thickness and thickness uniformity of the layers.

The SPR instrument consists of a two-arm reflectometer which measures the reflected optical power from the film sample in the flow cell as a function of angle of incidence. A laser diode with a wavelength of 854 nm was mounted on the source arm with a polarizer and compensation optics while the collection arm contained optics to image the reflected light onto a silicon detector with daylight blind filter. The two arms counter rotate at equal angle with an angular resolution of 0.001 degrees. The Kel-F® flow cell where the sample was optically probed was fixed at the center of rotation of the arms. The flow cell was a 0.5 mm deep elliptical pocket milled into a Kel-F® block with axes 7.0 mm by 2.1 mm, and a total volume of 40.8 μL. The elliptical dimension of the flow cell, as illustrated in Figure 23(a) allows smooth fluid movement and helps prevent the formation of air bubbles. The choice of material for the prism and substrate in the SPR instrument was SF11 for optical index matching. The SF11 substrate was placed with the metal-coated side facing the flow cell and held in place with vacuum. The O-ring around the flow cell seals the contact between the substrate and the flow cell. The

O-rings seals are Perlast® high performance perfluoroelastomer o-rings which are highly resistant to a wide range of chemicals. Approximately 5 µL of refractive index matching fluid was then dropped onto the top, uncoated side of the SF11 substrate. The refractive index matching fluid is a methylene iodide formulation purchased from Cargille Labs (n = 1.7650 ± 0.0005). A SF11 hemi-cylindrical prism with radius of 0.375 inches was slowly lowered to rest on the SF11 substrate. This was done carefully to avoid air bubbles being trapped in the index-matching fluid between the substrate and the prism. Figure 23(b) shows the basic components of the SPR instrument used.

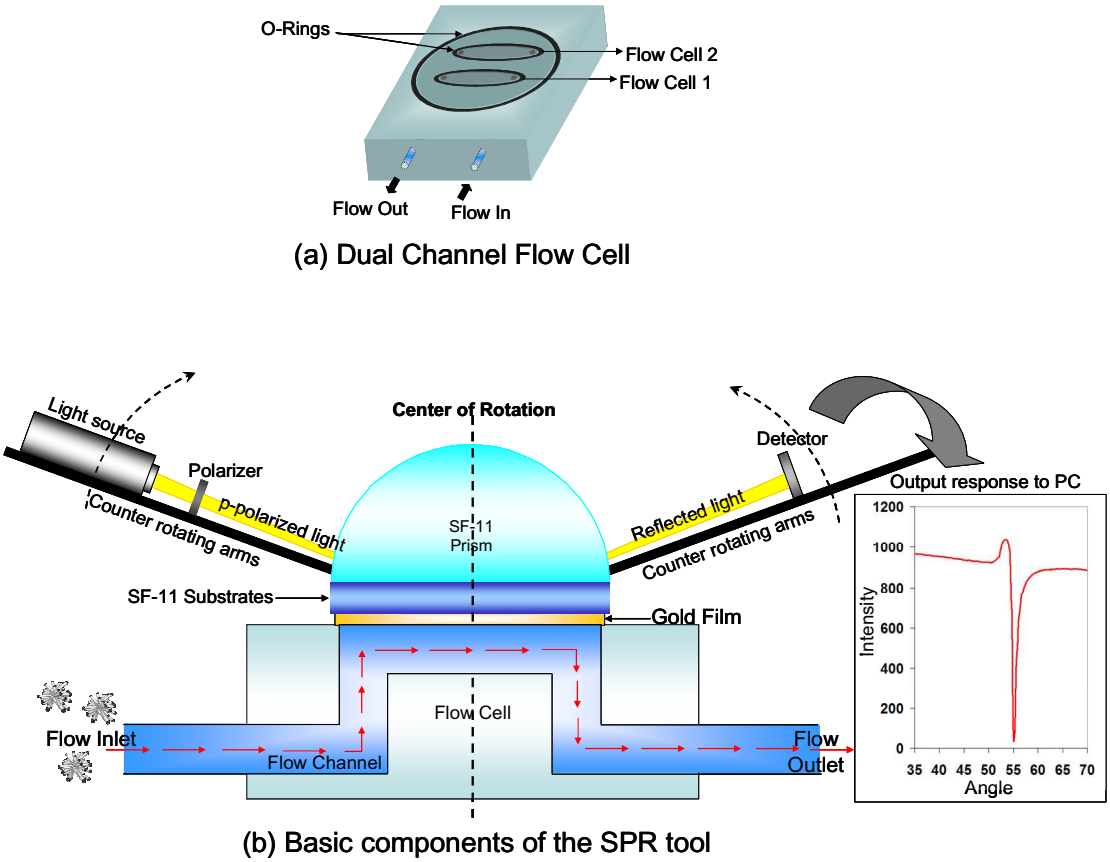

Figure 23. Diagram of (a) dual channel flow cell and (b) basic components of the SPR instrument.

Fluidics were incorporated into the SPR instrument to facilitate dynamic deposition of polymers. A 6-port valve was used to switch between the different types of solutions. Since the valve is known to have a sweeping volume, the ports were assigned to allow solvent or rinsing agent (*i.e.*, THF) to be added between the two polymer solutions to avoid mixing. The tubing used was Tefzel, a fluorocopolymer thermoplastic material with a wide range of chemical resistance that had a 1/16" OD and 0.030" ID. Figure 24 illustrates the manifold system used and the length of the sample tubing and the common tubing. Due to the use of organic solvents such as tetrahydrofuran (THF), the fluidics system had to be designed with THF-resistant materials. The sealing surface for the 6-port valve was made of ceramic while the connectors and tubing were made of Tefzel.

A baseline SPR signal was obtained by conducting an angular scan (intensity versus angle) with the desired solvent in the flow cell of the SPR instrument. From the baseline SPR scan, an angle was chosen at the point of inflection after the TIR and just before the resonance (minimum intensity). The SPR instrument was directed to the specific chosen angle for kinetic measurements. The SPR instrument was operated in the kinetic mode (intensity versus time) at a chosen angle during introduction of materials into the flow cell. The intensity versus time change was monitored as the polymers were injected into the flow cell to ensure equilibrium was achieved before each subsequent step. The change in intensity over time also provided information on the adsorption kinetics of each layer. A total of 2 mL of polymer solutions was injected at a flow rate of 1 mL/min into the flow cell using a syringe pump as previously explained using the

dynamic deposition method. The residence time of the polymer in the flow cell was calculated to be 1.5 minutes after subtraction of the volume of the tubing. The rinsing step requires 6 mL of rinsing solvent at 1 mL/min; hence the residence time of the rinsing solvent in the flow cell was 5.5 minutes. Since this was a positive flow system, precautions were taken to ensure that the correct port on the valve was opened before starting the syringe pump to prevent pressure build up. All used lines were purged with the rinsing solution and acetone to remove residual polymers after use.

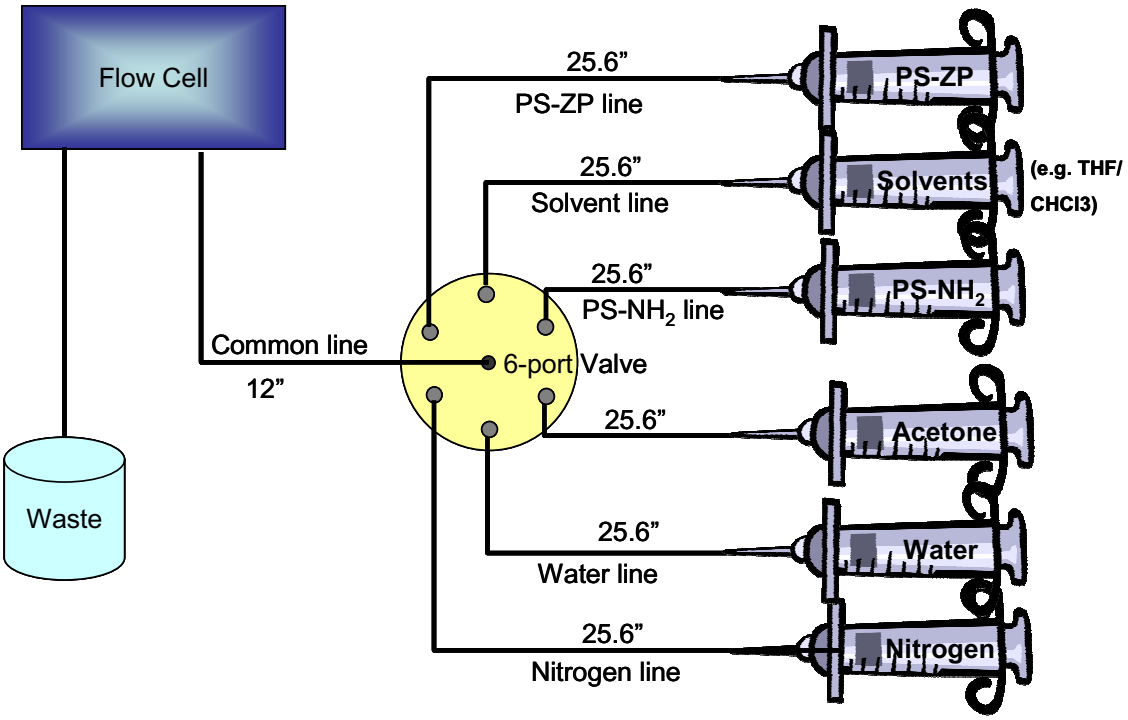

Figure 24. Manifold system for dynamic depositions in a flow cell.

Kinetic mode of operation was stopped after every layer deposition and angular SPR response (intensity versus angle) was collected. As the star polymer films were being deposited on the SiO_2 surface, the resonance angle shifts due to changes in the index of refraction. This angular shift was monitored to determine if each layer was uniform in thickness. Prior to analyzing the shift in resonance angle after each polymer layer deposition, the point at where total internal reflection (TIR) occurs on the SPR signals was ensured aligned as shown by the red dotted line in Figure 25. The resonance angle from the experimental SPR data was determined by fitting the data with the KNS function developed by Kurihara *et al.* [37].

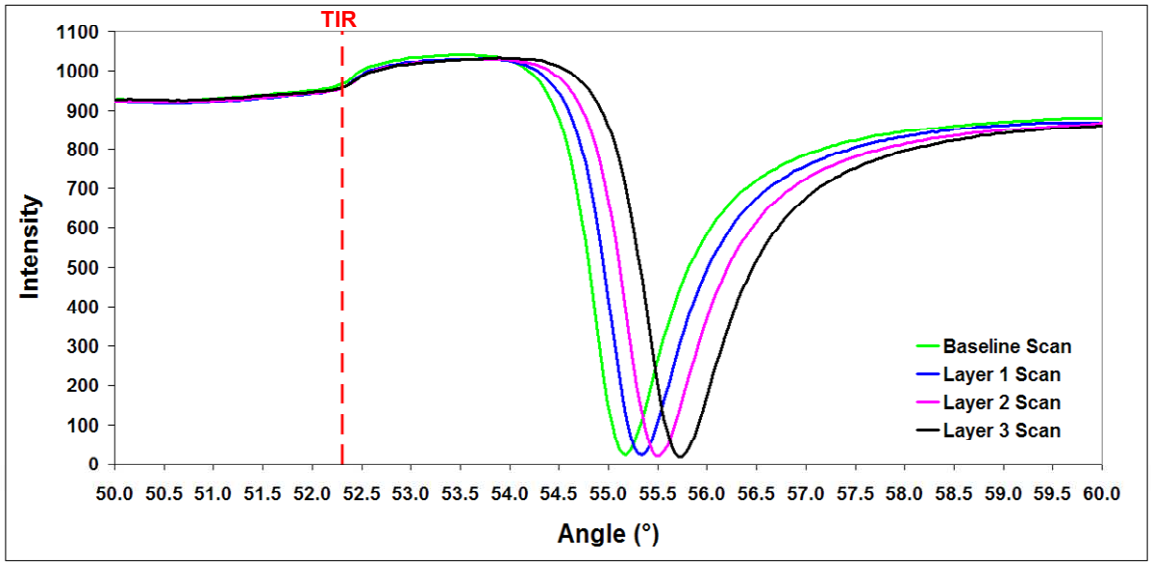

Figure 25. Overlay of successive SPR signals with TIR aligned.

The angular SPR response is related to the fixed-angle kinetic response as shown in Figure 26. When the flow cell was filled with the baseline solvent such as THF, and θ_0 was fixed as the angle for kinetic measurements, a constant reflectivity of ~ 0.2 was

recorded over time. The introduction of dichloromethane (notated as DCM in the figure) caused the refractive index in the flow cell to increase and the plasmon resonance shifted to a larger angle. This change in reflectivity could be resolved in the kinetics mode since the maximum reflectivity was attained. The introduction of polystyrene in dichloromethane and the formation of a polystyrene layer further increased the resonance angle which is not detected in the kinetic view. When dichloromethane was replaced by THF in the flow cell, the reflectivity dropped to a level (~ 0.6) that was higher than the original baseline THF level due to the shift in resonance angle caused by the formation of a polystyrene layer.

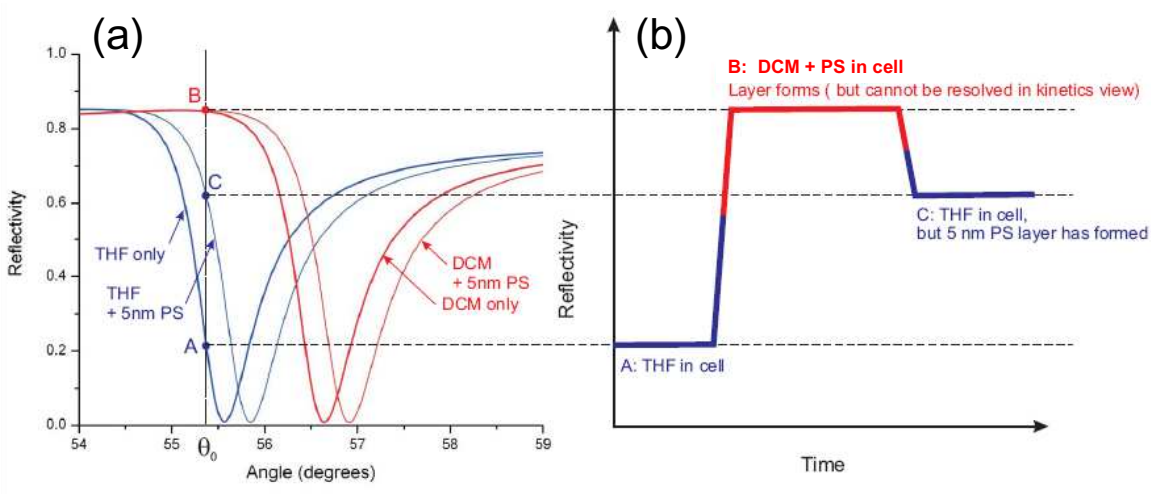

Figure 26. Relationship between (a) angular SPR response, and (b) fixed-angle kinetics measurement [81] (reprinted with permission from William P. Risk).

Concurrent to the LBL experiments using the SPR instrument, Dr. William Risk from IBM Almaden Research Center wrote a Matlab program for the determination of the minimum angle from the collected surface plasmon resonance signal by fitting the SPR data with the KNS function described by Kurihara *et al.* [37]. The program searches

for a set of coefficients that produces the least square error between KNS function and the experimental data and reports the minimum angle together with a plot of the data (black circles) and the best fit KNS function (red line) as shown in Figure 27.

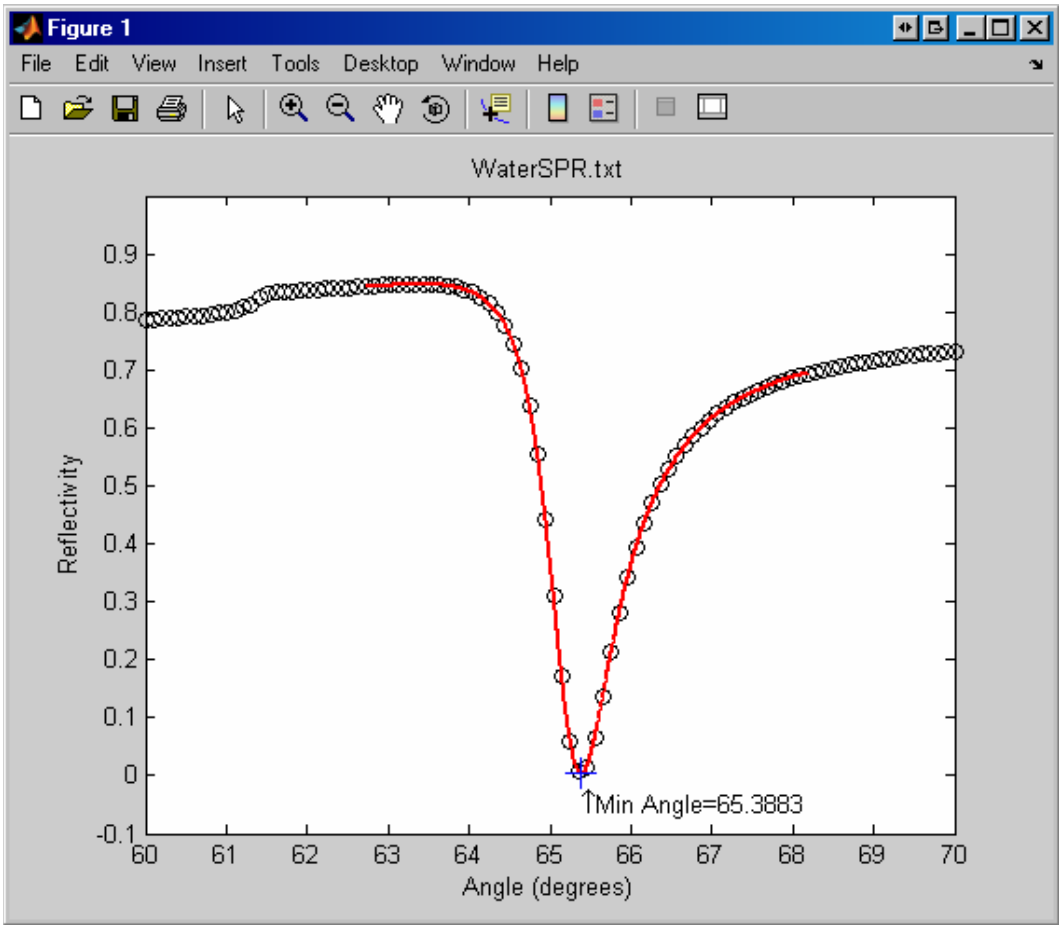

Figure 27. Plot of experimental data (black circle) together with best KNS fit (red line) produced by Matlab fitting program written by Dr. William Risk.

4.3.2 Quartz Crystal Microgravimetry (QCM)

The quartz crystal microbalance (QCM) was employed to examine the coverage of the polymer layers and to determine if each polymer layer was a monolayer. The QCM consists of a Kel-F® flow cell with a quartz crystal sandwiched between two electrodes. The quartz crystal was held in place with vacuum. Gold-plated steel springs

were used to make electrical contact with the electrodes of the crystal. The flow cell allows the use of the dynamic deposition method described in previous section. Figure 28(a) illustrates the basic set-up of the QCM flow cell while Figure 28(b) shows a schematic of the QCM. The same manifold system used for the SPR instrument was used on the QCM with similar precautions. The quartz crystal oscillates at its resonance frequency, *i.e.*, 5 MHz, when an AC voltage is applied across the electrodes. Any change in mass due to the deposition of each polymer layer would result in change in the resonance frequency. This change of frequency was monitored and recorded in real-time on the computer. The correlation between mass and frequency change was derived from the Sauerbrey equation shown in Equation 1. Computing the mass for each layer provided information on whether the same amount of polymer was being deposited for each polymer layer type.

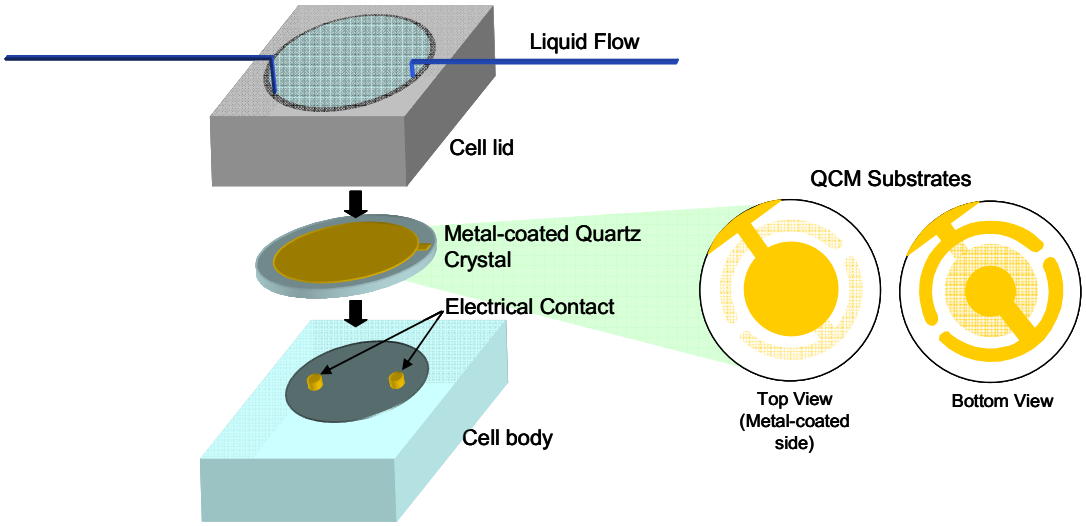

(a) Basic QCM flow cell set-up

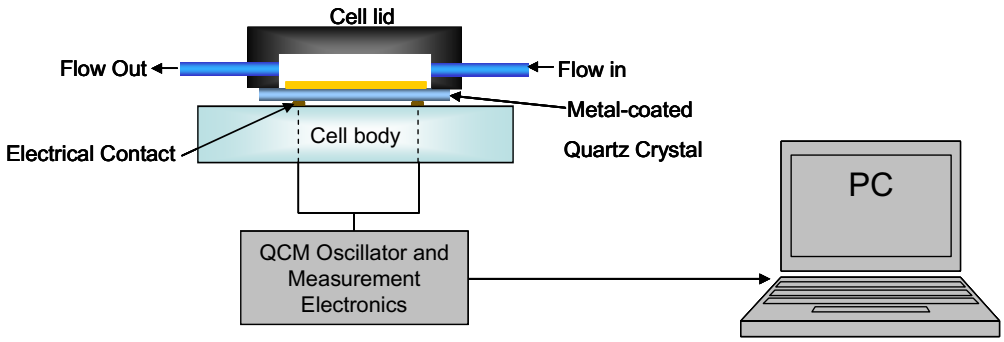

(b) Side view of the QCM tool

Figure 28. Schematic diagram of the (a) Basic QCM flow cell set-up and (b) Side view of the QCM.

4.3.3 Atomic Force Microscopy (AFM)

Atomic force micrographs were acquired using a Digital Instruments 3100 atomic force microscope in tapping mode at a scan rate of 1 Hz using a silicon nitride cantilever with 1 N/m spring constant. An illustration of the AFM set-up is shown in Figure 29. Deflection of the cantilever is measured using a laser spot reflected from the top of the

cantilever onto a photo-detector and is plotted as a topographic profile. The topography and the coverage of the different types of functionalized polymers both on wafer surfaces and on polymer were studied using this method. After establishing tip-sample contact, fine-tuning was performed to ensure continuous contact as the image was collected. 1 μm and 5 μm images were collected. All images were processed to remove imaging artifacts and set to a 10 nm color scale (z-height) to enable comparison. The AFM images were analyzed using the manufacturer's off-line software to obtain the root-mean-square (RMS) roughness. Smooth films had low RMS values which signify homogeneous and uniform coverage. The phase image, collected simultaneously with the topography image from the damping of the modulated cantilever in tapping mode, showed contrast if a different type of material was present. Both the height image and phase image were used for complete analysis of the film.

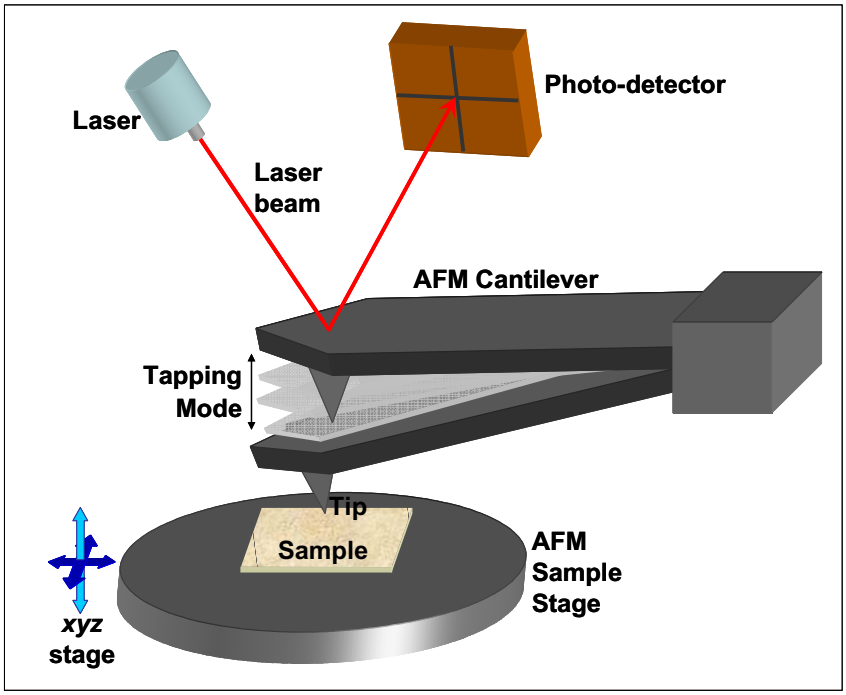

Figure 29. AFM set-up in tapping mode.

4.3.4 UV-Vis Spectroscopy

Absorption spectra were obtained after every layer deposition using an Agilent UV-Vis Spectrophotometer. The dipping method was used to prepare the samples. Zinc-porphyrins are strongly absorbing dyes that absorb light in the visible light region. Due to this feature, the formation of the dye-containing film was observed by UV-Vis spectroscopy. The deposition of PS-ZP resulted in a peak in the range of 420 to 460 nm depending on whether the zinc-porphyrins were fully bound, partially bound or not at all bound by coordination. The peak absorption of the zinc-porphyrin layer shifted slightly upon coordination with the next amine layer. This experiment provided information on the number of arms interacting within a monolayer of PS-ZP and confirmed the role of coordination chemistry in layer formation.

CHAPTER FIVE
RESULTS AND DISCUSSION

5.1 Atomic Force Microscopy

This chapter deals with efforts to assess the quality and stability of the polymeric films generated using layer-by-layer self-assembly of functionalized star polymer. Atomic force microscopy (AFM) was used to study the topography and coverage of the individual polymer layers formed in the LBL process. The polymeric films are designated based on their layer number throughout the results and discussion chapter as illustrated in Figure 30.

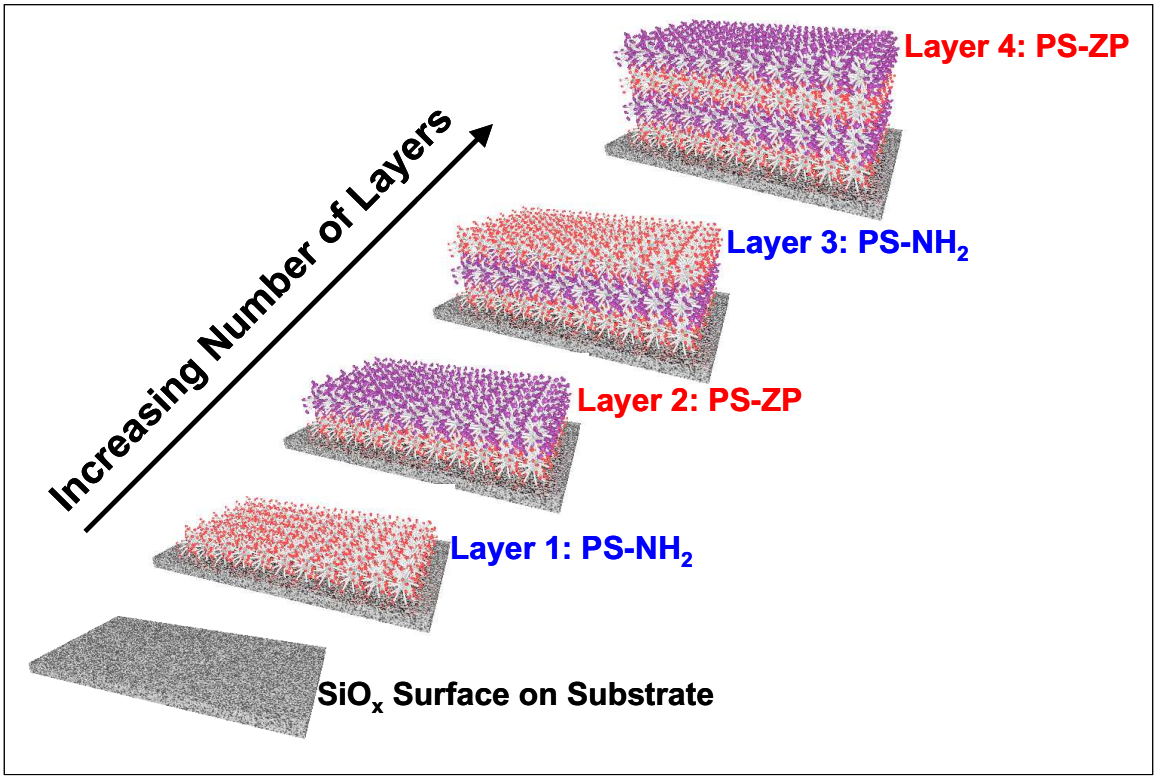

Figure 30. Schematic of the LBL self-assembly process for four polymeric layers.

The AFM height image can be used to show the morphology of the surface while the phase diagram can reveal information on the homogeneity of the film. Combined, the height and phase images provide insights on self-assembled film coverage and film stability. The stability of the film can be inferred from AFM data collected over time. In this chapter, the results from AFM studies and their implications are discussed in three sections: (i) self-assembled polymeric films on substrates, (ii) self-assembled polymeric films on complementary polymer layers, and (iii) layer-by-layer self-assembled polymeric films. The overall results and conclusions as to the effectiveness of AFM for the purpose of this research are presented below.

5.1.1 Self-Assembled Star Polymer Layer on Silicon Dioxide Surface

Optimal conditions for the formation of a complete and stable initial polymeric layer on silicon dioxide surface were investigated in order to ensure successive LBL self-assembly of alternating functionalized star polymers. The star polymer of choice for the base polymer layer formation on silicon dioxide surfaces was the amino-functionalized star polymer, PS-NH_2. Reasons for the preference of PS-NH_2 as the base film instead of zinc-functionalized star polymers, PS-ZP, were supported by AFM data and are discussed in ensuing paragraphs.

The silicon wafer has a native oxide layer and was used as the substrate of choice in the AFM study of surface coverage and stability of self-assembled polymeric films on silicon dioxide surfaces due to the smooth and flat background. The featureless surface of the silicon wafer allows easy distinction of surface features after polymer deposition. A typical surface of a silicon wafer after UV-ozone and Milipore water treatment is

shown in Figure 31. The root mean square (RMS) roughness of the silicon wafer surface from the 5-µm image in Figure 31(b) is approximately 0.6 nm.

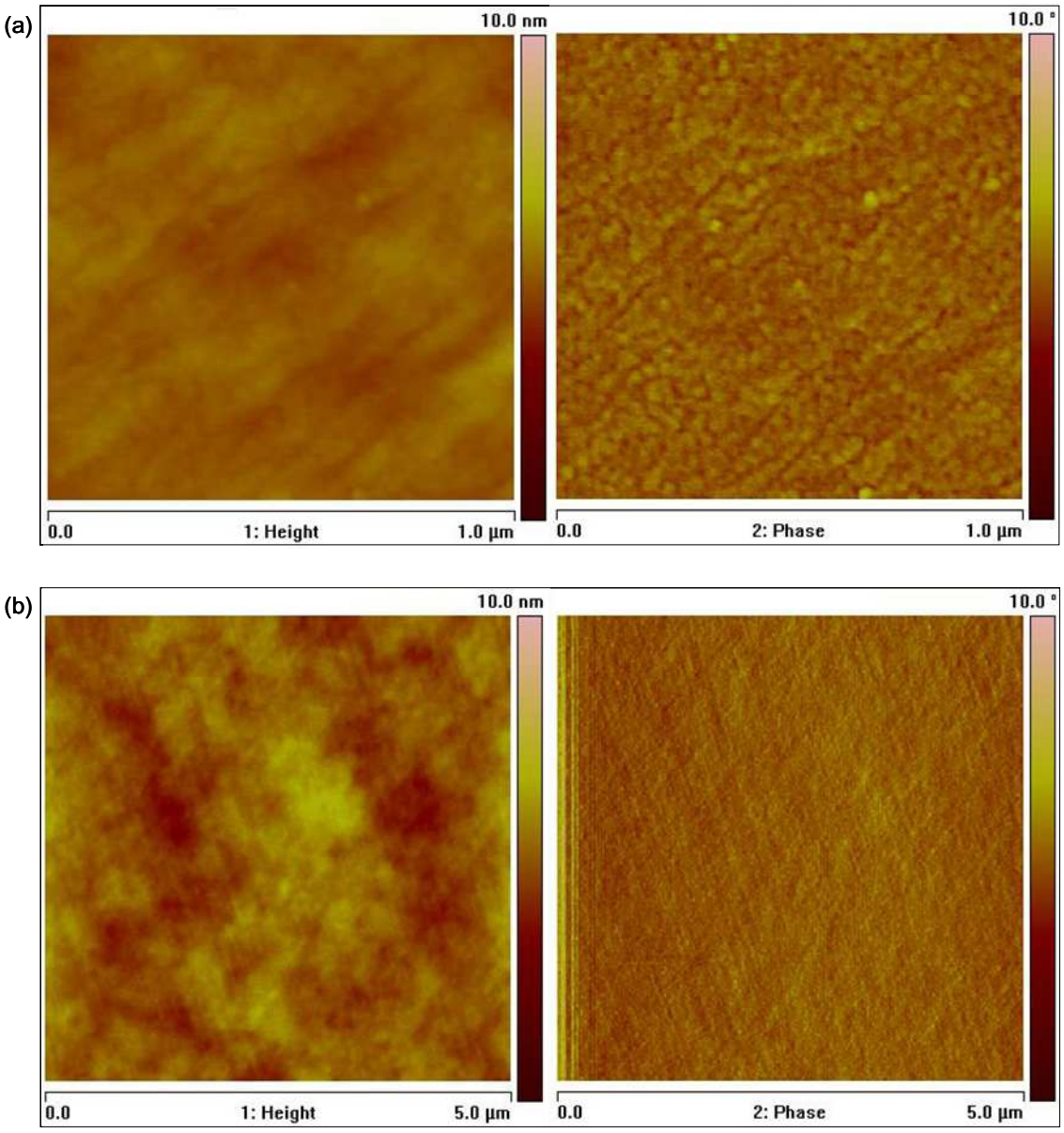

Figure 31. AFM height (left) and phase (right) images of silicon wafer after UV-ozone and Milipore water treatment, at (a) 1 µm x 1 µm (RMS ≈ 0.3 nm) and (b) 5 µm x 5 µm (RMS ≈ 0.6 nm).

Self-assembled star polymer films can be generated using two methods as explained in the materials and methods chapter: the flow-system and the dipping method. The flow-system allows the deposition to be carried out in an enclosed system and minimizes the effect of contamination from the environment. Samples for AFM analysis were initially generated using the dipping method. However it was found that the dipping process required a lot of sample handling which exposed the films to contamination and produced irregular films. A comparison of films formed from PS-NH_2 on a silicon wafer surface generated using the flow-system and using the dipping method under the same solvent conditions (dichloromethane deposition with THF wash) is shown in Figure 32. The film prepared from PS-NH_2 using the dipping method in Figure 32(b) shows structured and non-structured features on the surface. The structured features may be polymeric in origin or may arise from non-specifically bound polymers that were not removed by the washing step. The non-structured features could be particle contamination since the films were generated in an open environment. It was concluded from the atomic force micrographs that the flow system produced films of a better quality due to less handling and exposure to the environment. Subsequent AFM results were obtained from samples generated using the flow system. In addition, films produced using the flow-system are more comparable in preparation to the films produced in the flow cell of the SPR and QCM instruments (Section 5.2 and Section 5.3).

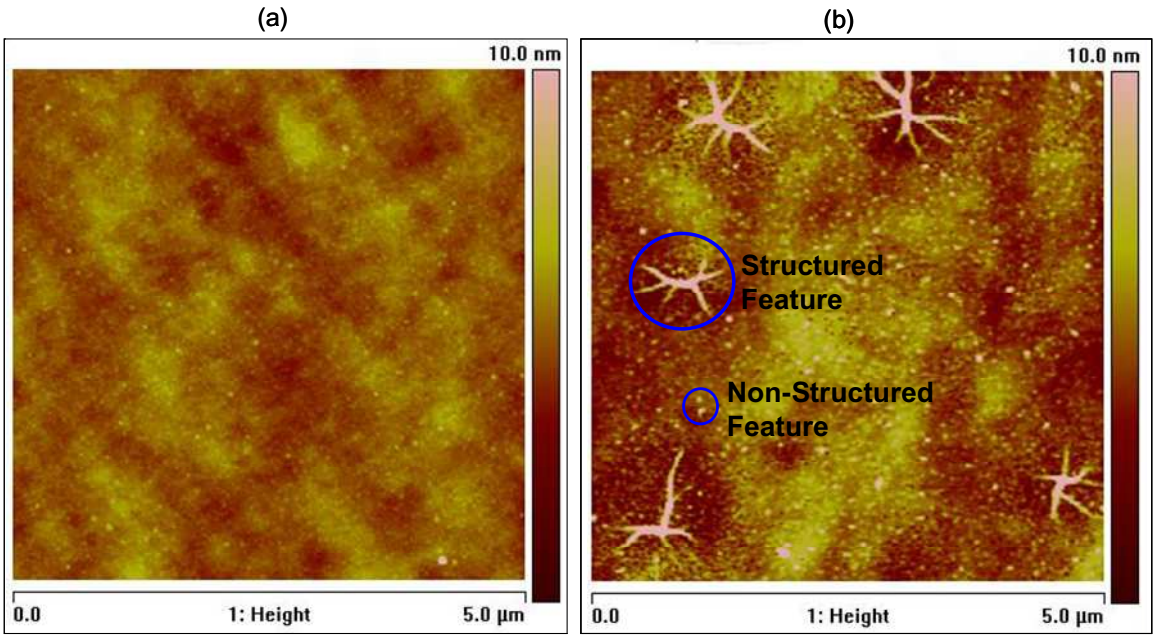

Figure 32. Comparison of AFM height images of PS-NH_2 film on silicon wafer generated using (a) flow system (RMS ≈ 0.6 nm), and (b) dipping method (RMS ≈ 1.7 nm). Films were prepared using dichloromethane deposition with a final THF wash.

It was observed from the AFM results that solvent plays an important role in determining the morphology of the first polymer layer on silicon dioxide surface. Initial experiments using THF as a solvent for PS-NH_2 polymer deposition with THF wash (THF/THF) produced a more textured surface as observed in the AFM image in Figure 33 compared to the film shown in Figure 32(a) which was prepared using dichloromethane deposition with a final THF wash post-deposition (CH_2Cl_2/THF). The RMS roughness of the surface from the THF/THF process is approximately 1.3 nm, compared to 0.6 nm for the CH_2Cl_2/THF process. A complete and contiguous PS-NH_2 film was formed on the silicon wafer despite its textured surface as shown in Figure 33(b). It is concluded from this observation that THF is a good solvent for deposition of

the first, PS-NH_2 polymer layer although the resulting film is not particularly smooth. The choice of solvent could affect the size and shape of the polymer during self-assembly into a film due to the degree of solvation or it could affect the interactions between the functional groups on the polymer with other functional groups. In general, star polymers with amino-functionalized moieties, PS-NH_2 interact strongly with the silanols on the surface of the silicon wafer yielding an amine-silanol complex [82] through electrostatic interaction. The electrostatic interaction between the amines on the star polymer and the silanols on the silicon dioxide surface involves proton transfer from the silanol to the amine group as illustrated in Equation 3. The pK_a value of some acids depends on the water content in THF as substantiated by a study done by Barron *et al.* on the pK_a value for different acid components of pH reference materials in varying THF-water mixtures [83]. Assuming that this observation applies also for silanols on the SiO_2 surface, when THF is used as the solvent for PS-NH_2, the pK_a value becomes important in determining whether the silanols on the silicon dioxide surface actually protonate the amines on the star polymer to form a cationic species. It is postulated that anhydrous THF when used in the PS-NH_2 deposition, does not support the deprotonation of the silanols on the surface of the silicon wafer, hence when anhydrous THF was used, the interaction involved between the amino (-NH_2) group and the silanols is hydrogen bonding which is a weaker type of interaction compared to electrostatic interaction. This may be the reason behind the textured surface seen in Figure 33.

$$PS-NH_2 + R_3Si-OH \Leftrightarrow PS-NH_3^+ + R_3Si-O^- \Leftrightarrow (PS-NH_3)^+(R_3Si-O)^-$$

Equation 3

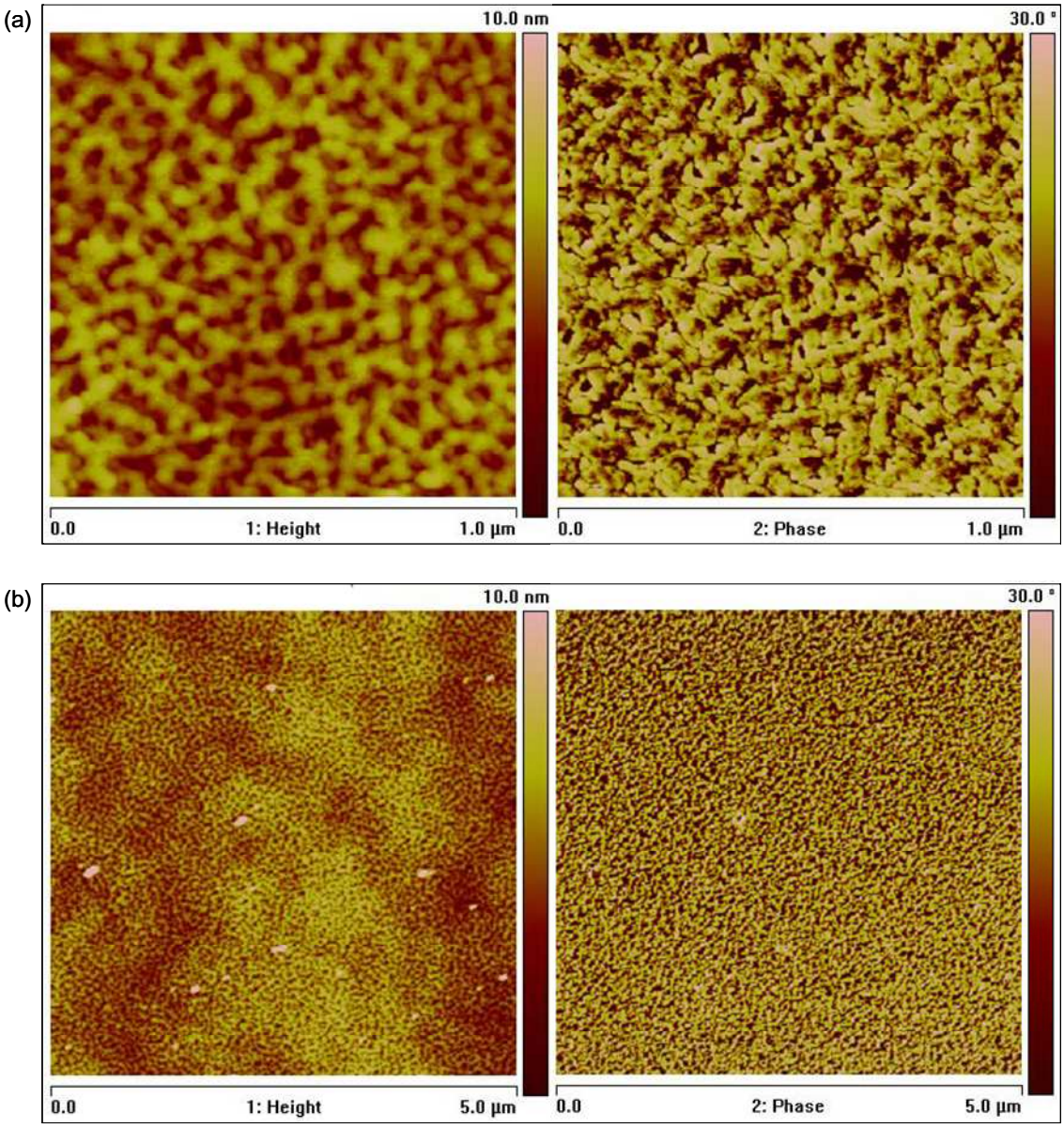

Figure 33. AFM height (left) and phase (right) images of layer 1 PS-NH_2 on silicon wafer with THF as both the deposition and wash solvent, (a) 1 µm x 1 µm (RMS ≈ 1.2 nm), and (b) 5 µm x 5 µm (RMS ≈ 1.3 nm).

The importance of the surface-polymer interaction for the formation of a smooth and complete first polymer layer for subsequent self-assembly is further highlighted by the results of experiments using zinc-porphyrin-functionalized star polymer, PS-ZP as the first layer instead of PS-NH_2. The film coverage is rough and apparently incomplete as shown in Figure 34. The PS-ZP polymer appears to cluster yielding a rough surface. The RMS roughness of the surface is approximately 1.5 nm. Hence, PS-ZP is unsuitable to be used as a first layer as it forms rough and non-contiguous films owing presumably to weaker Van der Waals interactions between zinc-porphyrins and the silanols on the surface of the silicon wafer.

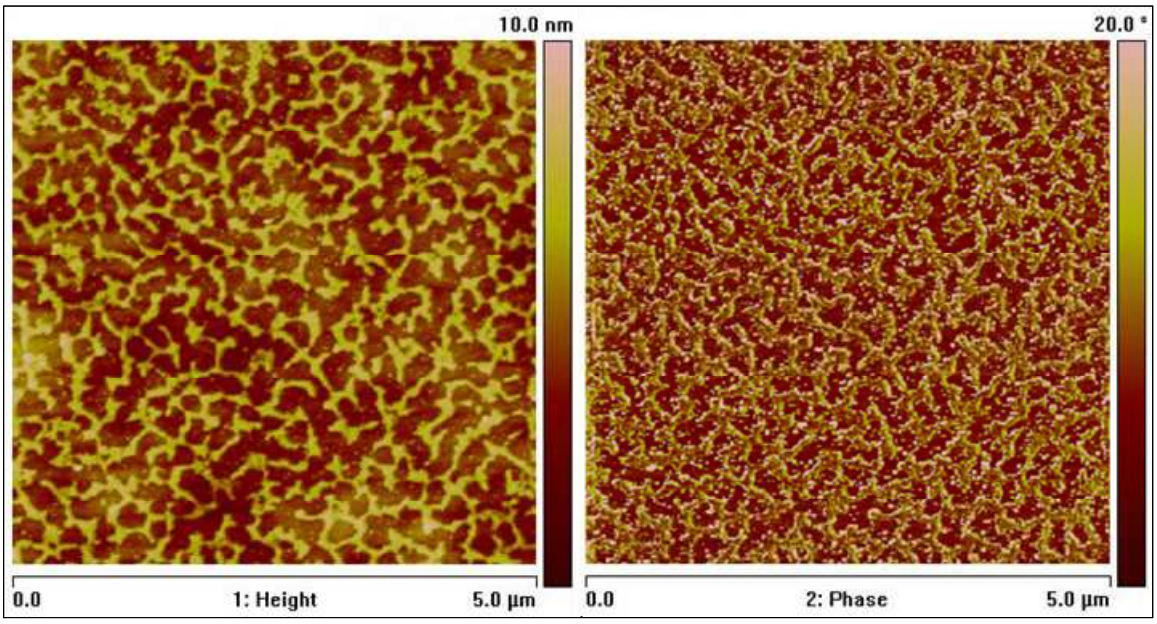

Figure 34. AFM height (left) and phase (right) images of PS-ZP on silicon wafer with THF as the solvent for deposition and washing, 5 µm x 5 µm (RMS ≈ 1.5 nm).

When chloroform is used as the solvent for deposition and wash of the initial film from PS-NH_2, dewetting of the film is observed after 24 hours of deposition, as shown in the 5-μm images in Figure 35.

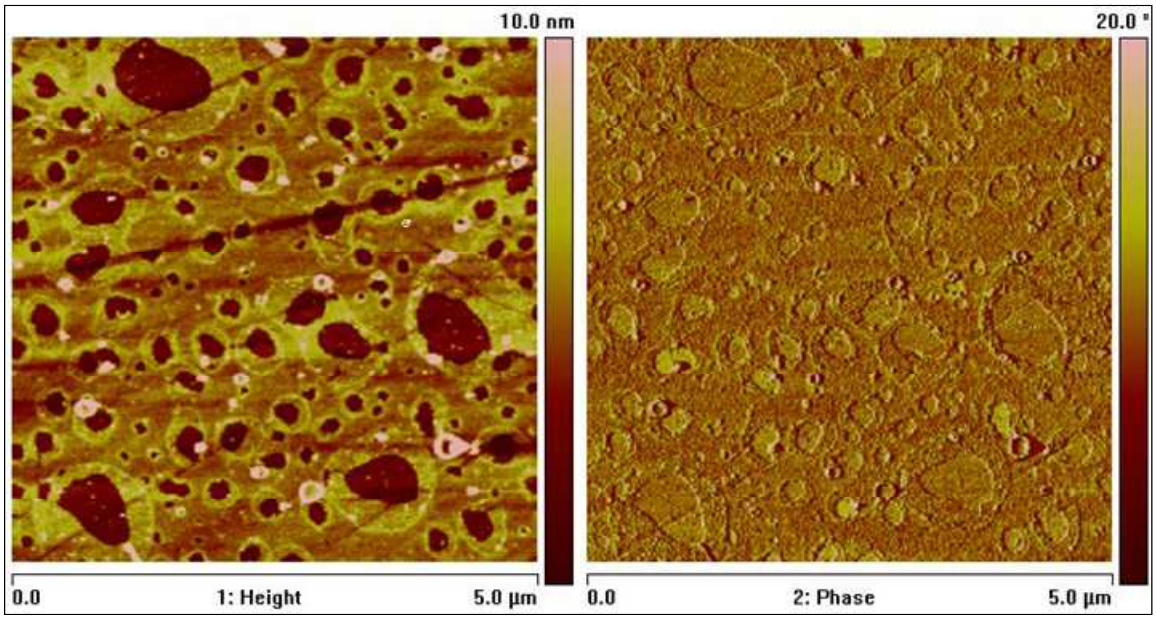

Figure 35. AFM height (left) and phase (right) images of layer 1 PS-NH_2 on silicon wafer with chloroform as the solvent for deposition and washing, 5 μm x 5 μm (RMS ≈ 3.1 nm).

The stability of the first layer can be significantly improved by finally exposing the film to THF post-deposition. Star polymer, PS-NH_2 deposited onto silicon wafer surface using dichloromethane (a solvent chemically similar to chloroform), followed by a final rinse with THF is shown in Figure 36. Dichloromethane was chosen instead of chloroform due to easy accessibility to pure dichloromethane through the Pure Solv solvent dispenser. The RMS roughness of the surface was approximately 0.6 nm.

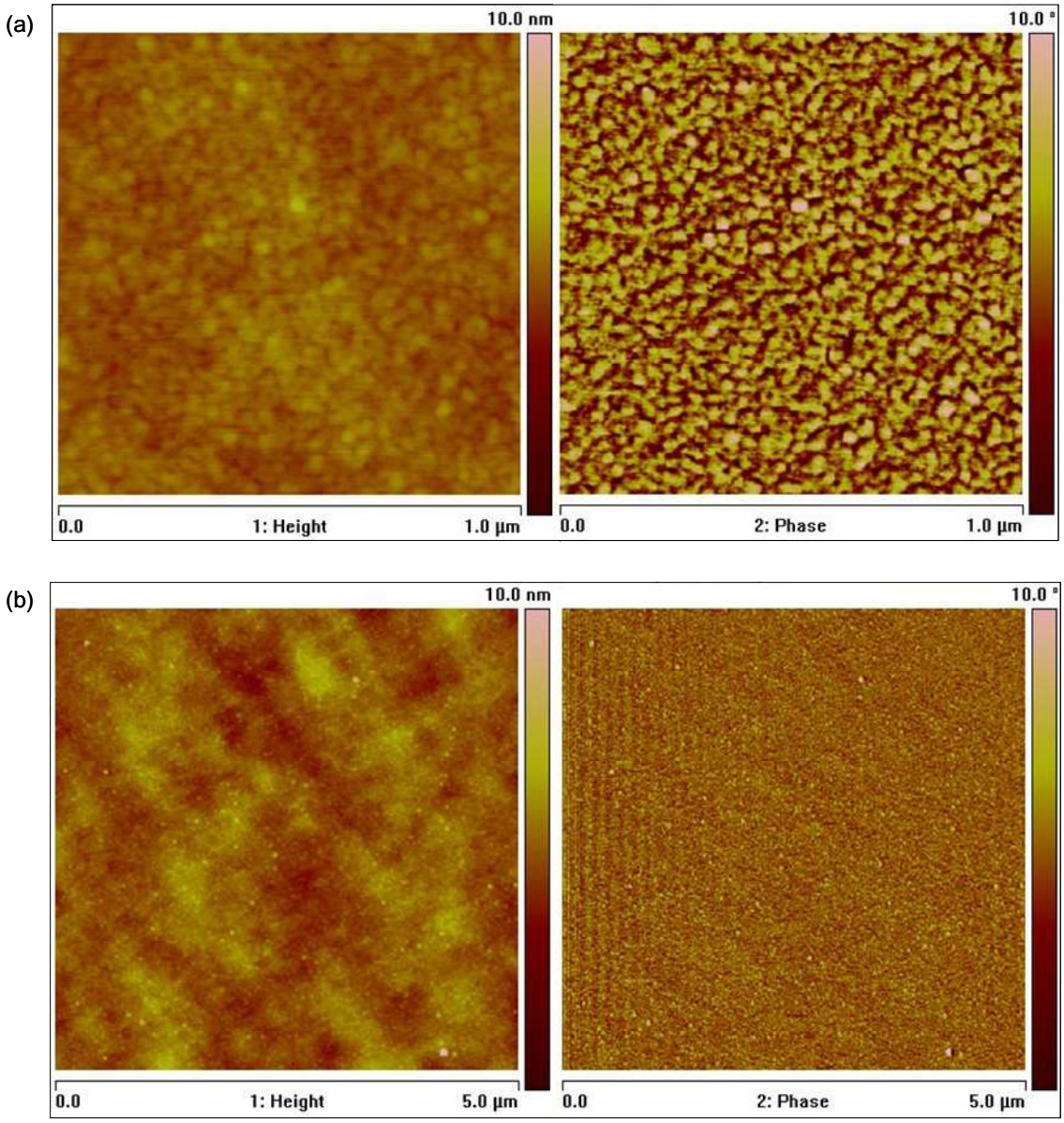

Figure 36. AFM height (left) and phase (right) images of layer 1 PS-NH_2 on silicon wafer with dichloromethane, CH_2Cl_2 as the solvent for deposition and THF as the final rinse solvent, (a) 1 µm x 1 µm (RMS ≈ 0.3 nm) (b) 5 µm x 5 µm (RMS ≈ 0.6). Vertical ripples seen in the phase diagram in (b) is due to imaging artifact.

The film generated using dichloromethane deposition followed by a THF wash was less grainy compared to the film generated using THF alone as shown in Figure 37. The three-dimensional rendition of the AFM images in Figure 37 provides an alternate view of the films and enables easier comparison. The interaction involved in the formation of the PS-NH_2 layer on silicon wafer is the electrostatic interaction shown in Equation 3. This observation led to the conclusion that dichloromethane is the preferred solvent for the deposition process of the first layer to ensure a smooth film; while a final THF rinse is essential to preserve the stability of the film.

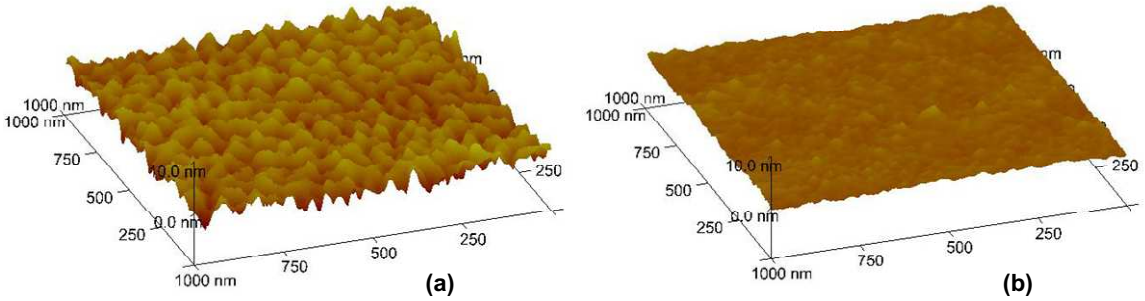

Figure 37. Comparison of PS-NH_2 film (1 μm x 1 μm images) on silicon wafer using (a) THF deposition and wash (RMS ≈ 1.2 nm), and (b) dichloromethane deposition followed by THF wash (RMS ≈ 0.6 nm).

While stable, the roughness of the resultant film formed from PS-NH_2 also depended on the length of time that the film had been exposed to THF during the rinse process. The roughness of the film increased with increase in THF rinse exposure time, as illustrated by the morphology of the surface of Layer 1 (PS-NH_2) shown in Figure 38. The RMS roughness of the film increases from 0.6 nm in Figure 38(a) to 0.7 nm in Figure 38(b) and 1.9 nm in Figure 38(c) as the THF-exposure duration was increased from 3 minutes to 9 minutes and 18 minutes, respectively. This agrees with the

proposition that the PS-NH_2 star polymer anchors reversibly on the silanol surface and the interactions between the surface and the arms of the star polymer exist at an equilibrium state. The solvent mediates the interaction between the surface and the arms on the PS-NH_2 star polymer. The exposure of the substrate-polymer to a different solvent (*e.g.*, THF) alters the equilibrium, causing re-structuring of the PS-NH_2 polymer molecule at the nano-scale. This capacity for post-deposition nano-restructuring of the films indicates the existence of the film as a self-assembled equilibrium structure.

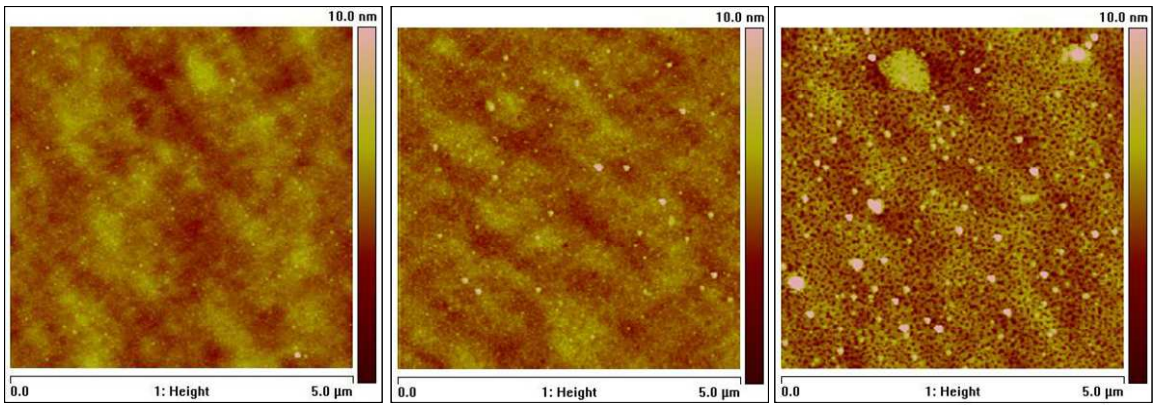

Figure 38. Effect of THF rinse exposure time, (a) 3 minutes (RMS ≈ 0.6 nm), (b) 9 minutes (RMS ≈ 0.7), (c) 18 minutes (RMS ≈ 1.9), on PS-NH_2 film deposited in CH_2Cl_2.

A summary of the RMS roughness analyses from AFM images of the base layer (Layer 1) prepared under different conditions is shown in Table 4. It can be deduced from the RMS roughness analysis and from visual inspection of the AFM images that PS-NH_2 can self-assemble into an acceptably smooth film on a silicon dioxide surface using dichloromethane as the solvent for deposition and THF as the final wash. The resultant film has an RMS roughness of 0.6 nm which is similar to the RMS roughness of a cleaned silicon wafer.

Table 4. Summary of RMS roughness analysis for functionalized star polymer self-assembly on silicon dioxide surfaces.

Case No.	Figure No.	Surface	Conditions	Deposi-tion Method	RMS Roughness
1	Figure 31(b)	Silicon wafer	Treated with UV Ozone/Milipore water	-	0.6 nm
2	Figure 34	PS-ZP layer	THF deposition and wash	Flow System	1.5 nm
3	Figure 33(b)	PS-NH_2 layer	THF deposition and wash	Flow System	1.3 nm
4	Figure 35	PS-NH_2 layer	Chloroform deposition and wash	Flow System	3.1 nm
5	Figure 32(b)	PS-NH_2 layer	Dichloromethane deposition and THF wash	Dipping	1.7 nm
6	Figure 38(a)	PS-NH_2 layer	Dichloromethane deposition and THF wash for 3 minutes	Flow System	0.6 nm
7	Figure 38(b)	PS-NH_2 layer	Dichloromethane deposition and THF wash for 6 minutes	Flow System	0.7 nm
8	Figure 38(b)	PS-NH_2 layer	Dichloromethane deposition and THF wash for 18 minutes	Flow System	1.9 nm

The AFM analysis done in this section established that a protocol of PS-NH_2 polymer flow deposition with dichloromethane followed by dichloromethane rinse and a final three-minute THF wash provided the optimal conditions to produce an initial contiguous and stable film from PS-NH_2 polymer with full coverage. As mentioned, PS-ZP is found to be an unsuitable candidate for the formation of a complete and contiguous base layer.

5.1.2 Self-Assembled Star Polymer PS-ZP Layer on Star Polymer PS-NH_2 Base Layer

After establishing the optimal deposition conditions for the initial PS-NH_2 polymer layer, conditions for depositing the second layer of star polymer with the complementary zinc-porphyrin functional group, PS-ZP, were explored. The zinc-porphyrin, ZP group interacts with the amino, NH_2 group through organometallic coordination. Initially, this second layer was deposited in the same manner as the first layer, *i.e.*, dichloromethane deposition with a final THF wash, to produce a film surface with an RMS roughness of approximately 0.8 nm as shown in the atomic force micrographs in Figure 39. The AFM micrographs showed complete second layer coverage. Although this RMS roughness value was similar to layer 1 (PS-NH_2 layer), visual inspection of the AFM height images suggested that the film surface appeared to adopt a grainier texture compared to the PS-NH_2 layer. The AFM height images in Figure 40 depict the change in surface morphology in the step-by-step process of depositing the base layer PS-NH_2 onto the silicon dioxide substrate, followed by the deposition of the second layer, PS-ZP.

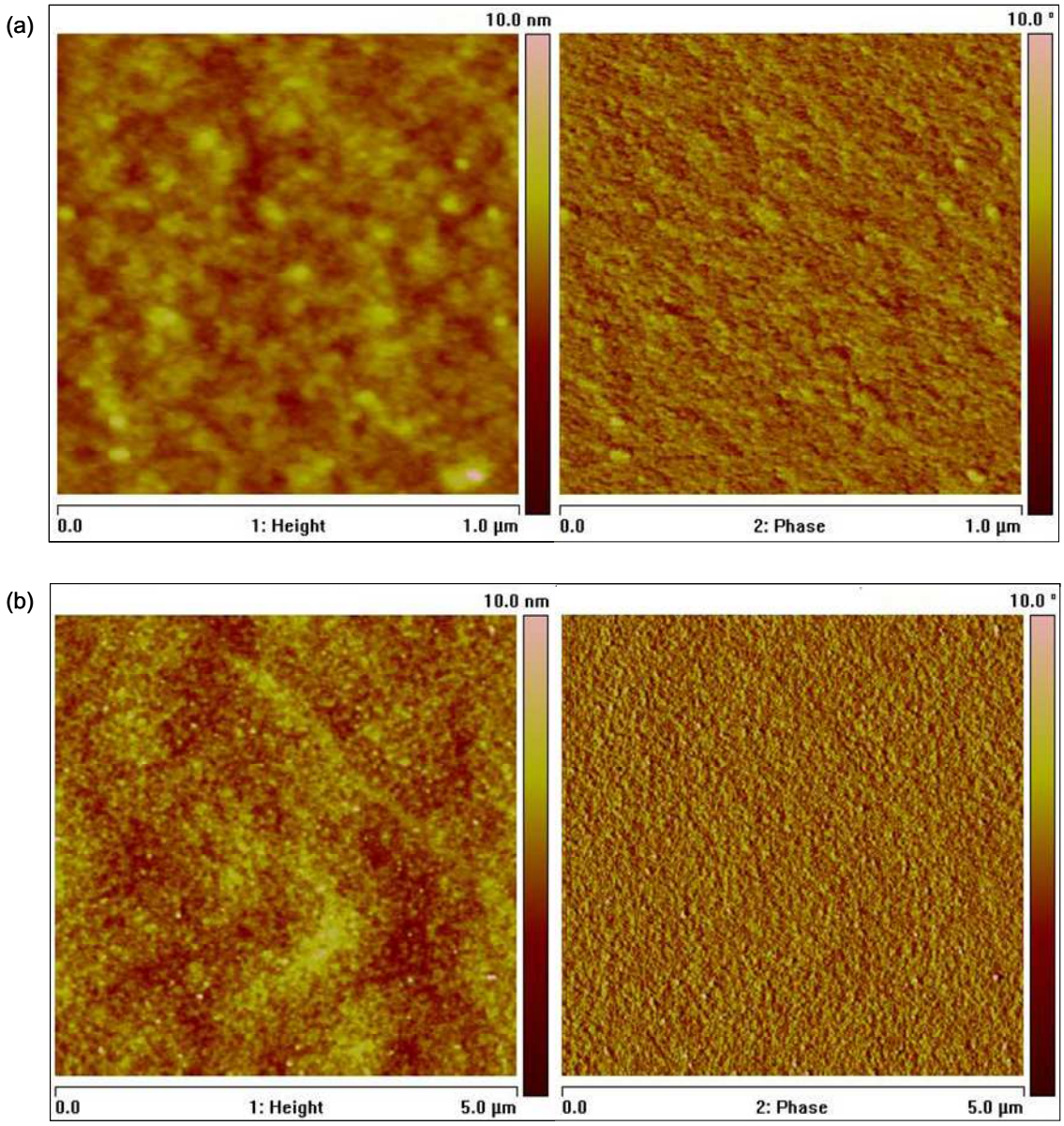

Figure 39. AFM height (left) and phase (right) images of the 2nd layer PS-ZP with dichloromethane, CH_2Cl_2 as the solvent for deposition and THF as the final solvent, (a) 1 µm x 1 µm (RMS ≈ 0.6 nm) (b) 5 µm x 5 µm (RMS ≈ 0.8 nm).

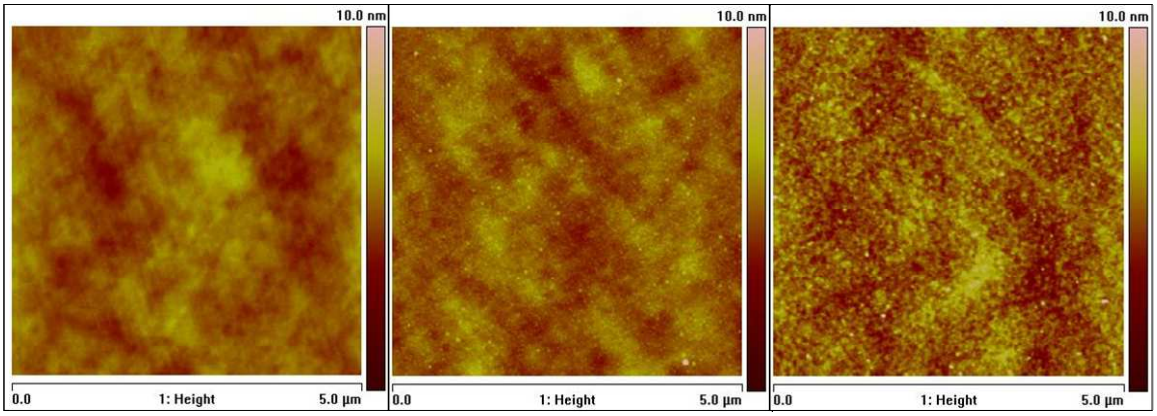

(a) (b) (c)

Figure 40. Comparison of AFM height images (5 µm x 5 µm) of the (a) silicon dioxide substrate (RMS ≈ 0.6 nm), and subsequent polymer layers deposited in dichloromethane with final THF wash, *i.e.*, (b) layer 1, PS-NH_2 (RMS ≈ 0.6 nm), and (c) layer 2, PS-ZP (RMS ≈ 0.8 nm).

The effect when THF was used as a solvent for deposition of PS-ZP on a PS-NH_2 film was investigated. Unlike layer 1 (PS-NH_2), there was no significant difference between a PS-ZP layer that was deposited in dichloromethane with THF wash and a PS-ZP layer that was deposited in THF with THF wash as shown in Figure 41. This is attributed to the fact that the interactions involved in formation of the PS-NH_2 film on a silicon wafer and the formation of the PS-ZP film on a PS-NH_2 film are different, *i.e.*, electrostatic interaction vs. coordination chemistry, respectively. It can be concluded from this observation that THF causes changes in the morphology of an electrostatic film (*i.e.*, the PS-NH_2 film on silicon wafer) but not in a film generated through coordination chemistry. Hence the dual solvent system - dichloromethane deposition with THF wash is not required after the first PS-NH_2 layer.

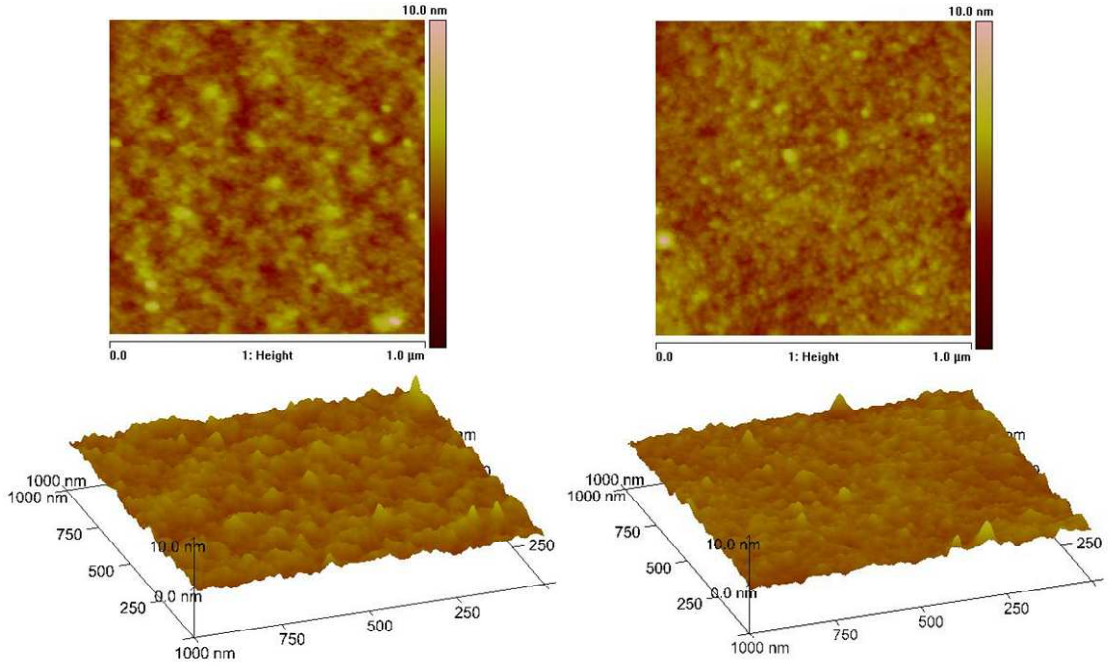

Figure 41. Comparison of AFM images (1 µm) of the PS-ZP layer deposited onto PS-NH_2 using (a) CH_2Cl_2/THF (RMS ≈ 0.6 nm), and (b) THF/THF (RMS ≈ 0.5 nm).

In summary, this section concludes that a dual solvent system (dichloromethane deposition with THF wash) is not required for the adsorption of PS-ZP molecules on a surface coated with PS-NH_2 molecules. A complete and contiguous second layer of PS-ZP can be formed from THF deposition with THF wash.

5.1.3 Layer-by-Layer Self-Assembled Film of Alternating Functionalized Star Polymers (PS-NH_2/PS-ZP)

After the deposition conditions had been determined for layers 1 (PS-NH_2) and 2 (PS-ZP), it was decided that subsequent alternating layers could be deposited in THF since the interaction involved in layer formation after the first layer is coordination chemistry. The morphology of the 3rd layer (PS-NH_2) is shown in Figure 42(a). Unlike the textured surface seen in layer 1 film of PS-NH_2 deposition from THF directly onto a

silicon wafer surface (Figure 33), the surface of the 3rd layer (PS-NH_2 deposited on PS-ZP in THF) is smoother and more complete with RMS roughness of approximately 1.2 nm. The atomic force micrographs show these films have slightly increased roughness compared to layer 2 (PS-ZP) and have complete polymer coverage. The 4th polymeric layer, PS-ZP, deposited in THF with THF wash in Figure 42(b) shows similar morphology to the 3rd layer and has a similar RMS roughness value of approximately 1.2 nm.

The three-dimensional AFM images summarizing the layer-by-layer self-assembly process of the first four layers are shown in Figure 43 while a summary of the RMS roughness of the surface after each polymer deposition is shown in Table 5. It was evident that the morphology of the surface changed slightly as additional layers were deposited, with a small and steady increase in RMS roughness of the surface of the films as each layer was being deposited. Film coverage remained complete in all cases.

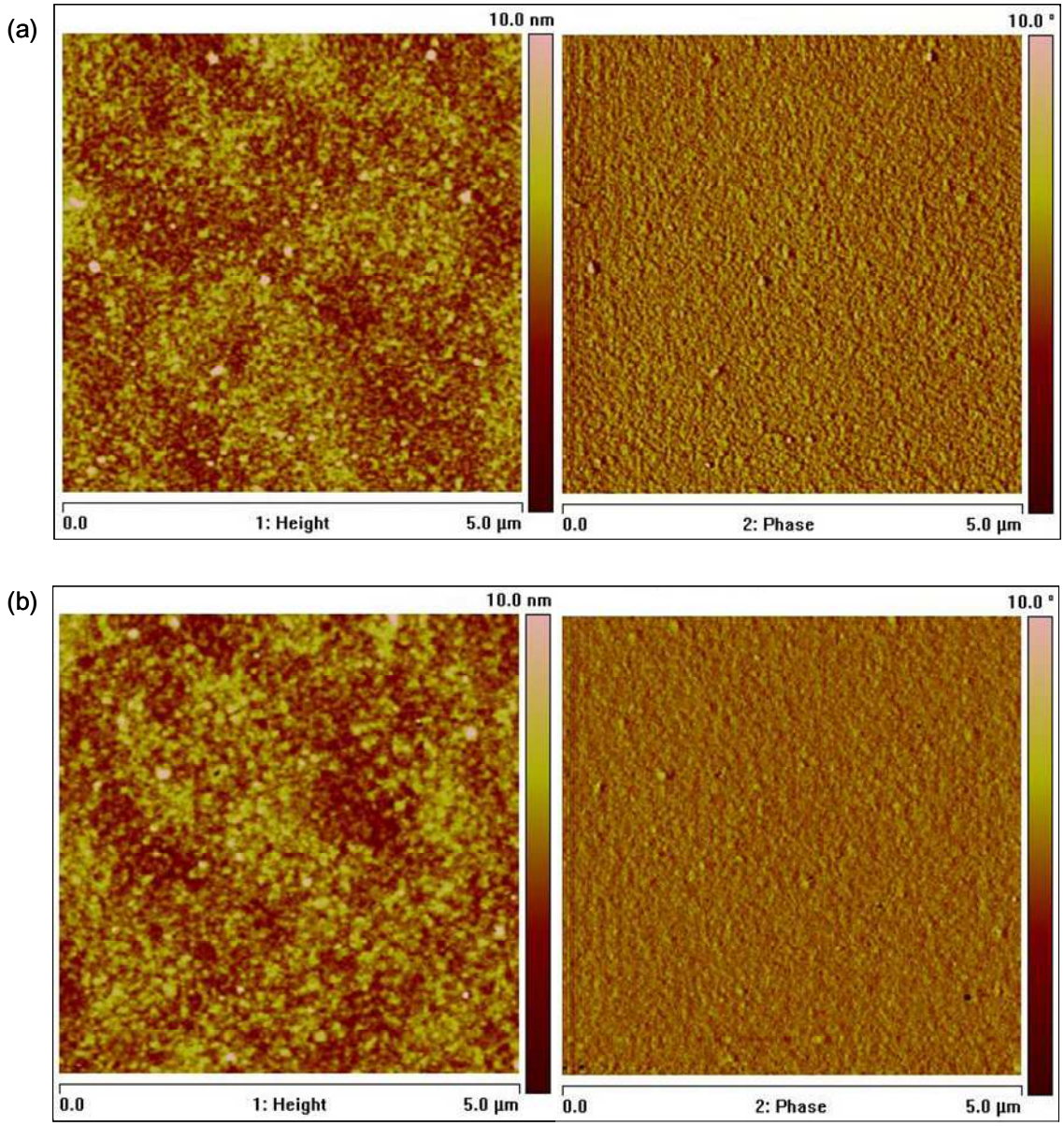

Figure 42. AFM height (left) and phase (right) images of (a) Layer 3, PS-NH_2 (on top of layers 1 and 2) (RMS ≈ 1.2 nm), and (b) Layer 4, PS-ZP (on top of layers 1, 2, and 3) (RMS ≈ 1.2 nm), deposited in THF/THF.

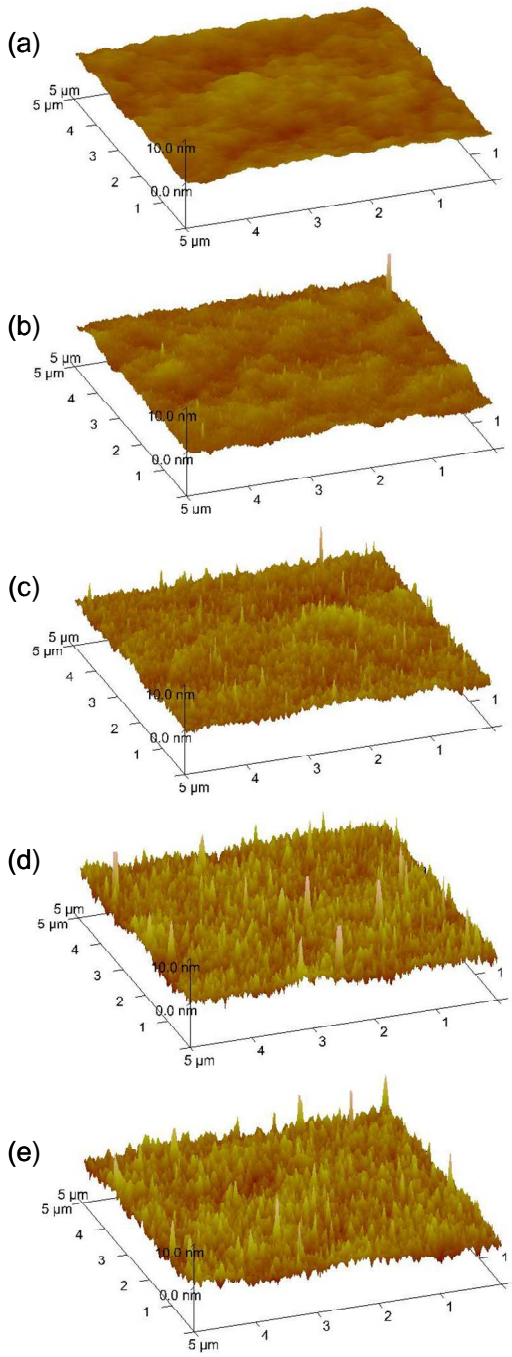

Figure 43. Three-dimensional AFM images of the four step process of creating the 4-layer film in Figure 30: (a) Silicon wafer (RMS ≈ 0.6 nm), (b) Layer 1, PS-NH_2 deposited in CH_2Cl_2 with THF wash (RMS ≈ 0.6 nm), (c) Layer 2, PS-ZP deposited in THF (RMS ≈ 0.8 nm), (d) Layer 3, PS-NH_2 deposited in THF (RMS ≈ 1.2 nm), and (e) Layer 4, PS-ZP deposited in THF (RMS ≈ 1.2 nm).

Table 5. Summary of the preparation conditions and RMS roughness values of the silicon dioxide surface and subsequent LBL deposition of four layers shown in Figure 43.

Layer No.	Material	Conditions	RMS Roughness
Substrate	Silicon dioxide	UV Ozone + Milipore water	0.6 nm
1	PS-NH_2	Deposition in CH_2Cl_2 and THF rinse	0.6 nm
2	PS-ZP	Deposition and wash in THF	0.8 nm
3	PS-NH_2	Deposition and wash in THF	1.2 nm
4	PS-ZP	Deposition and wash in THF	1.2 nm

In order to probe the stability of the multilayer film constructed through LBL, the top surface of the 4-layer film (described in Table 5 and shown in Figure 42(b)) was studied over a period of 2 weeks using AFM. The sample for the study was stored in a Fluoroware wafer container under ambient conditions and wrapped in aluminum foil to prevent contamination and photo-degradation of the polymers. The film was imaged 24 hours after deposition and subsequently 2 weeks after deposition and was found to be stable after two weeks with no signs of film dewetting as shown in Figure 44. In contrast, films that were deposited in chloroform showed dewetting 24 hours after deposition.

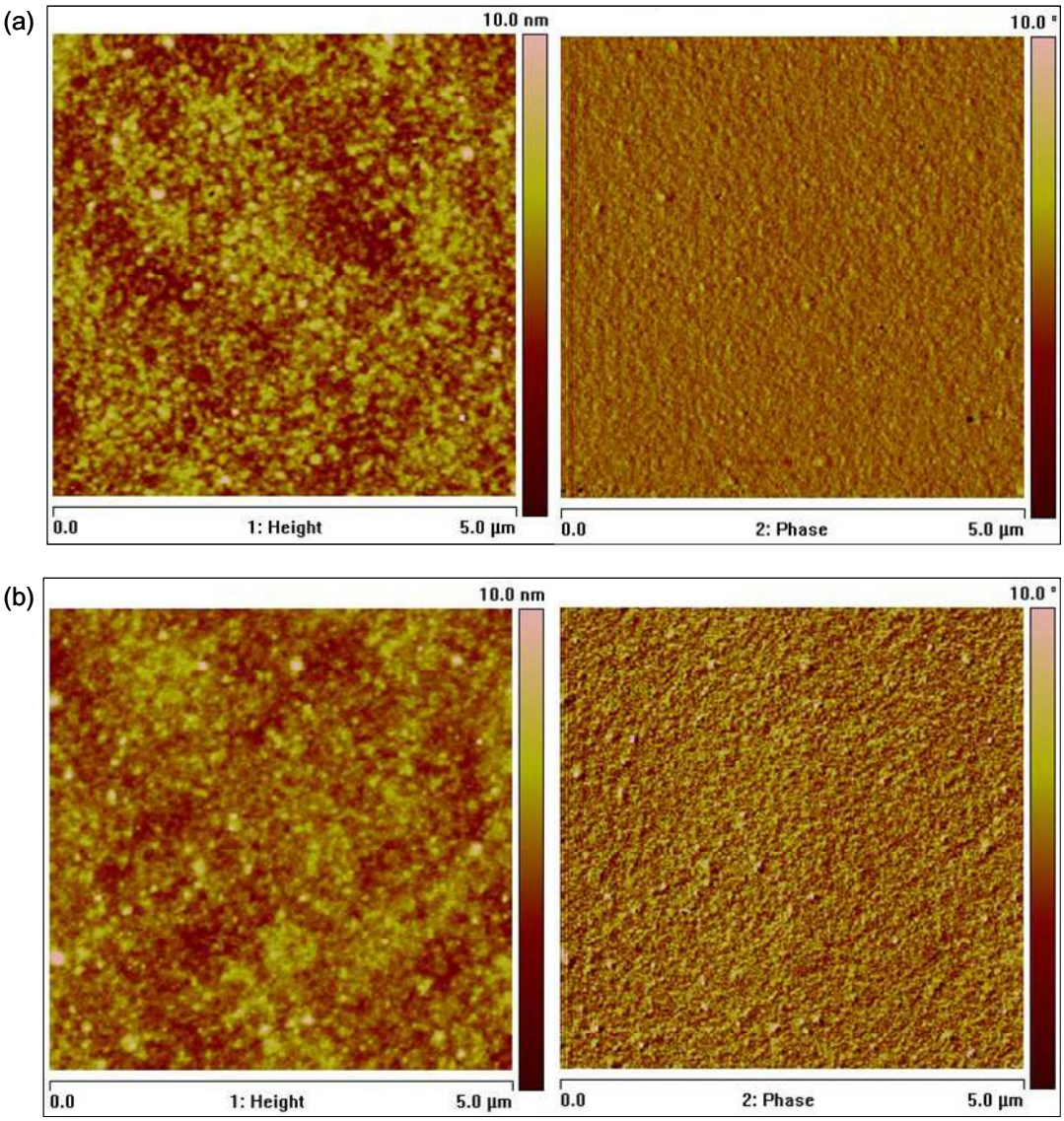

Figure 44. AFM height (left) and phase (right) images of Layer 4, PS-ZP (on top of layers 1, 2, and 3) (a) 24 hours after deposition (RMS ≈ 1.2 nm), and (b) 2 weeks after deposition (RMS ≈ 0.9 nm).

Figure 45 shows progressive deposition up to four polymer layers using THF as the solvent for deposition and wash while Table 6 is a summary of the RMS roughness after each polymer deposition and wash in THF. Visually, it was noted that the morphology of the films changed as layers were deposited while still maintaining

complete polymer coverage. Multilayer formation from the star-polymer detected by SPR and QCM seemed not to have been hindered by an initial rough base layer as detected by AFM.

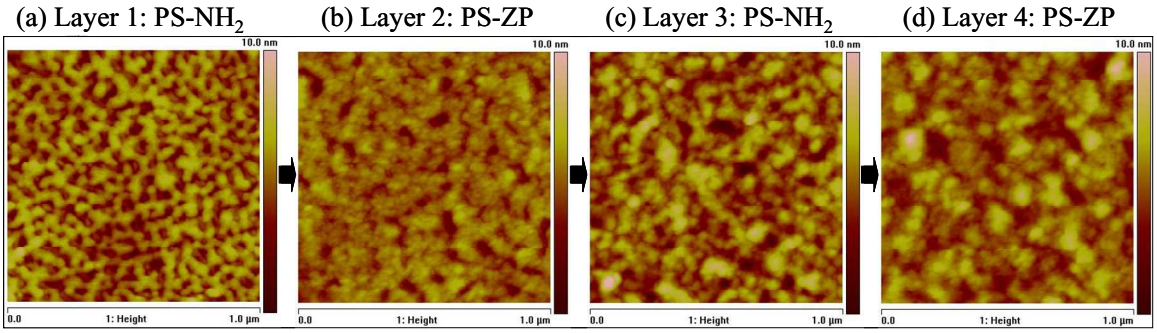

Figure 45. Effect of textured first layer on layer-by-layer self-assembly in THF.

Table 6. Summary of the RMS roughness values of polymer surface after every layer deposition in THF up to four layers as shown in Figure 45.

Layer No.	Material	Conditions	RMS Roughness
1	PS-NH_2	Deposition and wash in THF	1.2 nm
2	PS-ZP	Deposition and wash in THF	0.8 nm
3	PS-NH_2	Deposition and wash in THF	1.2 nm
4	PS-ZP	Deposition and wash in THF	1.1 nm

Since the PS-NH_2/PS-ZP multilayers were also examined using both surface plasmon resonance (SPR) and quartz crystal microbalance (QCM), AFM analysis was also carried out on the multilayer films formed on SPR and QCM substrates (substrates more suited to the analytical tool compared to silicon wafer) to assess film coverage and morphology. The surface of the substrate used in SPR and QCM characterization was sputtered silicon dioxide, SiO_2 as opposed to the native oxide layer on the silicon wafer. Typical surface preparation of an SF11 substrate used in the SPR instrument included thermally evaporated Cr (3 nm) and Au (50 nm) finally 4 nm of sputtered SiO_2. Figure 46(a) shows an RMS roughness of the SiO_2 surface of approximately 0.9 nm. Visual

inspection of the AFM images showed that the SiO_2 surface sputtered onto gold was rougher than the surface of a silicon wafer. A 10-layer film composed of alternating PS-NH_2 and PS-ZP deposited from THF/THF with initial PS-NH_2 film deposited using CH_2Cl_2/THF was formed on the SPR substrate. AFM micrographs in Figure 46(b), show continuous coverage of polymer layer at the tenth layer (PS-ZP) on the sputtered SiO_2 surface. It can be seen in the 1-μm images that the film actually becomes smoother at the tenth layer (b) compared to the grainy surface of the sputtered substrate shown in (a).

The typical surface of a 5 MHz QCM substrate purchased pre-deposited with SiO_2 as shown in Figure 47(a) has an RMS roughness of approximately 1.6 nm and is visually rougher than the surface of a silicon wafer. A 12-layer film composed of PS-NH_2 and PS-ZP deposited from THF/THF with initial PS-NH_2 layer deposited from CH_2Cl_2/THF was formed on the QCM substrate. Atomic force micrographs of the 12^{th} layer (PS-ZP), shown in Figure 47(b), show complete polymer coverage.

AFM results of the multilayer polymer films on substrates for SPR (SF11) and QCM confirm the feasibility of the self-assembly process through coordination chemistry in generating a continuous film surface on the multilayer of alternating functionalized star polymers.

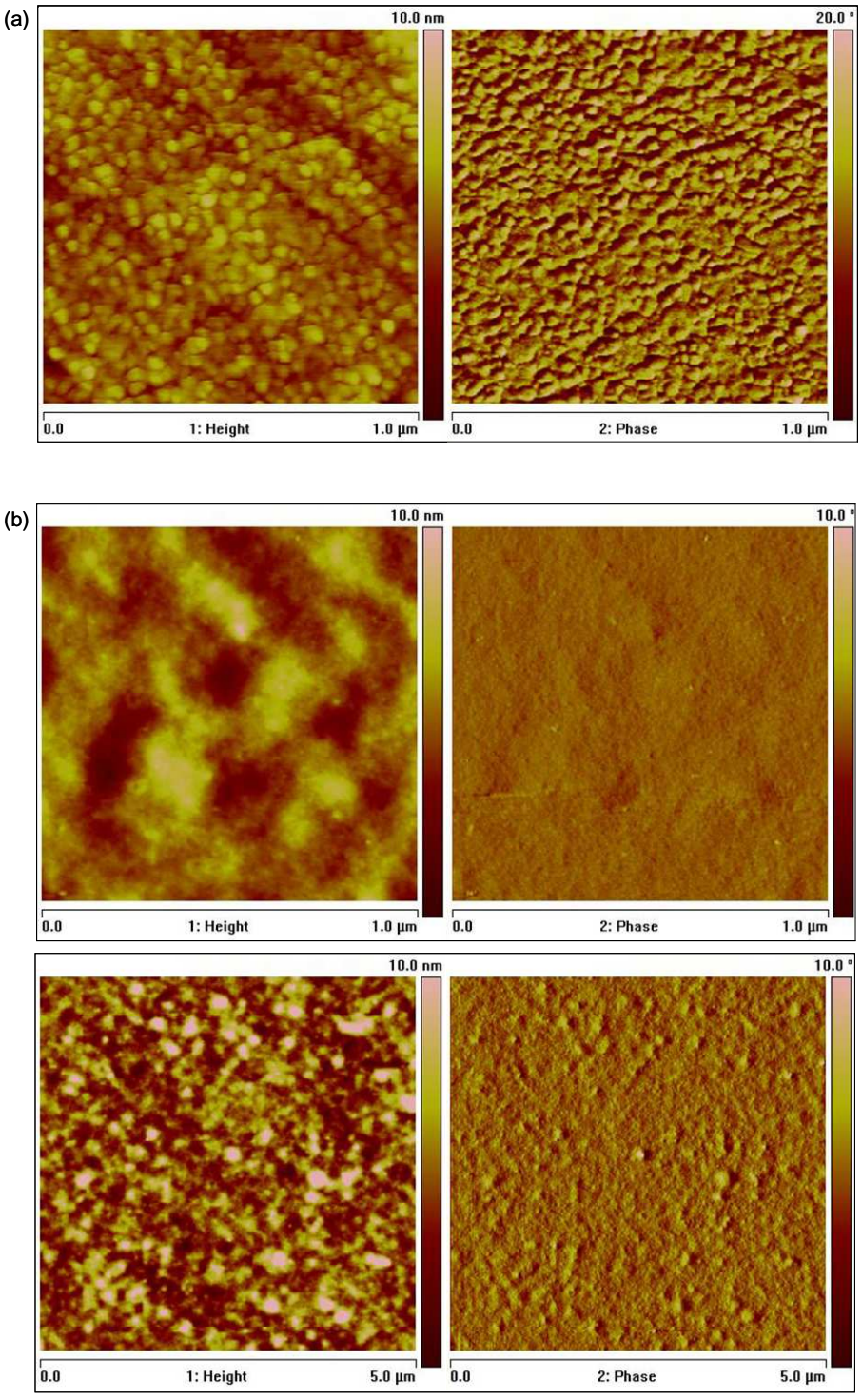

Figure 46. AFM height (left) and phase (right) images of (a) SiO_2 surface sputtered onto a gold covered SF11 wafer at 1 µm x 1 µm (RMS ≈ 0.9 nm), (b) tenth-layer (PS-ZP) on SF11 at 1 µm x 1 µm (RMS ≈ 1.2 (top)) and at 5 µm x 5 µm (RMS ≈ 2.1 nm (bottom)).

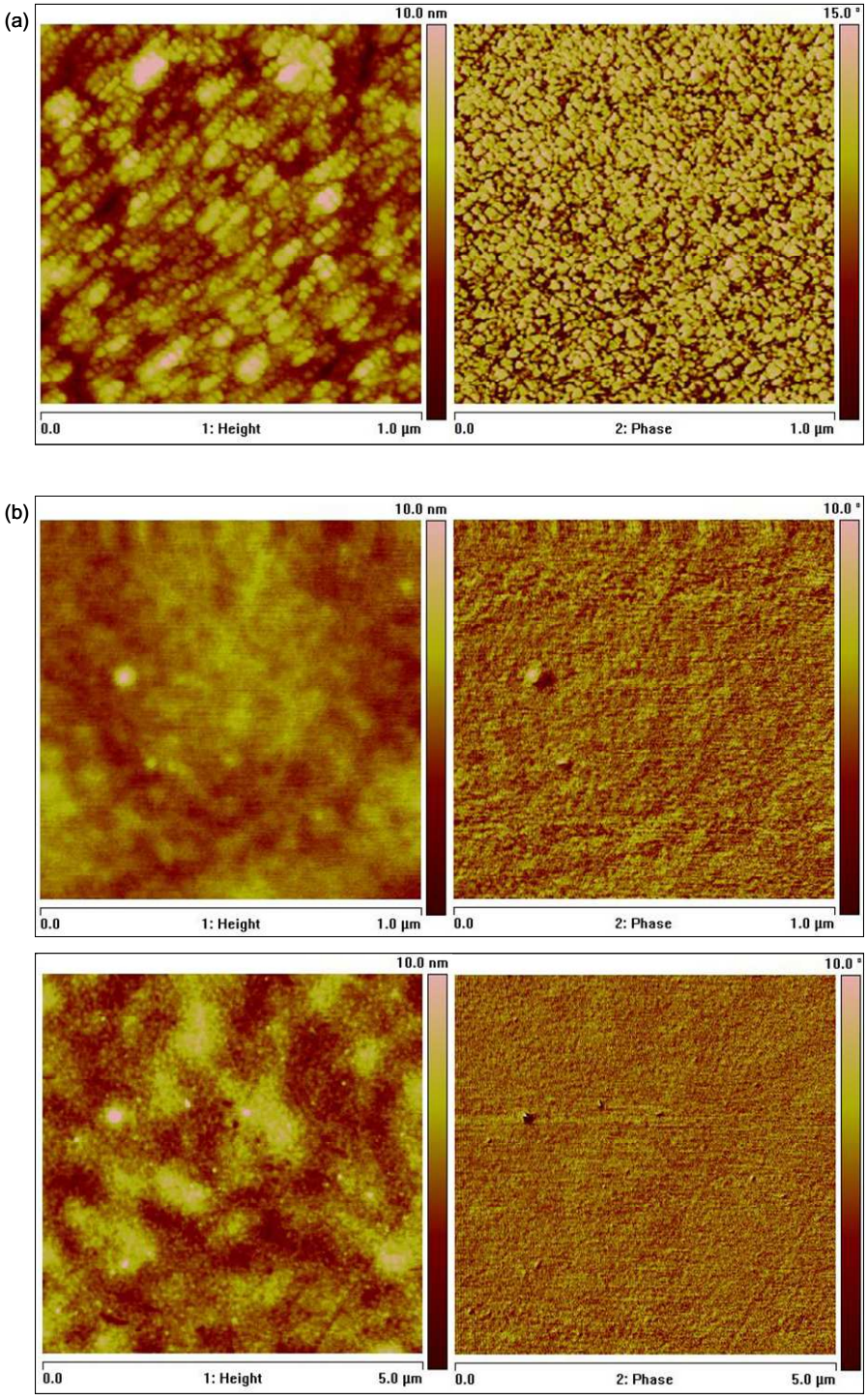

Figure 47. AFM height (left) and phase (right) images of (a) SiO_2 surface on a 5 MHz QCM substrate at 1 µm x 1 µm (RMS ≈ 1.6 nm), (b) twelfth-layer (PS-ZP) on QCM substrate at 1 µm x 1 µm (RMS ≈ 0.8 nm (top)) and at 5 µm x 5 µm (RMS ≈ 1.3 nm (bottom)).

5.1.4 Summary of AFM Analyses

Several parameters, *i.e.*, film preparation, stability, and quality, have been successfully monitored by AFM. It can be concluded from the AFM analyses that the flow system produces films of superior quality compared to a film produced through the dipping method. It can also be concluded that the dual solvent system (dichloromethane deposition with THF wash) is preferred for the deposition of the amino-functionalized star polymer (PS-NH_2) on silicon dioxide surfaces to obtain a complete and stable base layer. The best film quality is obtained when a final short THF wash (3 minutes) is introduced after dichloromethane deposition of PS-NH_2. Subsequent layers can be successfully deposited using THF alone. The self-assembled polymer layers are stable over a period of at least two weeks and are shown to have continuous surface coverage for up to ten layers.

The effect of solvents and star polymer type for the deposition of the first polymer layer on silicon dioxide surface was also elucidated through the AFM data presented in this section. PS-ZP is unsuitable for use as the initial polymer layer for subsequent LBL self-assembly of alternating star polymers due to the incomplete and non-contiguous nature of the PS-ZP film formed on the silicon dioxide surface. The solvent used in the deposition of the initial PS-NH_2 layer on silicon dioxide surfaces is found to strongly influence the morphology and coverage of film generated due to the effect of the solvent on the substrate-film interactions involved in forming the base polymer layer.

5.2 Surface Plasmon Resonance (SPR) Spectroscopy

After the solvent conditions had been established for a complete and stable self-assembled film formation (Section 5.1), surface plasmon resonance (SPR) experiments were conducted to study the LBL thin film deposition of alternating functionalized star polymers. The substrate used was alkaline silicate glass, SF11, on which was deposited a gold sensing layer (with an underlying chromium adhesion layer) and an overlying protective cap of sputtered SiO_2. The substrates were cleaned with UV Ozone followed by a wash with Millipore water prior to use as discussed in the Materials and Methods chapter. The profiles collected using the kinetic mode (intensity vs. time scan) of the SPR instrument can provide information on the time required for layer formation and can be used to evaluate the stability of the polymeric thin layer while the angular scan mode can provide information on the shifts in resonance angle after the formation of a complete layer. The results from SPR experiments will be discussed in three sections: (i) polymer self-assembly on substrate, (ii) polymer self-assembly on complementary polymer, and (iii) LBL polymer self-assembly.

5.2.1 Self-Assembly of Functionalized Star Polymer on Silicon Dioxide Substrate

SPR studies on the deposition of the first PS-NH_2 polymer layer on silicon dioxide (SiO_2) surface were conducted (i) to obtain information on the time required for layer formation on a silanol surface from the kinetic profile, (ii) to determine the SPR angular shift from baseline after the formation of a complete layer, and (iii) to assess film stability of the polymeric thin layer.

SPR experiments were carried out using CH_2Cl_2/THF solvent system for the deposition of PS-NH_2 on a sputtered SiO_2 surface. The SPR angular response of the THF baseline was obtained prior to dichloromethane injection into the SPR flow cell. Dichloromethane injection is vital to ensure that the solvent environment in the flow cell and the substrate surface is suitable for PS-NH_2 deposition which is in dichloromethane. The kinetic profile for PS-NH_2 deposition was collected using dichloromethane as the baseline. The refractive indices for THF and dichloromethane are different and the rate of layer formation cannot be effectively observed if THF is used as the baseline in the kinetic mode of the SPR instrument. A dichloromethane wash was then introduced followed by a quick THF wash. An angular scan of the first PS-NH_2 layer on SiO_2 surface in THF was collected. The angular response for the THF baseline and PS-NH_2 deposition (in dichloromethane) after THF wash in Figure 48 shows a change in the resonance angle denoting that there was PS-NH_2 polymer adsorption on the SiO_2 surface. The resonance angle was obtained from the experimental SPR data using a fitting function proposed by Kurihara *et al.* [37] that mimics the distinctive shape of the SPR signal, which is generally steeper on one side of the minimum compared to the other side of the signal. The 95% confidence interval (mean plus standard deviation) of the fitting process is ± 0.002°. Using this fitting function, the minimum angles for SPR data of the THF baseline scan and the SPR data of layer 1 (PS-NH_2) in THF were determined to be 55.16° ± 0.002° and 55.33° ± 0.002°, respectively as shown in Figure 49, translating into a shift of 0.17° ± 0.003° in the resonance angle.

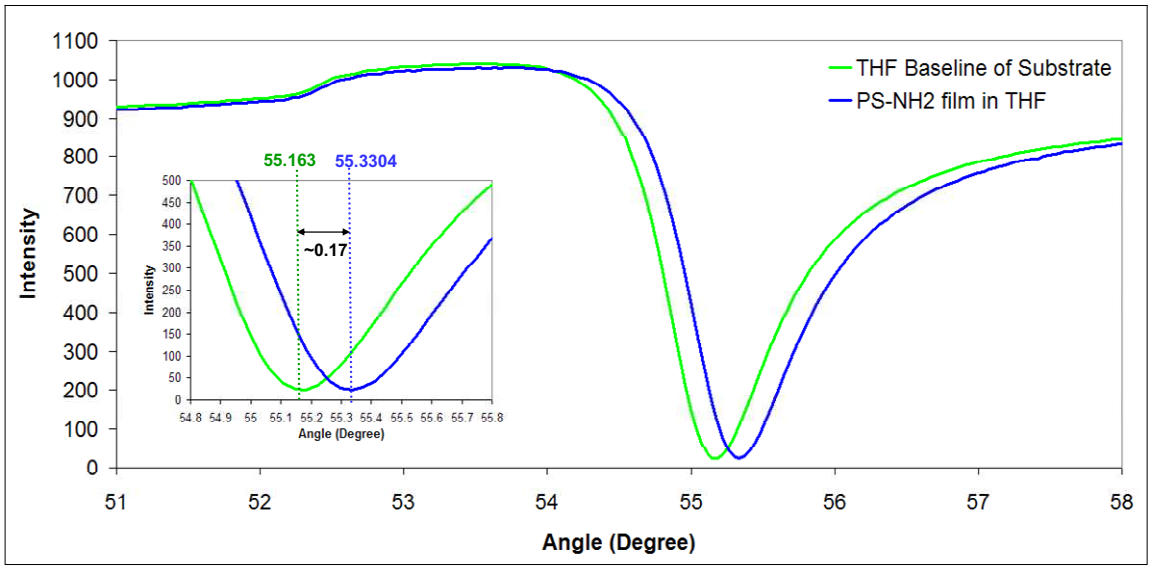

Figure 48. SPR angular response of amino-functionalized star polymers, PS-NH_2 deposited in dichloromethane with THF wash on silicon dioxide surface with reference to THF baseline.

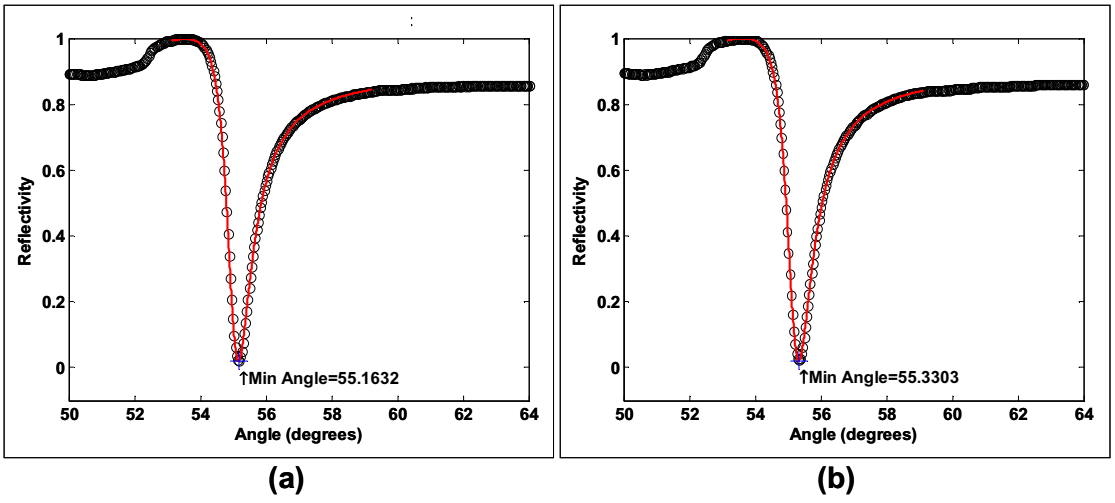

Figure 49. Minimum SPR angle obtained through experimental SPR data fitted to a function proposed by Kurihara *et al.* for (a) THF baseline on SPR substrate, and (b) PS-NH_2 layer on SPR substrate in THF.

The kinetic profile for the deposition of PS-NH_2 on a SiO_2 surface using dichloromethane, shown in Figure 50 could not be correlated to the SPR angular response in Figure 48 as discussed in the materials and methods section since the angular response and the kinetic profile were collected using different solvents as the baseline. The kinetic profile was collected by setting the SPR instrument to a reference angle chosen along the baseline SPR angular scan (*e.g.*, dichloromethane baseline in this case). At a fixed reference angle, the intensity over time signal changes due to changes in the effective refractive index in the SPR flow cell. As observed in Figure 50, the signal changed as the PS-NH_2 polymer was being deposited onto the SiO_2 surface in dichloromethane and changed again after a dichloromethane wash as non-adsorbing polymer molecules were washed away. The red dotted line in the kinetic profile in Figure 50 illustrates the expected profile if the PS-NH_2 polymers were completely washed away from the surface, *i.e.*, the signal reverted back to the original dichloromethane baseline. Comparing the solvent baseline on the substrate of the pre- and post- PS-NH_2 deposition, it is evident that the amino-functionalized star polymer, PS-NH_2, forms a layer on the silicon dioxide surface.

From the kinetic profile in Figure 50, the self-assembly of the first PS-NH_2 layer on the substrate appears to achieve steady-state approximately 10 seconds after polymer injection which supports an extremely rapid PS-NH_2 layer formation as compared to 15 minutes for the formation of a single amino-polymer layer using linear polymers as observed in a study done by Yoo *et al.* [10]. During the dichloromethane washing step, the intensity did not change despite undergoing 5 minutes of dichloromethane flow. This

shows that a stable PS-NH_2 layer was formed and the PS-NH_2 molecules remained anchored onto the SiO_2 surface even though there was prolonged contact with the solvent. The initial increase in intensity can be attributed to the deposition of PS-NH_2 polymer on the SiO_2 surface. The increase in intensity after approximately 75 seconds after the signal seemed to have attained steady state is not typically seen in a kinetic profile for a PS-NH_2 layer formation and may be due to experimental error. Not shown in the kinetic profile is the THF wash after dichloromethane wash that was discovered by AFM studies to improve the stability of the film. The PS-NH_2 layer deposited using CH_2Cl_2/THF on SiO_2 surface is complete and stable as shown by the AFM experiments done in Section 5.1.1.

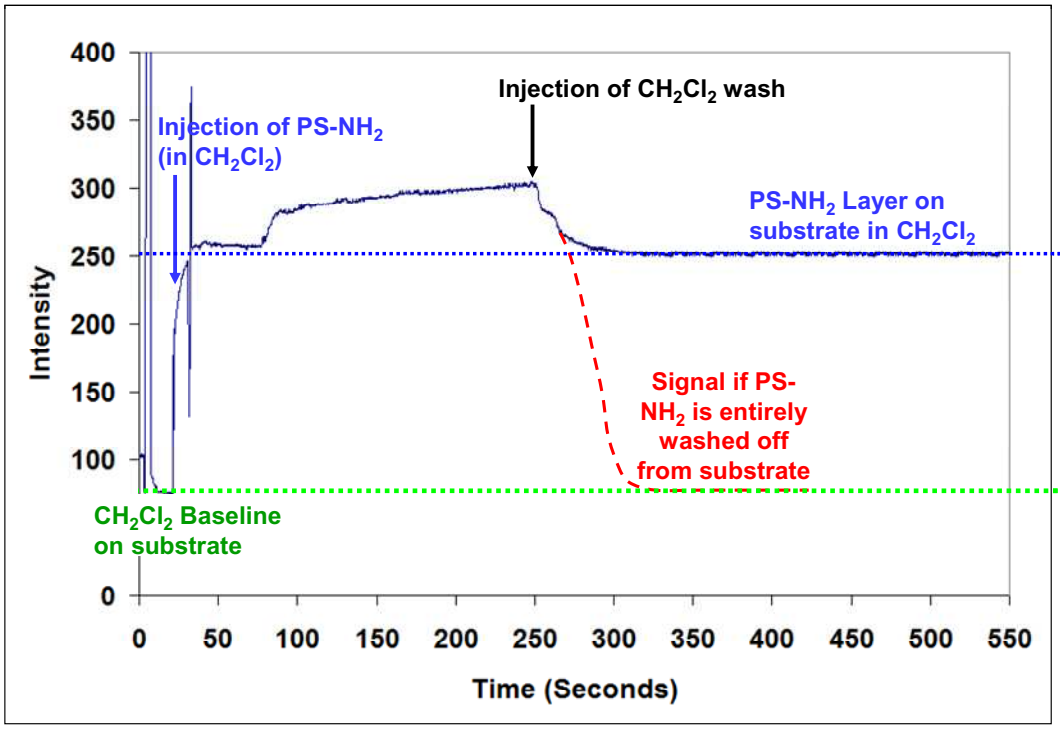

Figure 50. Kinetic profile of amino-functionalized star polymer, PS-NH_2 deposited in dichloromethane with dichloromethane wash on silicon dioxide surface. Not shown in the figure is the THF wash after dichloromethane wash.

The effect of solvent in the deposition of PS-NH_2 layer on SiO_2 surface was investigated using SPR. The changes in angular resonance and the kinetic profile when the initial PS-NH_2 layer was deposited in THF with THF wash (THF/THF) were collected. PS-NH_2 polymer molecules were deposited on the SiO_2 surface as substantiated by the change in SPR angle and the baseline change in the kinetic profile in Figure 51. The change in SPR angle was approximately 0.13° ± 0.003° and this was less than the shift seen when PS-NH_2 was deposited on the substrate using the CH_2Cl_2/THF solvent system (0.17° ± 0.003°). Since the resonance angle is a function of film thickness and refractive index, a smaller resonance angle shift may suggest that either the thickness or the effective refractive index of the PS-NH_2 film prepared using CH_2Cl_2/THF is less than when THF/THF was used. This could be due to one or more of the following reasons: (i) the PS-NH_2 molecules arranged themselves differently on the substrate in THF compared to dichloromethane (causing the polymer to solvent ratio to be different), (ii) there were fewer PS-NH_2 molecules deposited onto the SiO_2 using the THF/THF solvent system compared to CH_2Cl_2/THF, or (iii) there were solvent molecules trapped within the film (some CH_2Cl_2 may still be trapped within the film causing a difference in the refractive index of the PS-NH_2 film prepared through CH_2Cl_2/THF). This is in agreement with AFM results (Section 5.1.1) which showed that although the PS-NH_2 polymer molecules were successfully adsorbed onto the SiO_2 surface, the resultant layer is textured and rough (Figure 33). This might be due to hydrogen bonding between PS-NH_2 molecule and silanols on the surface in anhydrous THF instead of the stronger electrostatic interaction when dichloromethane is used as the solvent for polymer

deposition. From the kinetic profile in Figure 51(b), the system appeared to achieve steady state in seconds. This can be related to rapid PS-NH_2 layer formation on SiO_2 surface despite the probability of a weaker hydrogen bonding interaction between the amino group on PS-NH_2 and the silanols on the SiO_2 surface.

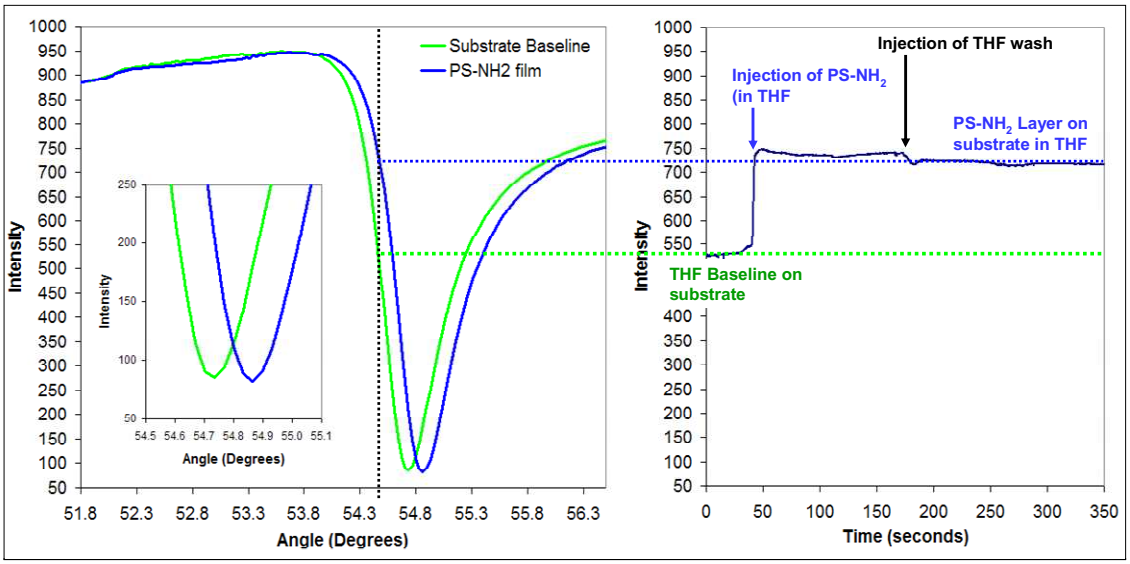

Figure 51. (a) SPR angular response and (b) kinetic profile of amino-functionalized star polymers, PS-NH_2 deposited in THF with THF wash on silicon dioxide surface.

Theoretical calculations carried out by Dr. William Risk (APPENDIX A) in conjunction with this experimental work revealed some preliminary insights on the polymeric film thickness generated by the deposition of PS-NH_2 polymer on SiO_2 surface. The assumptions used in the calculation were that the PS-NH_2 self assembles into a monolayer of hexagonally packed hard polystyrene (PS) spheres with the polystyrene occupying 60.5% of the volume of the monolayer while the interpenetration of THF occupies 39.5% of the volume of the monolayer as shown in Figure 52.

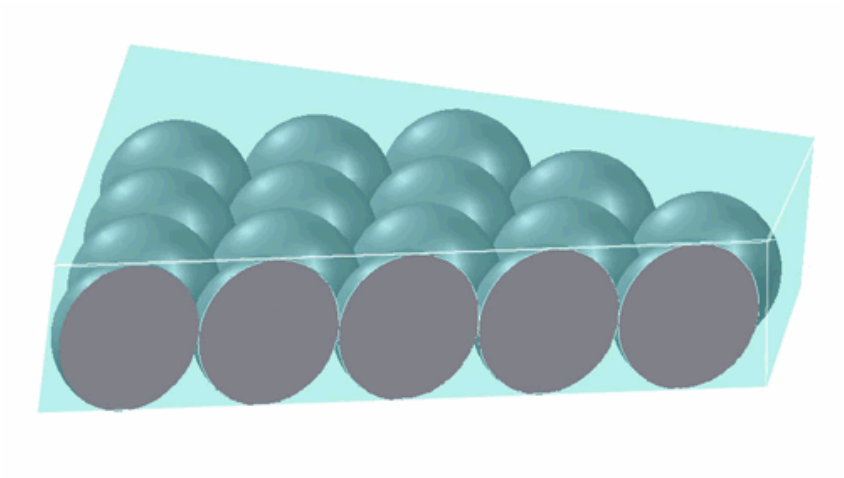

Figure 52. Monolayer of hexogonally-packed hard polystyrene spheres with interpenetrating THF [81] (reprinted with permission from William P. Risk).

The surface plasmon resonance angle, θ is dependent on the effective refractive index (n) and film thickness (t), *i.e.*, $\theta = f(nt)$. The effective refractive index of the solvated layer was calculated using Maxwell-Garnet theory [84] and the computed layer thickness with respect to the SPR resonance angle shifts is shown in Table 7 and Figure 53.

Table 7. Change in SPR resonance angle and the corresponding star polymer layer thickness.

Change in SPR Resonance Angle	Calculated Layer Thickness
0.1°	3 nm
0.2°	6 nm
0.3°	9 nm

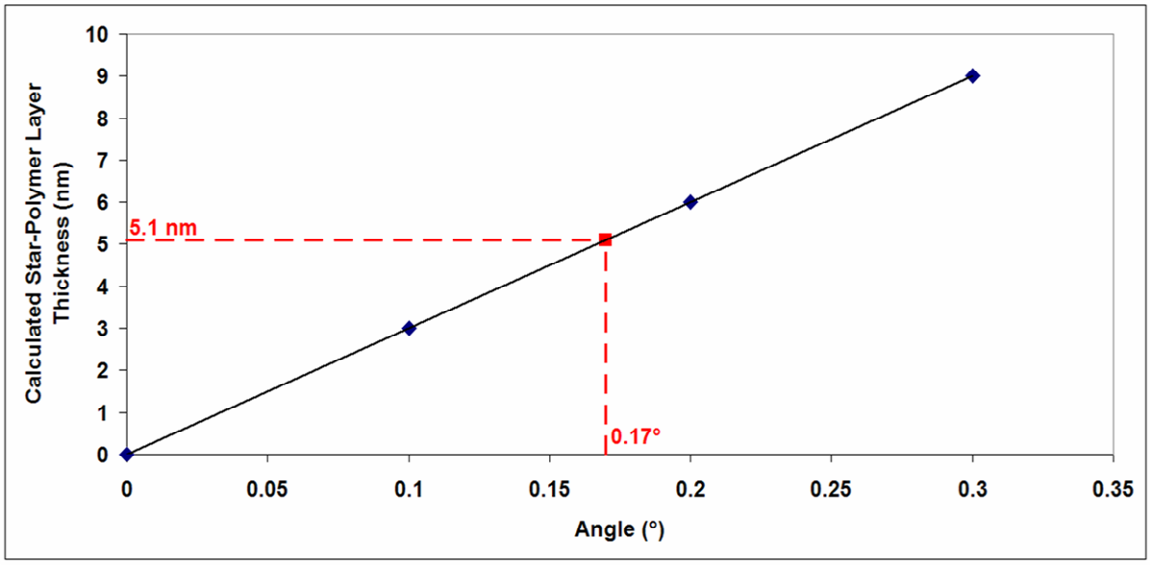

Figure 53. SPR angular shift with respect to star polymer layer thickness.

The resonance angle shift of 0.17 nm for the PS-NH_2 layer (in CH_2Cl_2/THF solvent system) on SiO_2 surface corresponds to a thickness of approximately 5.1 nm as shown in Figure 53. This thickness compared to the hydrodynamic diameter of the star polymer molecule which is approximately 9 nm [78] may indicate that the star polymer molecules are soft and do not preserve their shapes when anchored onto the SiO_2 surface or it may signify a higher degree of solvent interpenetration, *e.g.*, more than 39.5% of the volume is solvent. As illustrated in Figure 54, the star polymers may be compressed to a certain degree when adsorbed on the surface of the substrate, similarly to what was observed with the dendrimers as reported by Tsukruk *et al.* [17]. While the assumption of star polymers being hard spheres in the model may no longer be valid, the volume of polymer to solvent used in the model generates a realistic value for a monolayer thickness of a star polymer film on SiO_2 surface. The model will require further refinement to account for the flexibility of the star polymer structure.

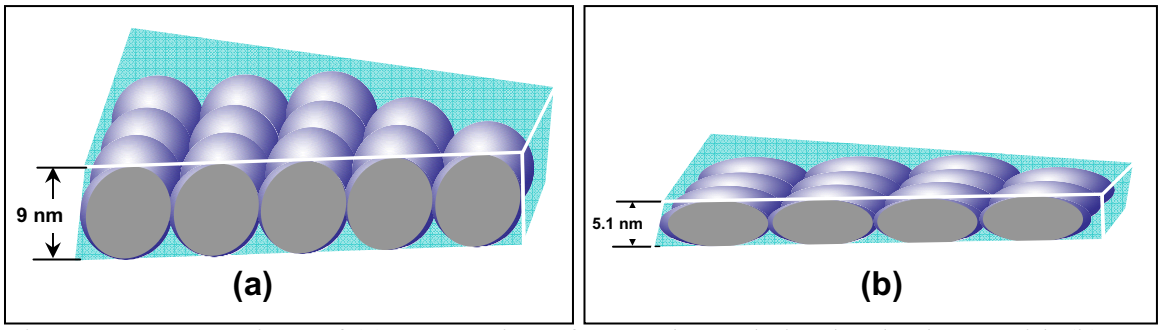

Figure 54. Comparison of (a) assumption of star polymer being hard spheres with (b) probable 57% compression of star polymer on SiO_2 surface.

The interaction of PS-ZP with the SiO_2 surface was then investigated using SPR. AFM analysis of the PS-ZP deposition on silicon wafer showed a patchy and incomplete PS-ZP layer formation (Figure 34) probably due to non-specific weak Van der Waals interaction. This observation was confirmed by SPR studies of the deposition of PS-ZP on the sputtered SiO_2 surface (SPR substrate) using THF/THF. The SPR resonance angles observed in Figure 55(a) for this process were 55.15° ± 0.002° (baseline) and 55.19° ± 0.002° (PS-ZP layer), resulting in a change of 0.04° ± 0.003° when the zinc-porphyrin-functionalized star polymer was deposited in THF as the first layer (after the rinsing step with THF) implying that there was a small amount of polymer adsorption onto the SiO_2 surface. The corresponding kinetic profile of the deposition of the zinc-porphyrin-functionalized star polymer, PS-ZP on a sputtered SiO_2 surface is shown in Figure 55(b). The kinetic profile was collected at a reference angle of 55.1° as shown by the vertical dotted black line in the figure. The change in intensity after THF wash, post PS-ZP deposition, is reflected by the corresponding SPR signal as represented by the horizontal red dotted line. The kinetic profile shows that although some PS-ZP polymer was deposited, most of the polymer was washed off during the solvent rinsing step as

there was a difference in intensities between the THF baseline recorded on silicon dioxide surface compared to the THF baseline recorded after PS-ZP deposition and THF solvent wash.

A complete layer as in the case of the PS-NH_2 deposited in CH_2Cl_2/THF solvent system showed a 0.17° ± 0.003° change in the resonance angle. Hence, the change of 0.04° ± 0.003° in resonance angle was relatively small compared to 0.17° ± 0.003°. This is consistent with the formation of either a thin uniform polymer layer (unlikely) or, as seen in the AFM image for PS-ZP layer on silicon dioxide surface, an incomplete and patchy polymer layer. This observation together with the AFM analysis done in Section 5.1.1 confirmed that the material deposited on the SiO_2 surface was a patchy layer of PS-ZP polymer.

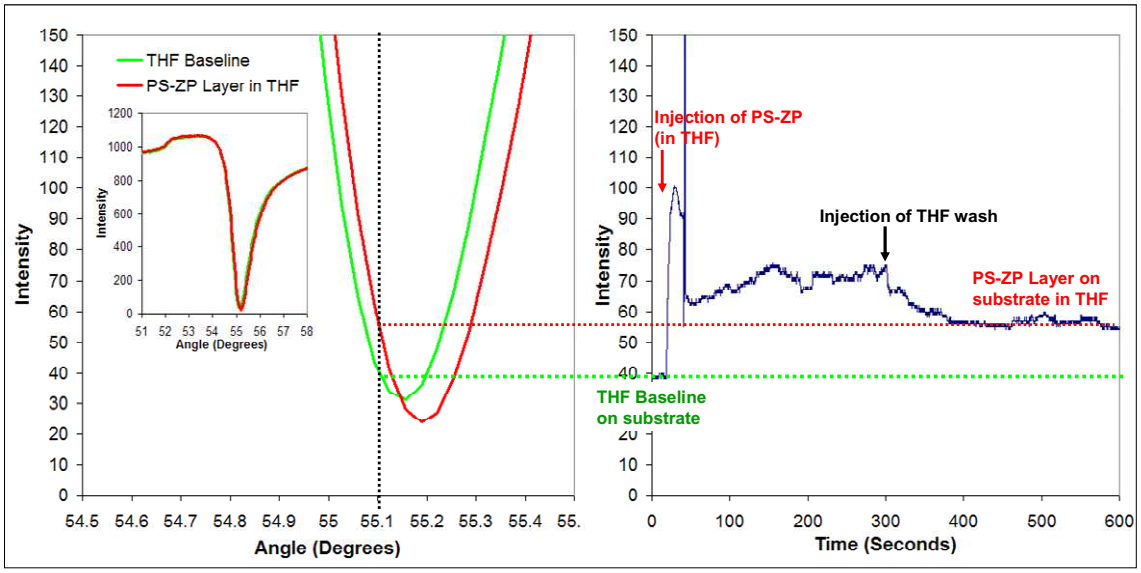

Figure 55. (a) SPR angular response and (b) kinetic profile, of zinc-porphyrin-functionalized star polymers, PS-ZP deposition on silicon dioxide surface.

SPR analysis of the deposition of the initial star polymer layer on SiO_2 surface correlated with the results of the AFM analysis described in Section 5.1.1. The small increase of 0.04° ± 0.003° when PS-ZP was deposited onto the substrate was consistent with the presence of a patchy and incomplete layer that was seen in the AFM images. In contrast, the formation of the PS-NH_2 layer was found to be rapid and stable as seen in the kinetic profiles of the polymer deposition in both dichloromethane and THF.

5.2.2 Self-Assembly of Functionalized Star Polymer on Star Polymer Layer

SPR experiments were conducted to investigate the deposition of a second layer of PS-ZP from THF onto the initial PS-NH_2 layer (deposited from CH_2Cl_2/THF). The deposition of the second PS-ZP layer was done using the THF/THF solvent system since it was concluded from AFM studies that THF does not compromise the quality of layers produced by coordination chemistry and can be used as the solvent for polymer deposition from the second layer onwards. The resonance angle of the PS-NH_2 layer shown in Figure 56(a) is 54.84° ± 0.002° while the resonance angle after the deposition of the PS-ZP layer is 54.91° ± 0.002°, resulting in an angular shift of approximately 0.07° ± 0.003°. This angular shift after the deposition of the PS-ZP layer was smaller compared to the base PS-NH_2 layer (0.17° ± 0.003°). Since the resonance angle is a function of the effective refractive index and film thickness, the smaller angular shift might be the result of (i) a patchy PS-ZP layer due to incomplete layer formation which was unlikely since AFM showed complete coverage of the second PS-ZP layer on the initial PS-NH_2 layer, (ii) a thinner PS-ZP layer than the initial PS-NH_2 layer due to a different degree of packing and solvation within the layer, or perhaps the PS-ZP

molecules might have arranged themselves differently on the PS-NH_2 film compared to the arrangement of PS-NH_2 molecule on a rigid SiO_2 surface, or (iii) the PS-ZP layer having a different effective refractive index due to varying amounts of solvent trapped within the film. Further experiments using a different characterization method such as QCM will provide more information on reasons behind the difference. From the kinetic profile in Figure 56(b), the self-assembly of the PS-ZP layer on the PS-NH_2 layer appears to achieve steady-state approximately 40 seconds after polymer injection which supports a rapid PS-ZP layer formation.

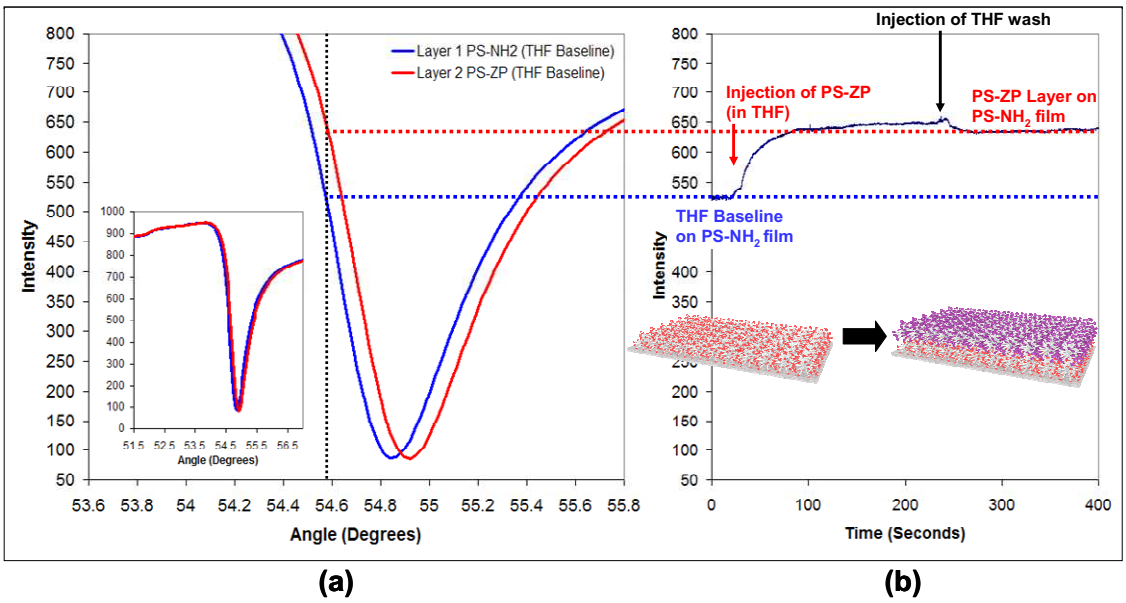

Figure 56. (a) SPR angular response, and (b) kinetic profile of zinc-porphyrin-functionalized star polymer, PS-ZP deposited in THF on a PS-NH_2 film.

Only the initial PS-NH_2 layer (Layer 1) requires the dual solvent system, CH_2Cl_2/THF, while subsequent PS-NH_2 layers are deposited using THF deposition and THF wash, THF/THF. The formation of the 3rd polymeric layer (PS-NH_2) on the 2nd layer (PS-ZP) is shown in Figure 57. The shift in the SPR minimum angle, Figure 57(a)

and the change in baseline signal in the kinetic profile, Figure 57(b) show that the amino-functionalized star polymers were being anchored onto their complementary polymer layer. The self-assembly of the PS-NH_2 layer on the PS-ZP layer achieved steady-state approximately 10 seconds after polymer injection which implied an extremely rapid PS-NH_2 layer formation, similarly to the rapid PS-NH_2 layer formation on the SiO_2 surface Figure 50. The angular difference between the resonance angle of the PS-ZP layer (2^{nd} layer) and the PS-NH_2 layer (3^{rd} layer) was approximately $0.08° \pm 0.003°$. This angular difference was smaller when compared to the first PS-NH_2 layer on SiO_2 surface which might suggest that the PS-NH_2 molecule self-assembled in a different arrangement on the PS-ZP film compared to the self-assembly of PS-NH_2 on a rigid SiO_2 surface. Alternatively, it may be due to different strength of interactions (*i.e.*, electrostatic for the first PS-NH_2 layer on SiO_2 substrate versus coordination chemistry for the 3^{rd} layer, PS-NH_2 on PS-ZP layer). Further discussion of the surface plasmon resonance angle after each layer deposition will appear in Section 5.2.3.

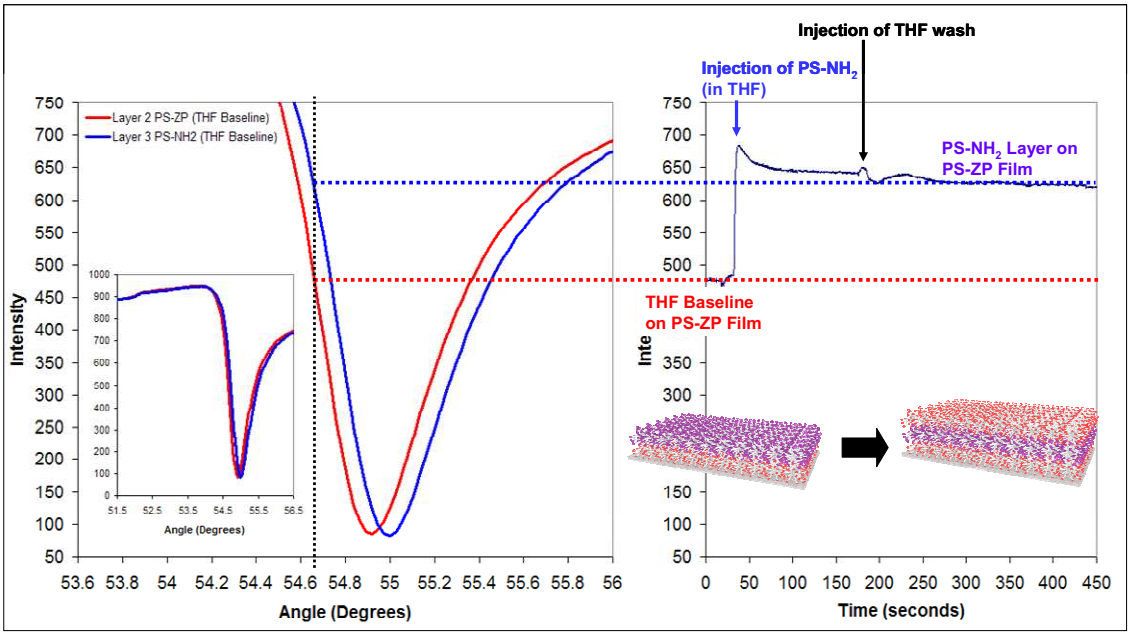

Figure 57. (a) SPR angular response, and (b) kinetic profile of PS-NH_2 deposited in THF on a PS-ZP film.

Since the first PS-NH_2 layer was deposited from CH_2Cl_2/THF solvent system onto a SiO_2 surface while subsequent polymer layers were deposited from THF/THF solvent system onto complementary polymeric layers, the first PS-NH_2 layer is not suitable to be used for comparison with Layer 2 (PS-ZP). Comparisons of PS-NH_2 and PS-ZP layers should be carried out using Layer 2 onwards. The kinetic profiles for the PS-NH_2 layer (Layer 3) and PS-ZP layer (Layer 2) are distinctly different. It can be surmised from the profiles that the PS-NH_2 layer formation achieves steady-state more rapidly compared to the PS-ZP layer after polymer injection. This may indicate that the formation of the PS-NH_2 layer is more rapid compared to the PS-ZP layer. The PS-NH_2 layer (Layer 3) and PS-ZP layer (Layer 2) formed were stable as the intensity remained constant during the THF washing step.

It is postulated that the self-assembly process is self-limiting due to the built-in functionalities at the periphery of the star polymer. Each PS-NH_2 and PS-ZP layer was suggested to be a single polymer molecule thick due to the specificity of the interactions involved between the complementary star polymers. The self-limiting characteristic of the self-assembly process was tested through SPR experiments.

PS-NH_2 polymer was injected onto the 3rd layer (PS-NH_2) using the THF/THF solvent system. The SPR response and kinetic profile of the injection of PS-NH_2 on a surface that has already been coated with PS-NH_2 film are shown in Figure 58. The resonance angle remained almost unchanged within limit of resolution of the SPR instrument as shown in the SPR response in Figure 58(a) while the kinetic profile shows that the intensity returned to the baseline intensity after THF wash, indicating that the PS-NH_2 polymer did not anchor onto the PS-NH_2 film and the non-specifically bound PS-NH_2 molecules were washed off the PS-NH_2 surface.

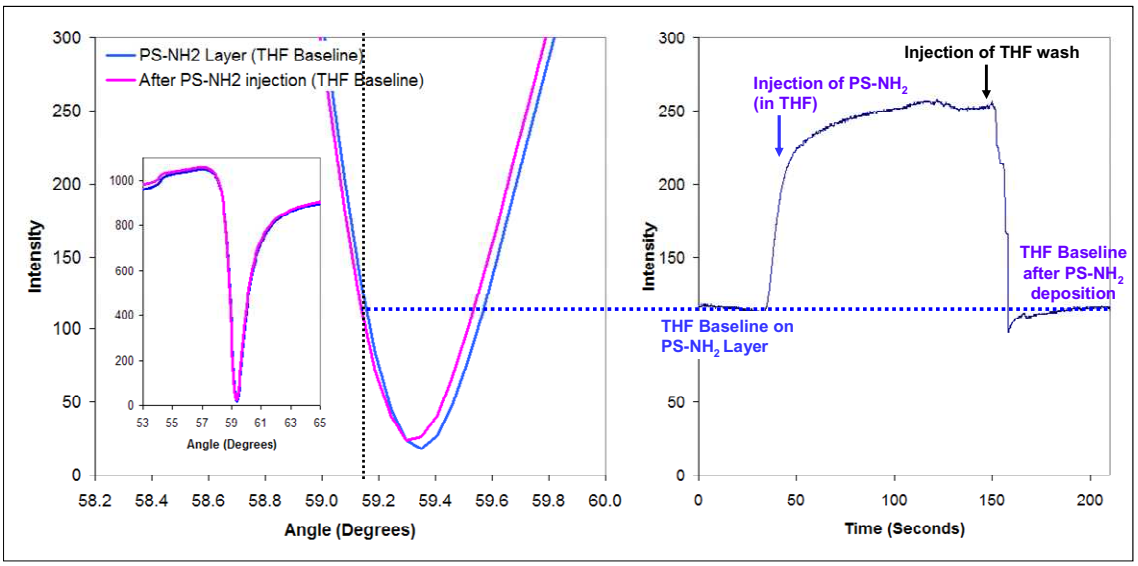

Figure 58. (a) SPR angular response and (b) kinetic profile of the injection of PS-NH_2 on a PS-NH_2 film.

Similarly, the self-limiting characteristic of the self-assembly process was tested on the 2nd Layer (PS-ZP). The SPR response and kinetic profile of the injection of PS-ZP on a PS-ZP film are shown in Figure 59. The kinetic profile of the PS-ZP injection on a PS-ZP film in Figure 59(b) suggests that there was a change in THF baseline after PS-ZP deposition which corresponded to an angular shift of approximately 0.04° ± 0.003° in the SPR signals shown in Figure 59(a). The small change in THF baseline and resonance angle compared to an angular shift of 0.07° ± 0.003° that appeared in the deposition of PS-ZP on PS-NH_2 layer may be due to the weak non-specific Van der Waals interaction of the PS-ZP molecules with the PS-ZP layer or the washing cycle with THF might not have been optimized to remove all non-specifically adsorbed polymers.

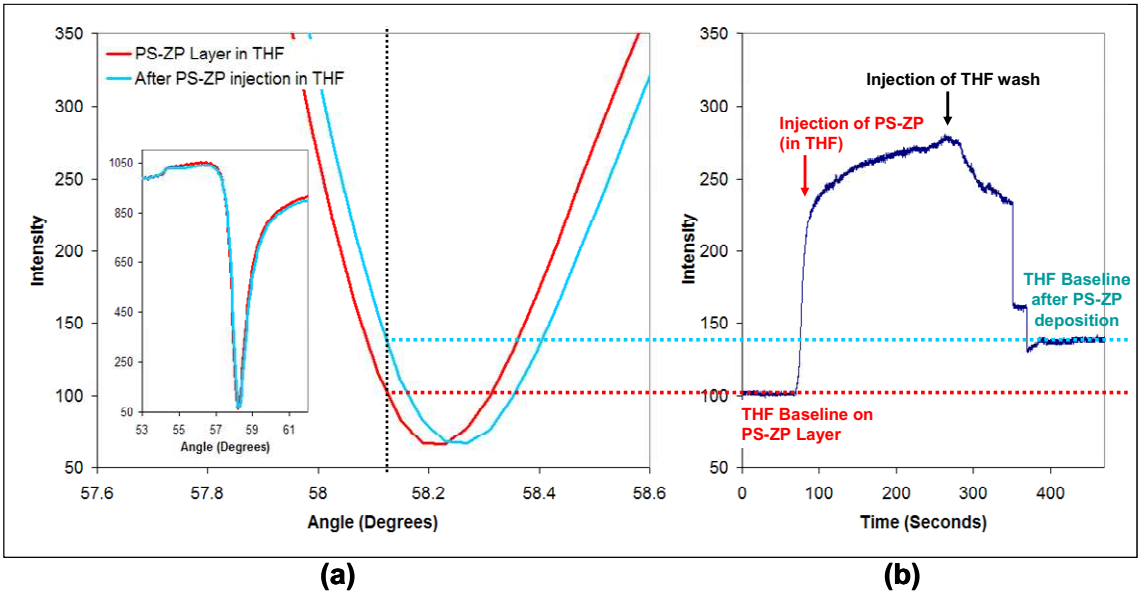

Figure 59. (a) SPR angular response and (b) kinetic profile of the injection of PS-ZP on a PS-ZP film.

The self assembly of polymer on a polymer layer is established to be feasible using THF as the solvent for deposition and wash. The kinetic profiles of the PS-NH_2 and the PS-ZP layer formation suggest that the self-assembly process is rapid and distinctively different for each polymer type. The resultant polymeric film is stable. The self-assembly process was verified to be self-limiting, although some polymer molecules may interact via weak non-specific Van der Waals interaction. The presence of non-specifically bound polymer does not impede the LBL self-assembly process, allowing the molecules to assemble as a monolayer.

5.2.3 Layer-by-Layer Self-Assembly of Alternating Functionalized Star Polymers (PS-NH_2/PS-ZP)

Using all the knowledge obtained through AFM and SPR studies, the LBL self-assembly process of alternating PS-NH_2/PS-ZP polymer layer was investigated using SPR. The LBL deposition of polymeric thin films was carried out with the initial PS-NH_2 layer deposited onto the SiO_2 surface using dichloromethane followed by a quick THF wash and subsequent alternating PS-ZP and PS-NH_2 polymer layers using THF deposition and THF wash. The SPR signal of the successive star polymer deposition shows an almost uniform bilayer change in resonance angle as depicted in the SPR angular scans in Figure 60. This bilayer results from the repeated difference in angular shifts between the PS-NH_2 layer and PS-ZP layer. The combination of a layer of PS-NH_2 and a layer of PS-ZP (PS-NH_2/PS-ZP) represents 1 bilayer. The PS-NH_2 layer shows a larger resonance angle shift compared to the PS-ZP layer within a bilayer. This could either indicate that the PS-NH_2 layers are thicker than the PS-ZP layers due to different molecular packing within the film and different degrees of film solvation, or the effective refractive index of the PS-NH_2 layers is not the same as the refractive index of the PS-ZP layers due to difference in solvent content within the solvated films.

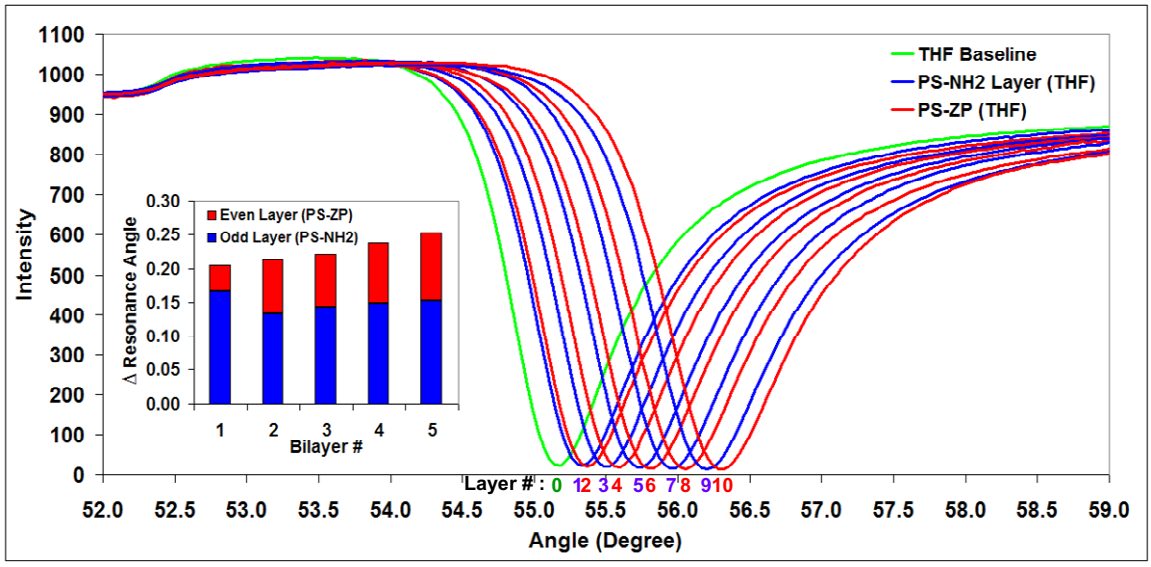

Figure 60. SPR angular scan and resonance angle change of bilayers (inset) of LBL self-assembly of star polymers on SiO_2 surface with CH_2Cl_2/THF as the solvent system for Layer 1 and THF/THF as the solvent system for subsequent layers.

The AFM results in Section 5.1 revealed that an initial PS-NH_2 layer deposited onto silicon dioxide surface in THF with THF wash produced a textured surface which visually appeared to become smoother as more layers were deposited (Figure 45), showing that the textured first layer could potentially be used as the base layer for LBL self assembly of alternating functionalized polymers. An experiment was carried out on the SPR instrument using THF/THF as the only solvent system for LBL self-assembly of the functionalized polymeric layer and the results are shown in Figure 61. For polymer layers deposited in THF, the SPR angle of the PS-NH_2 layer shows a shift of approximately 0.15° ± 0.003° while the PS-ZP layer shows a shift of approximately 0.08° ± 0.003°. Combined, the average SPR angular shift of a bilayer is approximately 0.23° ± 0.003° and is seen to be uniform as bilayers of PS-NH_2/PS-ZP are being deposited as shown in Figure 61.

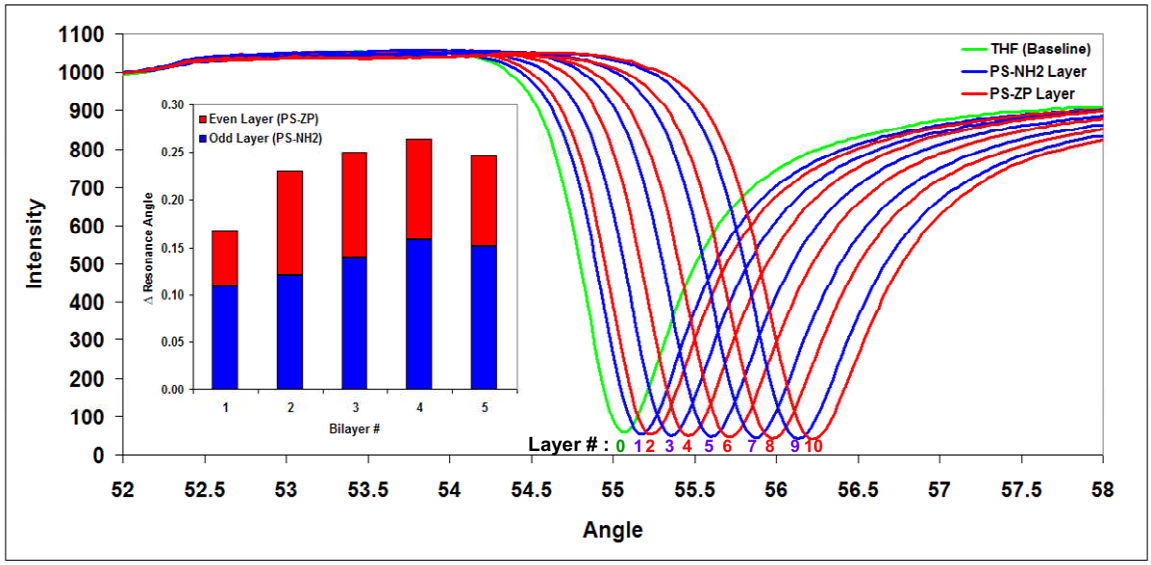

Figure 61. SPR angular scan and resonance angle change of bilayers (inset) of LBL self-assembly of star polymers on SiO_2 surface with THF/THF as the solvent system for all layers.

For ease of analysis, the SPR results for experiments using CH_2Cl_2/THF for the deposition of PS-NH_2 on SiO_2 surface with subsequent polymer layers using THF/THF (Figure 60) is denoted as Run 1 while the SPR results for experiment using THF/THF solvent system throughout the LBL self-assembly process (Figure 61) is denoted as Run 2. Comparing Run 1 to Run 2 in Figure 62, the trend seen in Run 2 is not very different from Run 1. Therefore, it can be concluded that the textured initial PS-NH_2 layer from THF/THF deposition does not impede the LBL self-assembly process. The LBL change in resonance angle for both runs fall within the experimental error of each other. The experimental error of 0.07° was determined using resonance angles measured for THF baseline collected for ten different SPR experiments (APPENDIX B). The error accounts

for the variability in the SiO_2 surface on the SF11 substrate and variability in the THF solvent quality.

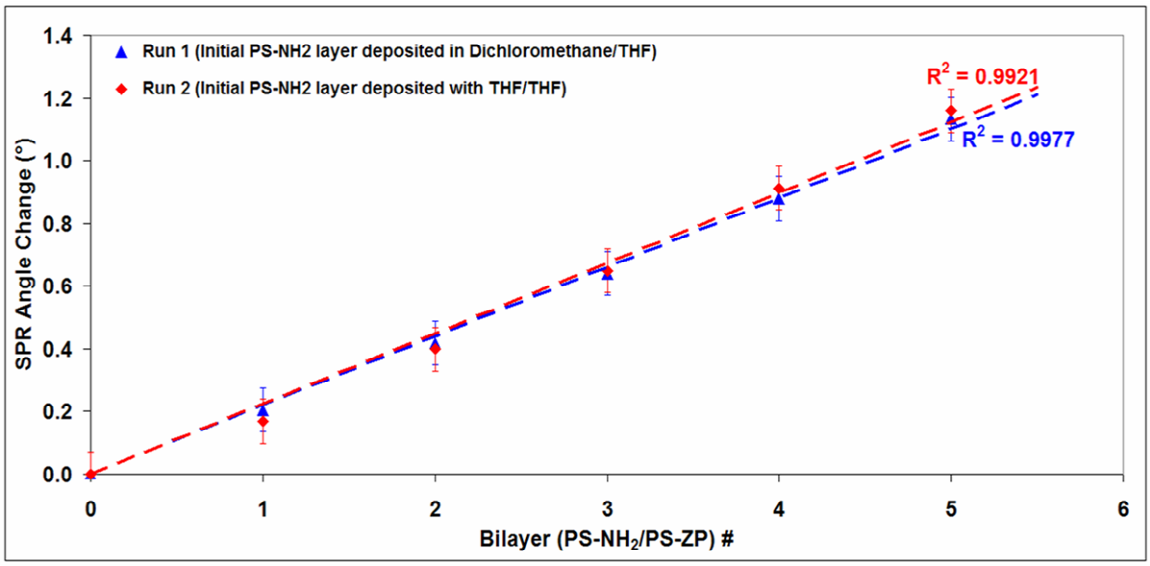

Figure 62. Comparison of SPR runs with initial layer deposited in THF/THF and CH_2Cl_2/THF.

Initial SPR experiments were conducted using toluene as the solvent for both polymer deposition and wash. SPR signals were collected for the toluene baseline and after deposition and wash of every polymer layer as shown in Figure 63. The resonance angle shows non-uniform shifts angular shifts which can be related to irregular polymeric film growth. The inset in Figure 63 shows that the change in resonance angle for a PS-NH_2/PS-ZP bilayer increases with respect to bilayer deposition, before achieving a maximum value at the 3rd bilayer (Layer 3 and Layer 4). Subsequent bilayers show a drop in angular shifts up to the ninth layer, where the self-assembly process appear to collapse. This observation leads to the conclusion that toluene is not a suitable solvent for LBL self-assembly of alternating PS-NH_2/PS-ZP star polymer layers. Irregular film growth as a result of solvent incompatibility may lead to a limited amount of functional

groups available on the surface of a polymeric film for interaction with subsequent layer and consequently impedes the self-assembly process.

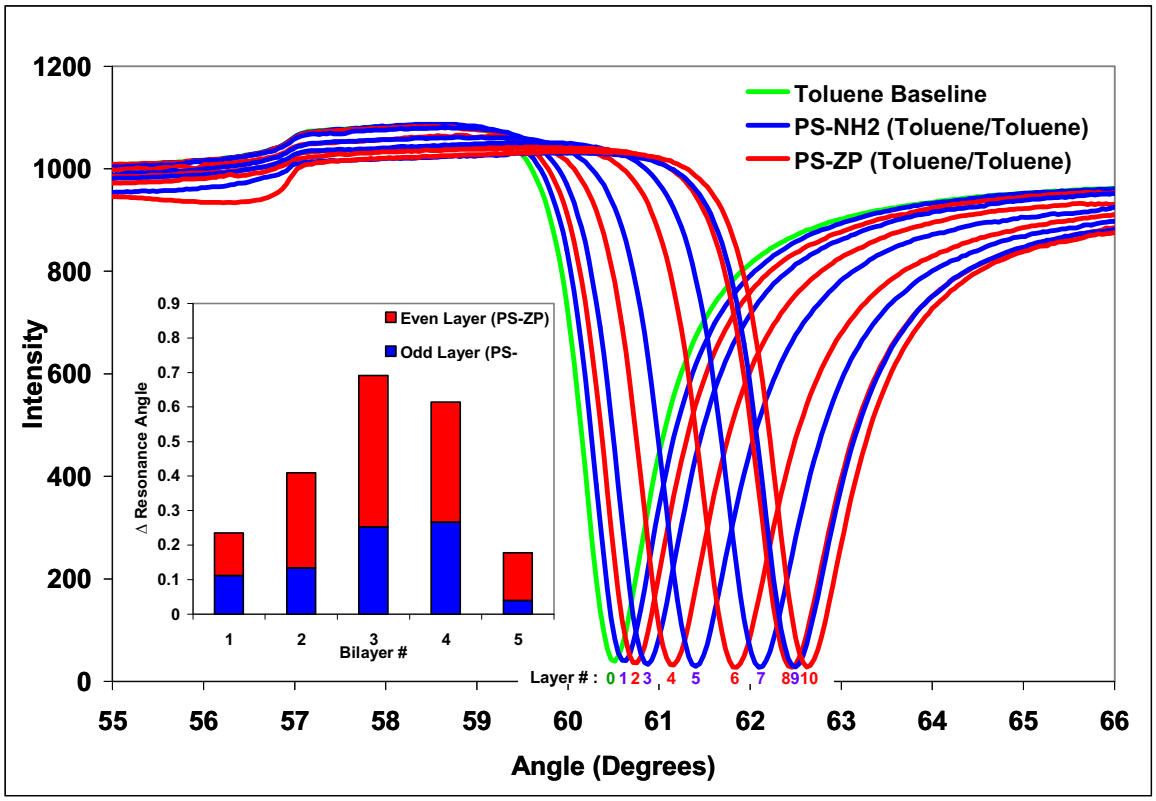

Figure 63. SPR angular scan and resonance angle change of bilayers (inset) of LBL self-assembly of star polymers on SiO_2 surface with toluene as the solvent for both polymer deposition and wash.

Similar behavior is observed when the star polymer deposition and wash step were done in chloroform as shown in Figure 64. The SPR angle change after the deposition of each polymer layer was not uniform. The resonance angle change for bilayer (PS-NH_2/PS-ZP) appeared to reach a maximum at the 4^{th} bilayer before decreasing at the 5^{th} bilayer. A comparison of SPR angle change from LBL self-assembly using toluene (Figure 63) and LBL self-assembly using chloroform (Figure 64) is shown in Figure 65. Similar irregular film growth behavior has been observed using toluene and chloroform.

Therefore, it can be concluded that both toluene and chloroform are not suitable solvents for LBL self-assembly of uniform star polymer layers.

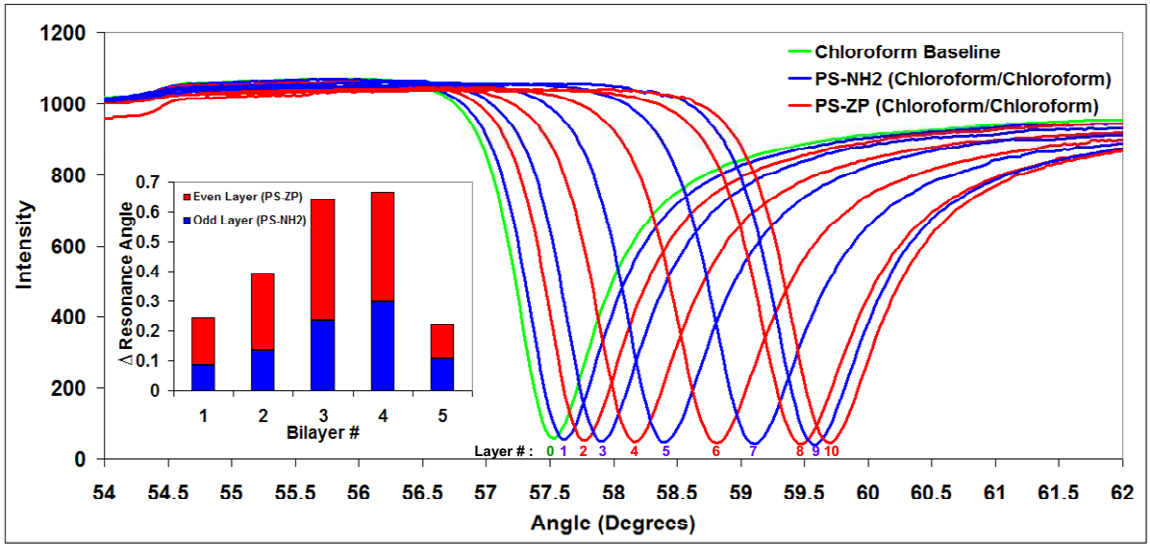

Figure 64. SPR angular scan and resonance angle change of bilayers (inset) of LBL self-assembly of star polymers on SiO_2 surface with chloroform as the solvent for both polymer deposition and wash.

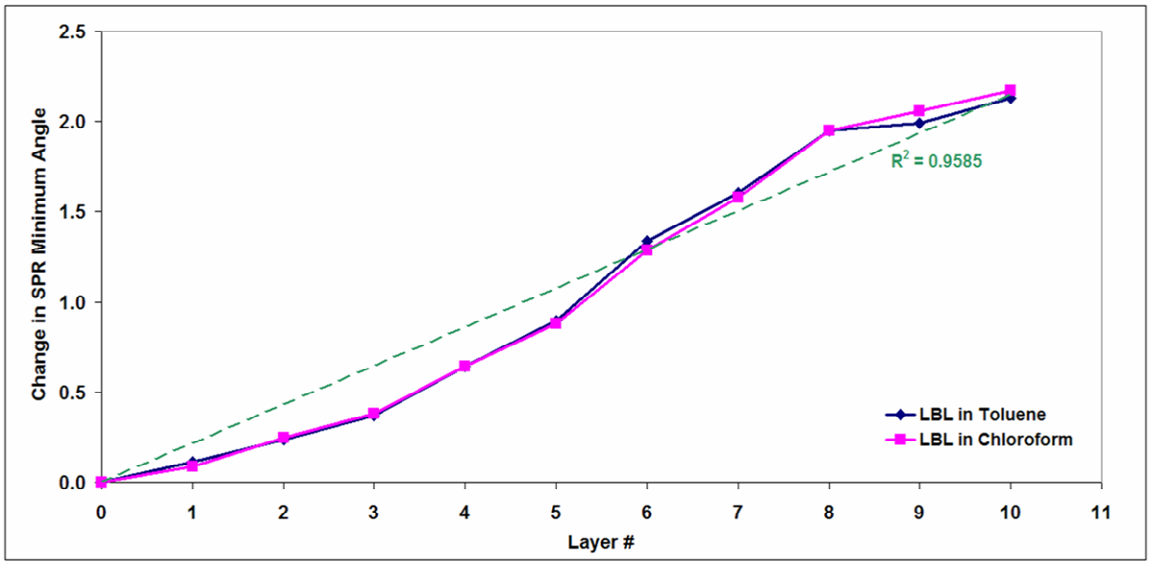

Figure 65. Comparison of SPR angle change with regards to LBL self-assembly of star polymers on SiO_2 surface with toluene and chloroform as the solvent.

Prior to using the SF-11 glass on the SPR instrument, SPR experiments were initially done using borosilicate crown glass, BK7 for the prism and the substrate. The substrate used was BK7 wafer, upon which was deposited a gold sensing layer (with an underlying chromium adhesion layer) and an overlayer protective cap of sputtered SiO_2. However due to the refractive index of the organic solvents used in the LBL process, the SPR detection of the LBL self-assembly process was carried out near the limit of the SPR instrument. Figure 66 shows the plasmon resonance response of the LBL self-assembly process done using the BK7 optical set-up with chloroform as the solvent for deposition followed by THF rinse for each polymer layer. As observed from the figure, the plasmon resonance signal for chloroform baseline (<79°) is at the limit of the angular scan. There are also signal distortions after 77° which may compromise the accuracy of the results. The SPR instrument was migrated to alkaline silicate glass (SF11) to increase the working limit of the instrument for organic solvents. The refractive index, n, of the BK7 material at 854 nm is 1.50978 while the refractive index of the SF11 at the same wavelength is 1.76196 [79]. Since the refractive index of SF11 is larger than BK7, the angle required to excite surface plasmons using the SF11 prism/wafer system is nearer to the center of the scan range as shown in Figure 67.

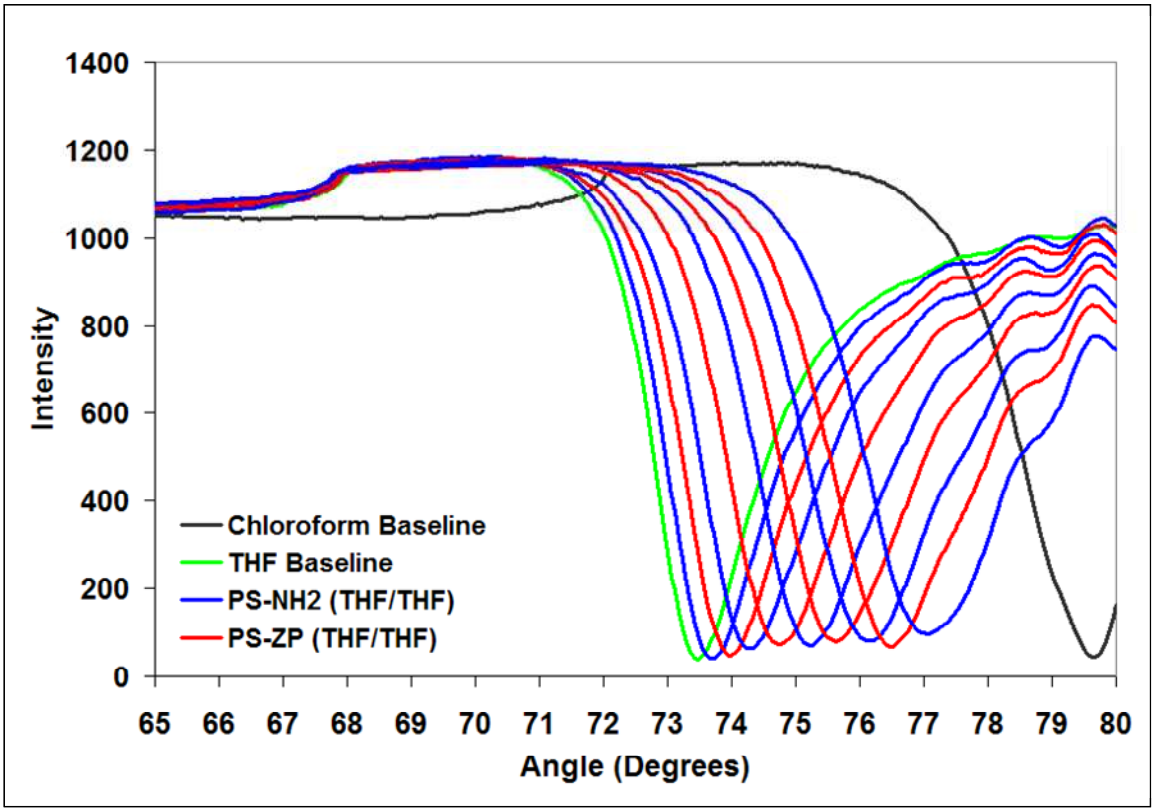

Figure 66. SPR signals of LBL self-assembly process on silicon dioxide surfaces using BK7 optical system.

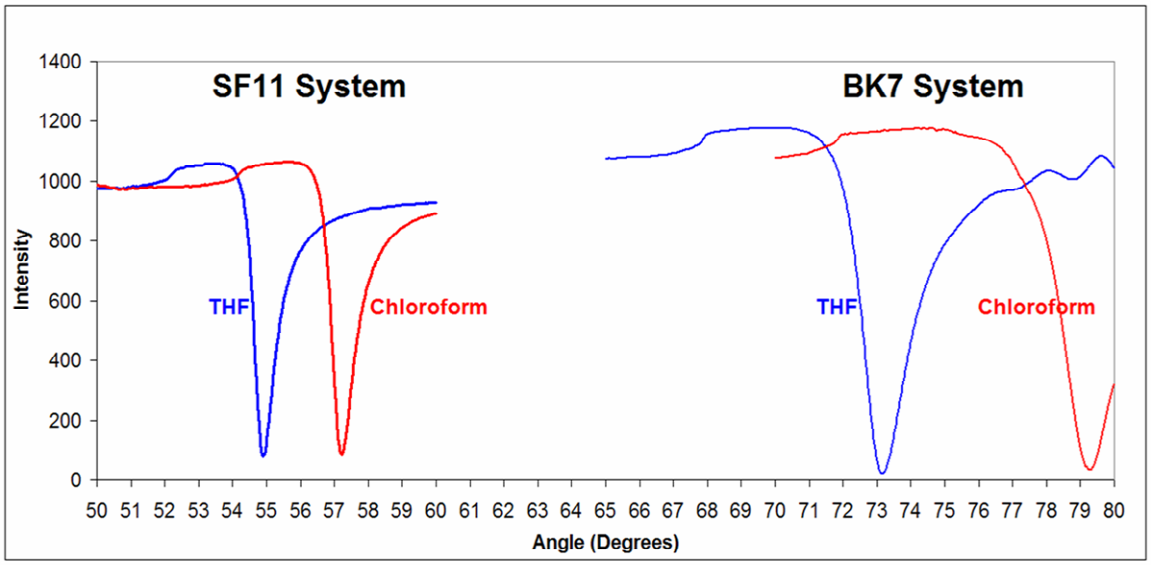

Figure 67. Comparison of SPR signals of THF and chloroform solvents using the BK7 optical set-up and the SF11 optical set-up.

SPR experiments were also carried out directly on gold to investigate the effect of surfaces on the layer-by-layer process. Unlike the electrostatic interaction involved in the anchoring of PS-NH_2 polymer on silicon dioxide surface, PS-NH_2 polymer interacts with gold through coordination chemistry. From the initial experiments shown in Figure 68, the LBL self-assembly can be carried out on gold surface. However, due to inconsistencies of the gold surface, SPR signals of the LBL process were erratic and also not repeatable. Efforts in the study of LBL self-assembly of alternating PS-NH_2/PS-ZP polymer on gold surfaces will be pursued in future work.

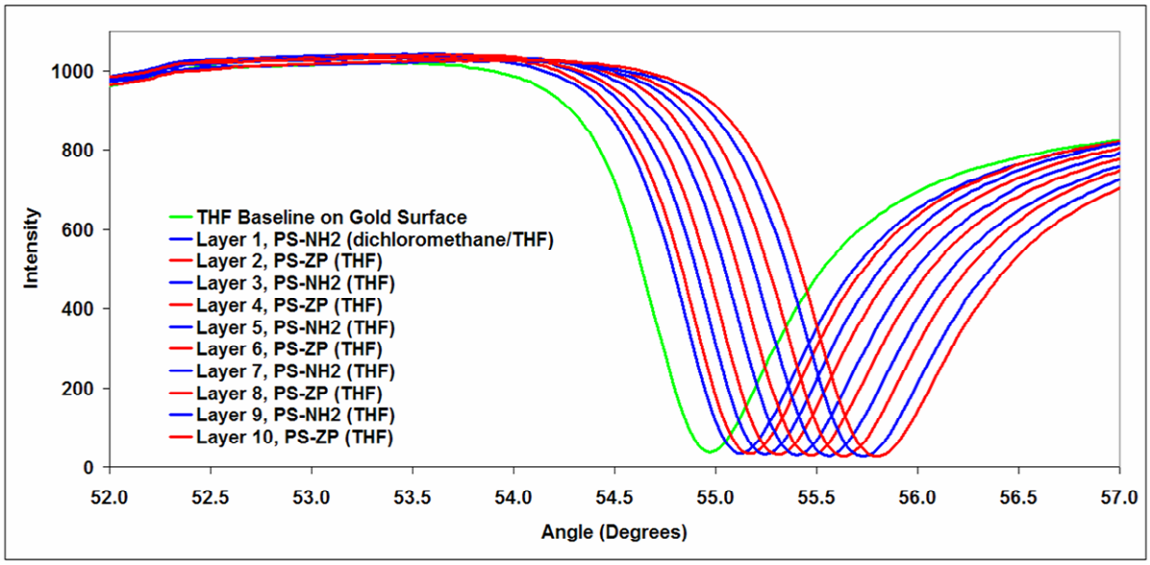

Figure 68. SPR angular response of the LBL self-assembly of star polymers on gold surface in THF.

The experiments described in this section suggest that the most suitable solvent for LBL self-assembly of star polymers after the formation of the first PS-NH_2 layer on substrate using CH_2Cl_2/THF was found to be THF/THF. THF is effective in washing off extraneous polymer that does not adsorb onto the polymeric film, however the duration for THF wash exposure still needs to be optimized. Uniform polymer bilayers PS-

NH_2/PS-ZP were obtained with the PS-NH_2 layer showing a bigger SPR angular shift compared to the PS-ZP layer. The polymeric film showed complete coverage at the tenth layer as seen in the AFM analysis (Figure 46). The self-assembly process continues despite a textured initial PS-NH_2 layer when THF/THF solvent system was used.

5.2.4 Summary of SPR Studies

The feasibility of using SPR to be used as a tool for *in-situ* analysis of layer deposition is validated as there is the advantage for real-time observation of layer formation through the collected SPR angular scans and kinetic profiles.

SPR studies together with AFM data confirm that the most suitable solvent system to be used in LBL self-assembly of alternating PS-NH_2 and PS-ZP star polymers is THF/THF. Although AFM analysis shows that dichloromethane deposition of PS-NH_2 as the initial layer followed by a quick THF wash produces the best film quality, SPR results shows that the LBL self-assembly process can continue despite a textured initial layer and uniform SPR shifts were observed for a polymer bilayer (PS-NH_2/PS-ZP). The SPR experiments also showed that the polymeric films formed through the self-assembly process were stable as demonstrated by the constant intensity signal in the solvent wash step despite prolonged solvent exposure. Besides the verification of the viability of the LBL self assembly process, the SPR experiments substantiated the self-limiting property of the process. Kinetic profiles obtained through the SPR instrument confirm that the PS-NH_2 polymer interacts strongly with the PS-ZP polymer to form a layer but interacts weakly with itself. This is similarly observed for the PS-ZP polymer.

The change in SPR resonance angle for the PS-NH_2 layer is larger than the change recorded for the PS-ZP layer which may be either due to (i) the PS-NH_2 being thicker than the PS-ZP film because of the difference in polymer molecule arrangement within the film or difference in the degree of film solvation, or (ii) it could be due to the PS-NH_2 film having different optical properties, *e.g.*, refractive index, compared to the PS-ZP film. Further analysis of the layer build-up using QCM may provide insights on the characteristics of the generated polymeric multilayers.

5.3 Quartz Crystal Microgravimetry (QCM)

The purpose of this section is to use quartz crystal microbalance (QCM) to measure mass changes for each polymer layer as it is deposited in the layer-by-layer process. Information from the QCM analysis together with AFM and SPR data discussed in previous sections will provide a more in-depth assessment of the LBL self-assembly process and the properties of the resultant films. The QCM measures frequency changes of a quartz crystal resonator as material adheres to (or is removed from) the surface of the quartz crystal. Also measured is the motional resistance which denotes energy loss due to damping of the oscillation. As this is closely linked to the physical properties of the deposited films and neighboring solvent [85], changes in the resistance as polymer layers are deposited may provide an evaluation of the properties of the polymeric film. QCM experiments also studies polymer deposition over a larger substrate area compared to the SPR instrument. Similarly to previous sections, QCM results are discussed with respect to (i) self-assembly of star polymer on SiO_2 surface, (ii) self-assembly of star polymer molecules on a star polymer layer, and (iii) LBL self-assembly of alternating

functionalized star polymers (PS-NH_2/PS-ZP). The substrates used in QCM analysis were quartz crystals with a resonant frequency of 5 MHz, purchased pre-sputtered with a layer of silicon dioxide over the gold. As discussed in the materials and methods section, the frequency change as polymer layers adsorb onto the quartz crystal is measured *in-situ* using a flow cell, which allows measurements of the frequency change of the polymer film both in the "wet" or "dry" state. Ultimately, QCM and SPR are complementary measurements for determination of the thickness of the self-assembled polymer films.

5.3.1 Self-Assembly of Functionalized Star Polymer on Silicon Dioxide Substrate

The change in frequency of the QCM quartz crystal as the first PS-NH_2 polymer layer was deposited onto SiO_2 surface using CH_2Cl_2/THF is shown in Figure 69. The oscillation frequency decreased as mass was added to the quartz crystal and increased as mass was removed from the quartz crystal. An increase in mass (decrease in oscillation frequency) was detected as THF was introduced first into the flow cell to establish a solvent baseline, followed by dichloromethane to prepare the flow cell and the SiO_2 surface for PS-NH_2 polymer deposition in dichloromethane. After that, a PS-NH_2 solution in dichloromethane was injected into the flow cell. Steady state was reached (*i.e.*, the oscillation frequency is almost constant) before the washing steps were performed with the introduction of dichloromethane into the flow cell and a subsequent injection of THF wash. The oscillation frequency remained unchanged even after 2 minutes of THF rinsing which suggested that a stable PS-NH_2 layer had been formed on the SiO_2 surface. Using THF as the baseline, the change in frequency after the formation of the first PS-NH_2 layer on the QCM substrate was approximately 50 ± 1 Hz. The

oscillation frequency after the deposition and wash of the PS-NH_2 polymer would return to the frequency of the THF baseline if no PS-NH_2 polymer was deposited on the SiO_2 surface.

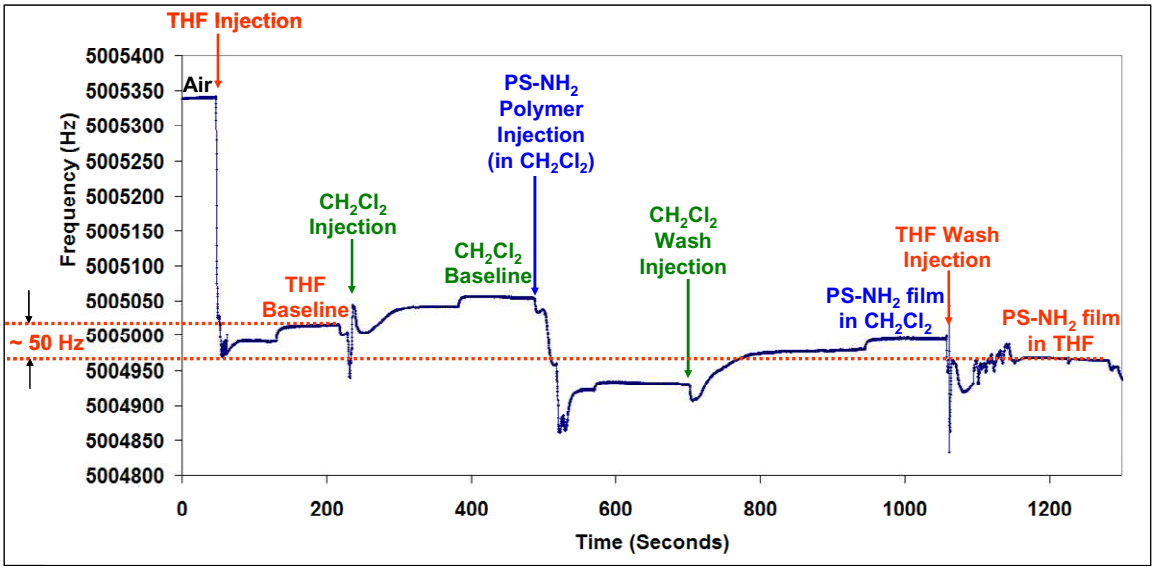

Figure 69. Frequency change of layer 1, PS-NH_2 deposition on SiO_2 surface using dichloromethane with a THF wash.

The effect of solvent on the self-assembly of the first PS-NH_2 layer on SiO_2 surface was investigated by QCM. When THF was used as the solvent for deposition and wash (THF/THF) of the PS-NH_2 layer, the frequency change was approximately 32 ± 1 Hz as shown in Figure 70. The lower frequency change compared to when CH_2Cl_2/THF was used (~50 ± 1 Hz) is consistent with SPR results discussed in Section 5.2.1, where a smaller change in resonance angle was detected for PS-NH_2 film prepared using THF/THF, as shown in Table 8.

Table 8. QCM and SPR results for the self-assembly of PS-NH_2 layer on sputtered SiO_2 surface using different solvent system.

Solvent System	QCM Δ Frequency (Hz)	SPR Δ Resonance Angle (°)
CH_2Cl_2/THF	50 ± 1	0.17 ± 0.002
THF/THF	32 ± 1	0.13 ± 0.002

The decrease in Δ frequency and Δ resonance angle may indicate that the amount of PS-NH_2 polymer that adsorbed onto the surface when the deposition was done in THF was less than when the deposition was done in dichloromethane. This may be due to a difference in packing of the PS-NH_2 polymer molecules when the molecules self-assembled into a monolayer on the SiO_2 surface under different solvent conditions. The detected difference in the QCM and SPR is consistent with the difference in morphology seen in the AFM analysis described in Section 5.1.1 (*i.e.*, rough vs. smooth). The PS-NH_2 film on a silicon wafer prepared using CH_2Cl_2/THF appeared to be smoother compared to the PS-NH_2 film prepared using THF/THF which was found to have a nanostructured morphology possibly due to packing within the film (Figure 33).

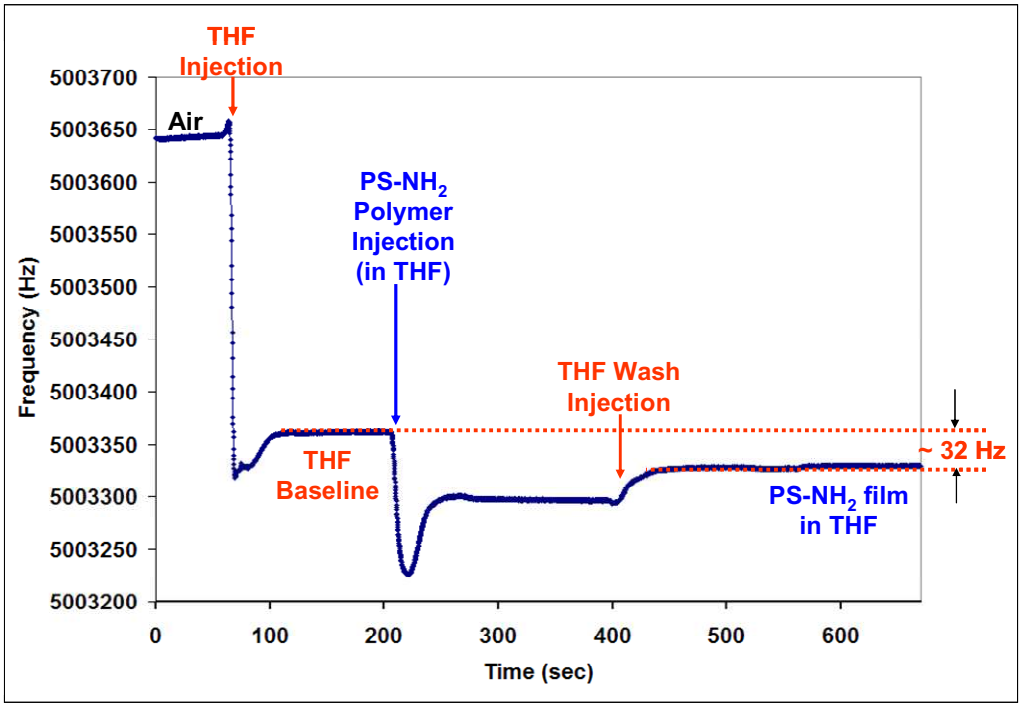

Figure 70. Frequency change of layer 1, PS-NH_2 deposition on SiO_2 surface using THF with THF wash.

5.3.2 Self-Assembly of Functionalized Star Polymer on a Star Polymer Layer

The interaction between PS-ZP star polymer with a PS-NH_2 layer and the interaction between PS-NH_2 star polymers with a PS-ZP layer were studied by QCM. The frequency curve for deposition of additional functionalized star polymer on a polymeric film, shown in Figure 71 for PS-ZP polymer (Layer 6) on PS-NH_2 film (Layer 5) and PS-NH_2 polymer (Layer 7) on PS-ZP film (Layer 6) using THF/THF solvent system, shows the continuous decrease in oscillation frequency as the LBL formation progresses. The THF/THF solvent system was used for deposition of polymer layers after the first PS-NH_2 layer which was deposited onto SiO_2 surface using CH_2Cl_2/THF, since evidence from AFM analysis suggested that a dual solvent system was not required after the first PS-NH_2 layer.

The PS-ZP polymer (in THF) was injected into the flow cell on a PS-NH_2 layer (Layer 5). After ensuring that the steady state was achieved, *i.e.*, constant oscillation frequency, THF was introduced as the wash to remove non-specifically adsorbed polymer. Equilibrium was achieved during the THF wash, denoting the formation of a stable PS-ZP layer (Layer 6). PS-NH_2 polymer (in THF) was then injected on the PS-ZP layer (Layer 6), followed by THF wash. The formation of PS-ZP layer (Layer 6) and PS-NH_2 layer (Layer 7) as shown in the figure resulted in an almost uniform decrease of approximately 75 ± 1 Hz in oscillation frequency per polymer layer. The 75 ± 1 Hz change observed for the seventh layer (PS-NH_2) was larger than the change seen in the first PS-NH_2 layer possibly due to the different interactions involved in layer adsorption, *i.e.*, electrostatic for the interaction between the first PS-NH_2 layer and SiO_2 surface, and coordination chemistry for the interaction between the PS-NH_2 layer and PS-ZP layer. The QCM profile for PS-NH_2 deposition and PS-ZP deposition are very different as shown in Figure 71. The PS-NH_2 layer appear to achieve equilibrium faster compared to the PS-ZP layer which suggests that the formation of the PS-NH_2 layer is more rapid than the formation of the PS-ZP layer.

The PS-ZP layer (Layer 6) and PS-NH_2 layer (Layer 7) still remained intact despite prolonged contact with THF solvent as confirmed by the constant oscillation frequency during the THF rinsing step denoting a strong interaction between the PS-ZP layers and the PS-NH_2 layers.

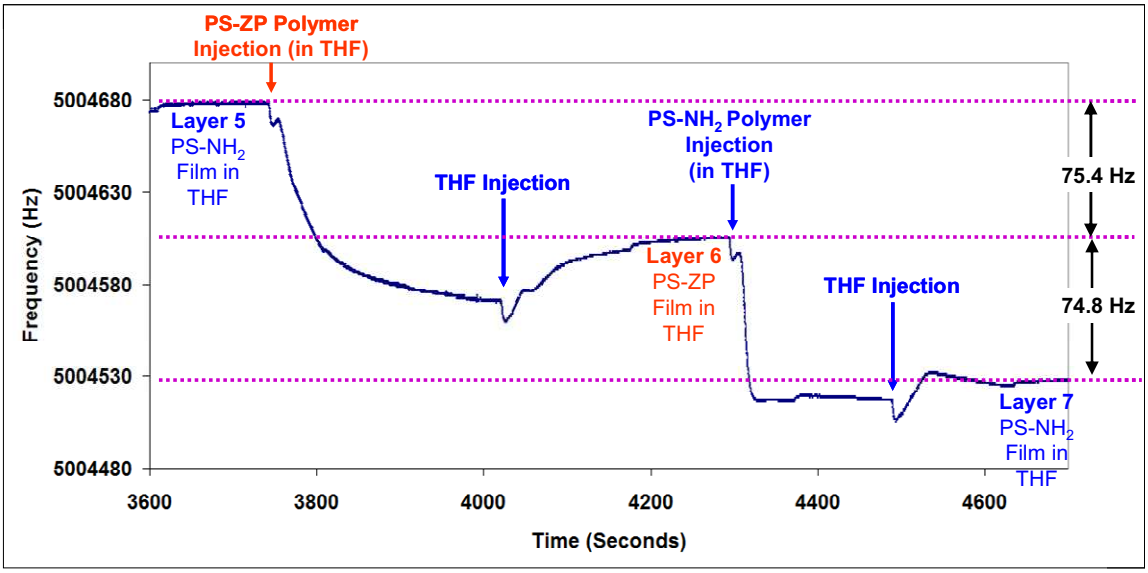

Figure 71. Frequency change of layer 6, PS-ZP deposition on PS-NH_2 film using THF/THF and layer 7, PS-NH_2 deposition on PS-ZP film using THF/THF.

The interaction between PS-NH_2 polymer molecules with a deposited PS-NH_2 layer was studied by QCM. The decrease in oscillation frequency when PS-NH_2 polymer was deposited on the 11th layer (PS-NH_2) was approximately 13 ± 1 Hz which was only 17% of the expected frequency decrease of 75 ± 1 Hz based on the previous PS-NH_2 layers. This may indicate that some PS-NH_2 molecules were non-specifically adsorbed onto the PS-NH_2 film because of weak Van der Waals interactions or the THF washing step might not have been optimized to remove the extraneous polymer molecules. SPR analysis of the interaction between PS-NH_2 polymers on PS-NH_2 layer (Section 5.2.2) shows no significant change in the plasmon resonance angle. Both the SPR and QCM results are consistent with the assertion that the interactions between PS-NH_2 polymer molecules are weak.

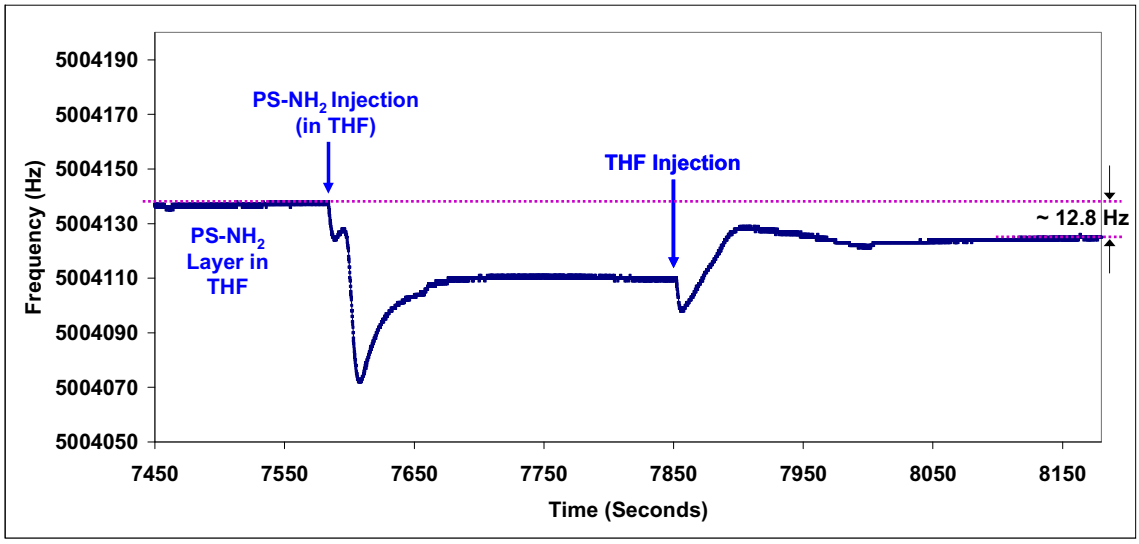

Figure 72. Effect of deposition of PS-NH_2 polymer on a PS-NH_2 layer using THF/THF.

A similar experiment was carried out with the deposition of PS-ZP polymer on a PS-ZP layer using THF/THF. The decrease in oscillation when PS-ZP polymer was deposited on the PS-ZP layer (Layer 11) was only 8 ± 1 Hz as shown in Figure 73. The decrease in oscillation frequency for PS-ZP polymer on PS-ZP layer was only 11% of the frequency decrease observed if a complete PS-ZP film was formed (approximately 75 ± 1 Hz). Hence the result may suggest that some PS-ZP polymer molecules were non-specifically adsorbed onto the PS-ZP film which, as discussed above, may not have been completely removed using the existing THF wash procedure.

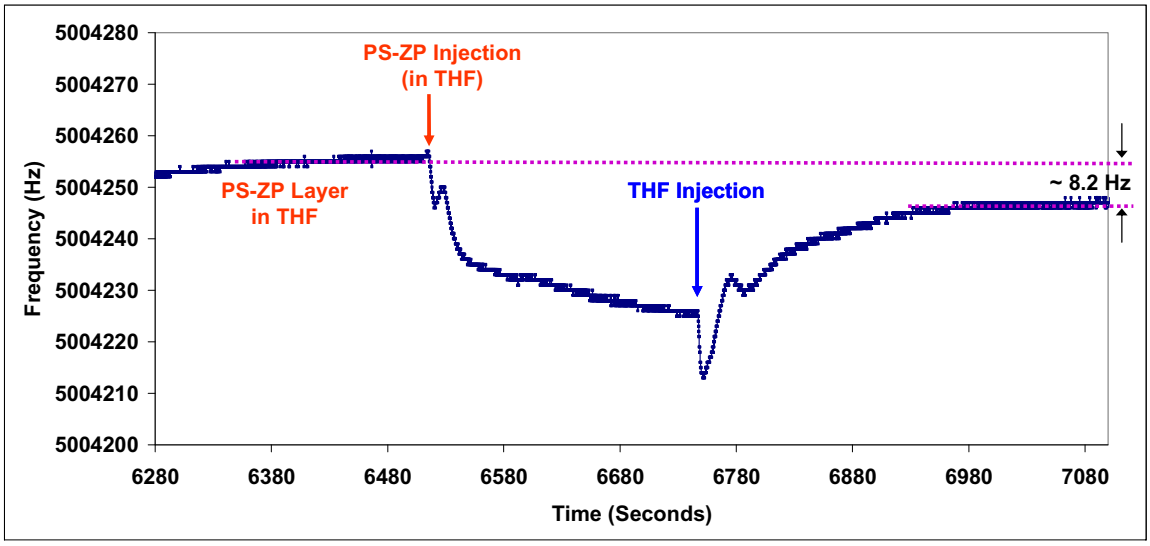

Figure 73. Effect of deposition of PS-ZP polymer on a PS-ZP layer using THF/THF.

5.3.3 Layer-by-Layer Self-Assembly of Alternating Functionalized Star Polymers (PS-NH_2/PS-ZP)

Since the AFM analysis in Section 5.1.1 shows that deposition of PS-NH_2 on silicon wafer using CH_2Cl_2/THF produces a contiguous and smooth polymer film, the QCM experiments were carried out using the CH_2Cl_2/THF solvent system for the deposition of the first PS-NH_2 on the SiO_2 surface of the quartz crystal while subsequent alternating PS-NH_2 and PS-ZP star polymer layers were deposited using THF/THF. The change in oscillation frequency for deposition of ten layers of alternating PS-NH_2 and PS-ZP star polymer using the described solvent system is shown in Figure 74.

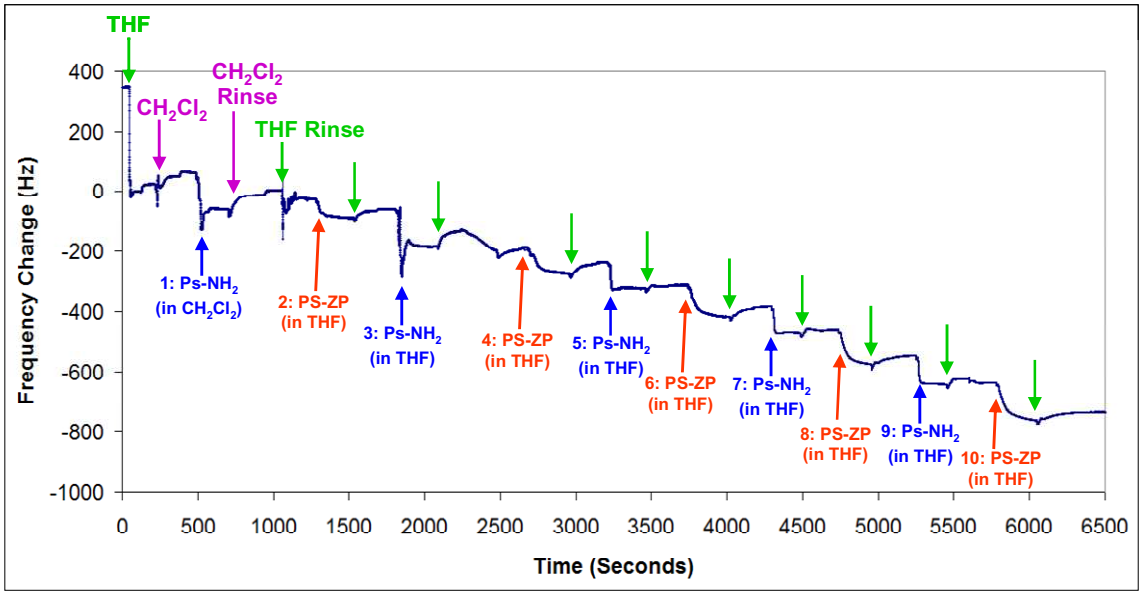

Figure 74. QCM profile of LBL self-assembly of star polymers using THF/THF with the first PS-NH_2 layer deposited on SiO_2 surface using CH_2Cl_2/THF.

The total frequency change for the self-assembly of ten layers of alternating PS-NH_2/PS-ZP shown in Figure 74 was approximately 760 ± 1 Hz. The frequency changes were almost uniform for each polymer layer as illustrated by the almost linear response ($R^2 = 0.9882$) shown in Figure 75. The linear relationship between layer number and frequency change is in agreement with the Sauerbrey equation, *i.e.*, the polymer layers behave like a thin, rigid film. On the contrary, the non-linear trend of the resistance change which is also shown in Figure 76, suggests that the PS-NH_2/PS-ZP multilayers behave more like a gel (P(MMA-MAA) [85]). Since the deviation from the Sauerbrey equation is governed by three parameters, *i.e.*, film thickness, film viscosity and the resonator frequency, the equation can be effectively applied for a non-rigid film as long as the polymeric film is thin enough [85, 86]. The resistance change profile with

deposited layer of polymeric film may imply that the PS-NH_2 layers behave differently compared to the PS-ZP layers.

The Δ frequencies for PS-NH_2 and PS-ZP within the bilayer appear to be uniform as seen from the 3rd bilayer (PS-NH_2/PS-ZP) onwards as shown in the inset of Figure 75. This suggests that the amount of PS-NH_2 and PS-ZP deposited within a bilayer is uniform for each PS-NH_2/PS-ZP bilayer.

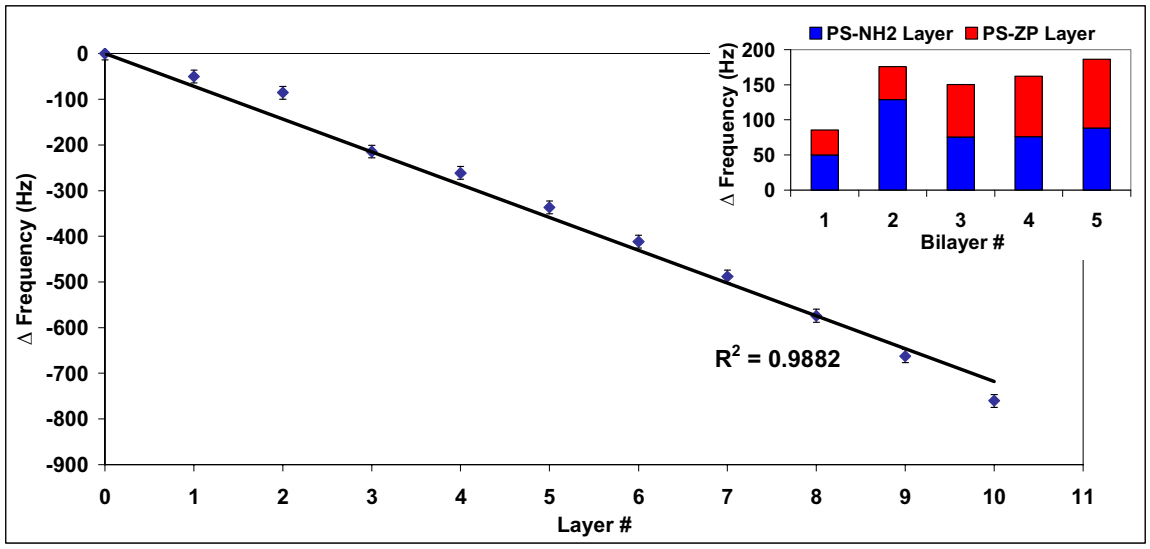

Figure 75. Frequency change for LBL self-assembly of ten layers of alternating PS-NH_2/PS-ZP using THF/THF with the first PS-NH_2 layer deposited using CH_2Cl_2/THF and Δ frequency with regards to bilayer # (inset).

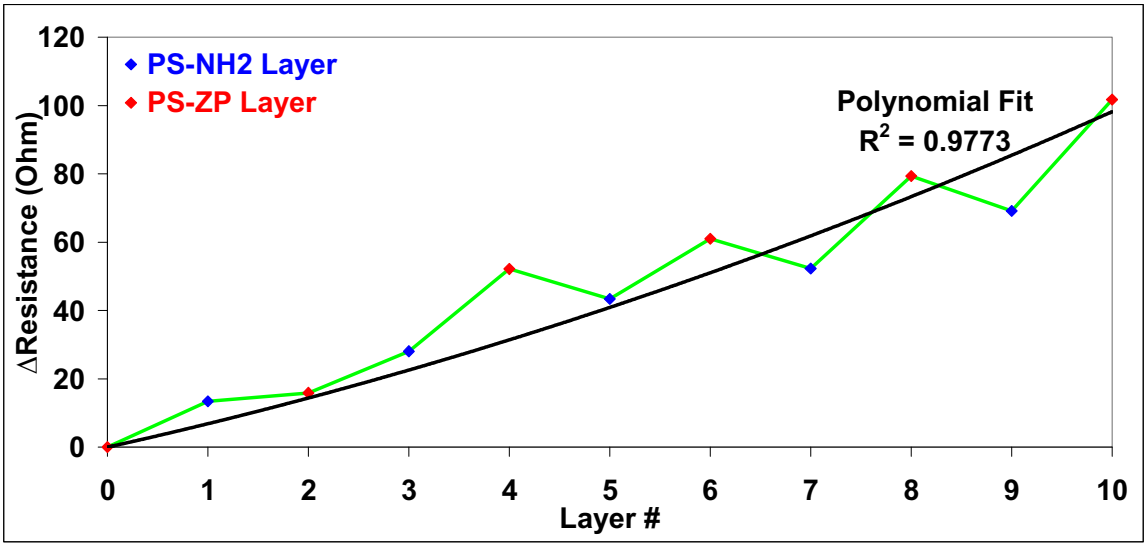

Figure 76. Resistance change for LBL self-assembly of ten layers of alternating PS-NH_2/PS-ZP using THF/THF with the first PS-NH_2 layer deposited using CH_2Cl_2/THF.

AFM, SPR and QCM analysis confirms that solvent plays a very important role in determining the efficiency of layer formation through self-assembly and determining the characteristics of the resultant multilayer of polymeric film. The polymeric films may become less rigid depending on the solvent used for deposition and the percentage of solvent in the film. As more solvent is absorbed into the films, deviations from the Sauerbrey equation may occur. QCM experiments using a single solvent system throughout (THF/THF) were studied for LBL self-assembly on SiO_2 surface. The decrease in the oscillation frequency for ten layers when the THF/THF solvent system was used was approximately 600 ± 1 Hz. This is shown in Figure 77. The figure shows the formation of 12 layers of alternating PS-NH_2 and PS-ZP layers deposited using THF/THF and is consistent with the AFM and SPR findings that THF is an appropriate solvent for LBL self-assembly of alternating PS-NH_2 and PS-ZP star polymers.

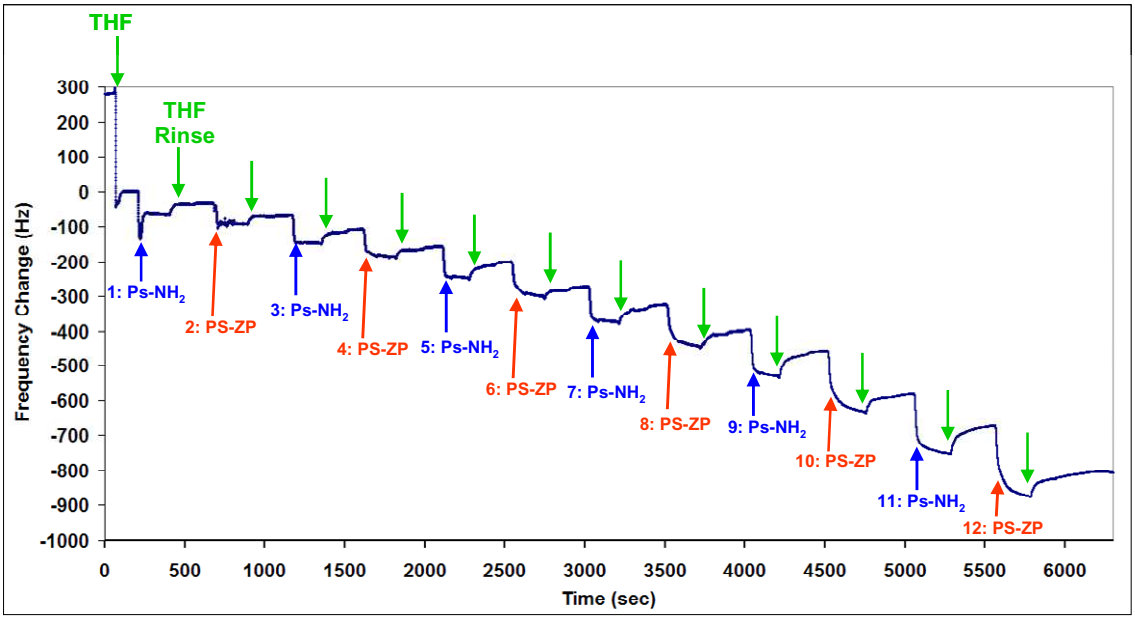

Figure 77. QCM profile of LBL self-assembly of star polymers using THF/THF.

The changes in frequency with regard to PS-NH_2/PS-ZP bilayer formation for three runs using different solvent systems are shown in Figure 78. The corresponding resistance changes for successive polymer layers are shown in the inset. The experiment using CH_2Cl_2/THF deposition sequence for the first PS-NH_2 layer on SiO_2 surface and THF/THF for subsequent layers, denoted as Run 3 in the figure, appears to provide the same linear behavior (same slope) as experiment conducted using CH_2Cl_2/THF throughout the deposition (Run 2). On the other hand, there was a change in frequency behavior when THF/THF was used throughout the deposition (Run 1). This may be due to the way the first PS-NH_2 layer was deposited onto the SiO_2 surface. The initial PS-NH_2 layer was deposited onto SiO_2 using CH_2Cl_2/THF solvent system for Run 2 and Run 3 while the deposition for PS-NH_2 on SiO_2 in Run 1 was done in THF/THF. AFM demonstrated that the first PS-NH_2 layer on silicon wafer had a nonstructured texture

when deposition was done in THF/THF and this could account for the differences in the way the polymer layers self-assemble on the first PS-NH_2 layer. This has brought about the differences seen in the QCM frequency profile. The resistance change with regards to layer number for the three runs (inset of Figure 78) shows a non-linear profile which is consistent with gel-like behavior of the polymeric multilayers. There are differences in the results shown in Figure 78 even though the final solvent of contact for every layer deposition was THF in all three runs. This may be due to the hygroscopic nature of the THF which may absorb water resulting in variable frequency changes between the runs.

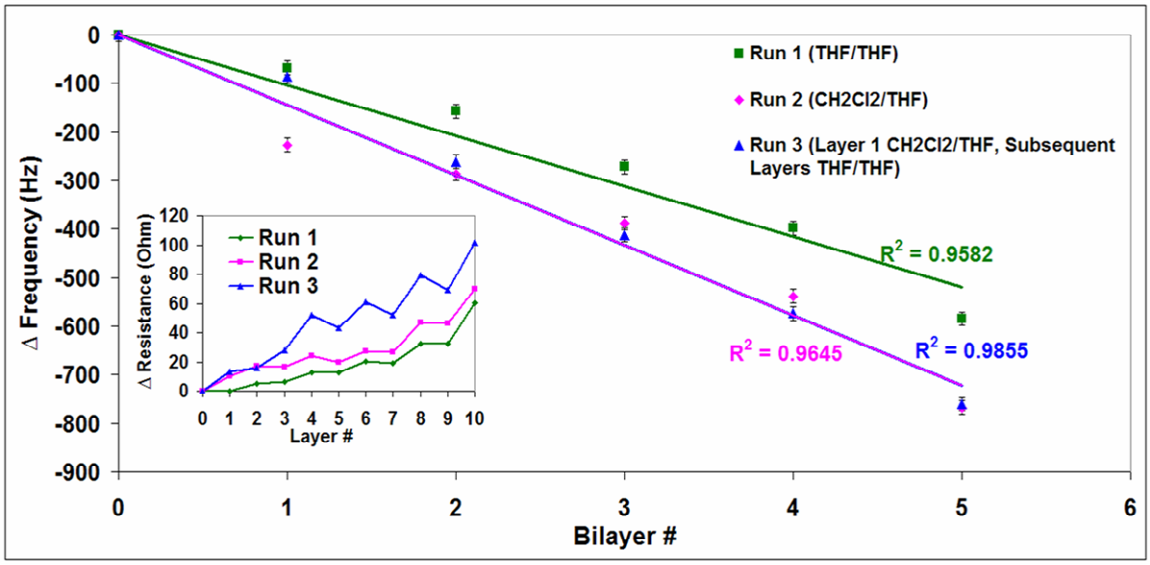

Figure 78. Comparison of QCM frequency change and resistance change (inset) for LBL self-assembly experiments using different solvent systems.

QCM experiments were also performed using chloroform for both the deposition and wash of alternating PS-NH_2 and PS-ZP star polymers. The QCM profile of the LBL self-assembly of star polymers using chloroform as shown in Figure 79 shows a change of approximately 2200 ± 1 Hz for nine polymeric layers and when the tenth layer was injected, the quartz crystal stopped oscillating, indicating that a very large amount of

energy was lost. This energy loss exceeds the capacity of the driver circuit in the QCM instrument to compensate for it. This may be due to the characteristics of the multilayer film assembly on the quartz crystal which may be very viscous and rubbery resulting in a large amount of internal friction. The large frequency decreases for layers prior to the impeded oscillation (at Layer 10) indicates a large amount of mass deposition implying thick polymeric films. This contradicts the premise that the polymers self-assemble into a thin film that is a single-polymer-molecule thick. This suggests that chloroform is not a suitable solvent to remove non-specifically adsorbed polymer molecules as it causes each layer to be more than a single molecule thick, subsequently triggering irregular film growth as layers deposition progresses. This result also agrees with the SPR results using chloroform as discussed in Section 5.2.3.

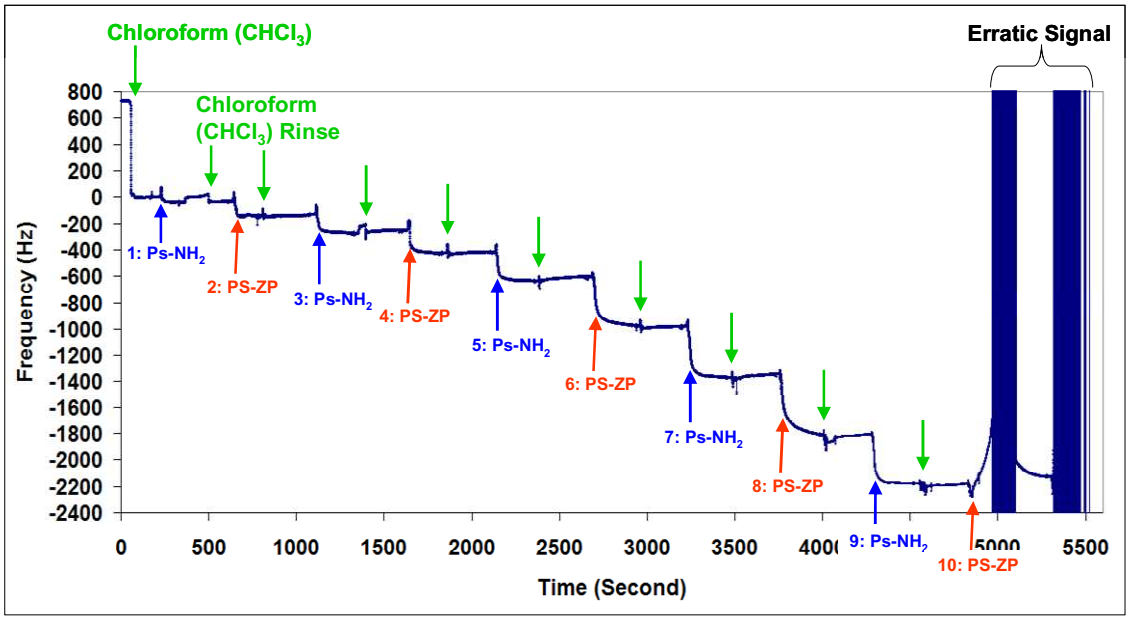

Figure 79. QCM profile of LBL self-assembly of star polymers using chloroform.

5.3.4 Summary of QCM Studies

The QCM instrument provides valuable information concerning the formation of alternating PS-NH_2 and Ps-ZP polymer layers. The almost linear response seen in the oscillation frequency decrease with increasing numbers of polymeric layers suggests that the mass deposited for each layer is uniform but the polymer films must be very thin since the resistance change shows a non-linear behavior which suggests a non-rigid, gel-like structure. The evolving theory of star polymer characteristics based on SPR analysis suggested that the star polymer films were heavily solvated when formed and this may provide the layers with gel-like characteristics.

The QCM results show uniform changes in frequency as the polymer layers were formed using THF/THF on an initial PS-NH_2 film deposited on SiO_2 using CH_2Cl_2/THF. Although the SPR result shows that the PS-ZP layer has a smaller angular shift compared to the PS-NH_2 layer, the QCM result appears to suggest that a uniform mass of polymer was deposited onto each layer. Comparing the SPR results to the QCM results, it can be postulated that the angular difference seen in the SPR data between the PS-NH_2 layer and the PS-ZP layer may be due to the difference in solvent retention within the PS-NH_2 layer and PS-ZP layer which will change the effective refractive index of the particular film.

5.3.5 Combined SPR and QCM Analysis

The SPR and QCM methods are complementary methods used in assessing the LBL self-assembly process and the resultant molecularly thin layers of alternating PS-NH_2 and PS-ZP star polymer films. The SPR probes the optical properties and thickness of the polymer films while the QCM provides a physical measurement of the amount of material deposited per polymer layer. The structure of the PS-NH_2/PS-ZP multilayer film can be inferred from collective analysis of the SPR and QCM results. SPR experiments revealed a bilayer characteristic, where the change in resonance angle for the PS-NH_2 layers was larger than the change in resonance angle for the PS-ZP layers suggesting that the PS-NH_2 and PS-ZP layers manifest different characteristics which may result from (i) differences in layer thickness, (ii) differences in layer affinity towards solvent, and (iii) differences in layer effective refractive index. QCM analysis suggested that equal amounts of star polymer molecules were deposited for each polymer layer.

From the previous model derived by Dr. William Risk on the expected SPR angle shift with regards to layer thickness and polystyrene-to-solvent ratio, a matrix for the prediction of the polymeric multilayer is compiled as shown in Table 9. The average SPR angular shift for the first PS-NH_2 layer deposited on SiO_2 surface is approximately 0.14° which corresponds to case 7 in the table. The matrix predicts an initial PS-NH_2 layer with an average layer thickness of 4.5 nm on SiO_2 surface which agrees with ~ 50% compression of the star polymer molecule. This first PS-NH_2 layer is predicted to have polystyrene to solvent ratio of 60.5 to 39.5. The average of SPR angular shift for subsequent PS-NH_2 layers (except the first PS-NH_2 layer on substrate) deposited with

THF/THF is 0.15° which also corresponds to case 7 in Table 9. The PS-NH_2 layers probably have the same thickness and solvent content despite the layers having been formed from different interaction and using different solvent system. The angular shift for the PS-ZP layers deposited using THF/THF is smaller, ~ 0.08°, which corresponds to either case 8 or case 11. The smaller shift in SPR angle can be either due to a thinner PS-ZP layer caused by higher molecular compression or to larger amounts of solvent trapped within the PS-ZP layer altering the polystyrene-solvent ratio. From the predictions in Table 9, the polymeric multilayer structure of the self-assembled PS-NH_2/PS-ZP film can probably occur in two different arrangements as shown in Figure 80.

Table 9. Predictions of polymeric structure with regards to change in resonance angle.

SPR, $\theta = f(n_e, t)$					
No.	Compression (%)	Layer Thickness, t (nm)	Polystyrene to Solvent ratio	Effective Refractive Index, n_e	Theoretical $\Delta\theta_{SPR}$ (°)
1	0	9	1 : 0	$n_e \approx n_{PS}$	$\theta_{SPR} \approx 0.51$
2	25	6.75	1 : 0	$n_e \approx n_{PS}$	$0.26 < \theta_{SPR} < 0.51$
3	50	4.5	1 : 0	$n_e \approx n_{PS}$	$\theta_{SPR} \approx 0.26$
4	75	2.25	1 : 0	$n_e \approx n_{PS}$	$\theta_{SPR} < 0.26$
5	0	9	60.5 : 39.5	$n_{THF} << n_e < n_{PS}$	$\theta_{SPR} \approx 0.3$
6	25	6.75	60.5 : 39.5	$n_{THF} << n_e < n_{PS}$	$0.15 < \theta_{SPR} < 0.3$
7	50	4.5	60.5 : 39.5	$n_{THF} << n_e < n_{PS}$	$\theta_{SPR} \approx 0.15$
8	75	2.25	60.5 : 39.5	$n_{THF} << n_e < n_{PS}$	$\theta_{SPR} < 0.15$
9	0	9	1 : 1	$n_{THF} < n_e < n_{PS}$	$\theta_{SPR} < 0.3$
10	25	6.75	1 : 1	$n_{THF} < n_e < n_{PS}$	$\theta_{SPR} << 0.3$
11	50	4.5	1 : 1	$n_{THF} < n_e < n_{PS}$	$\theta_{SPR} < 0.15$
12	75	2.25	1 : 1	$n_{THF} < n_e < n_{PS}$	$\theta_{SPR} << 0.15$

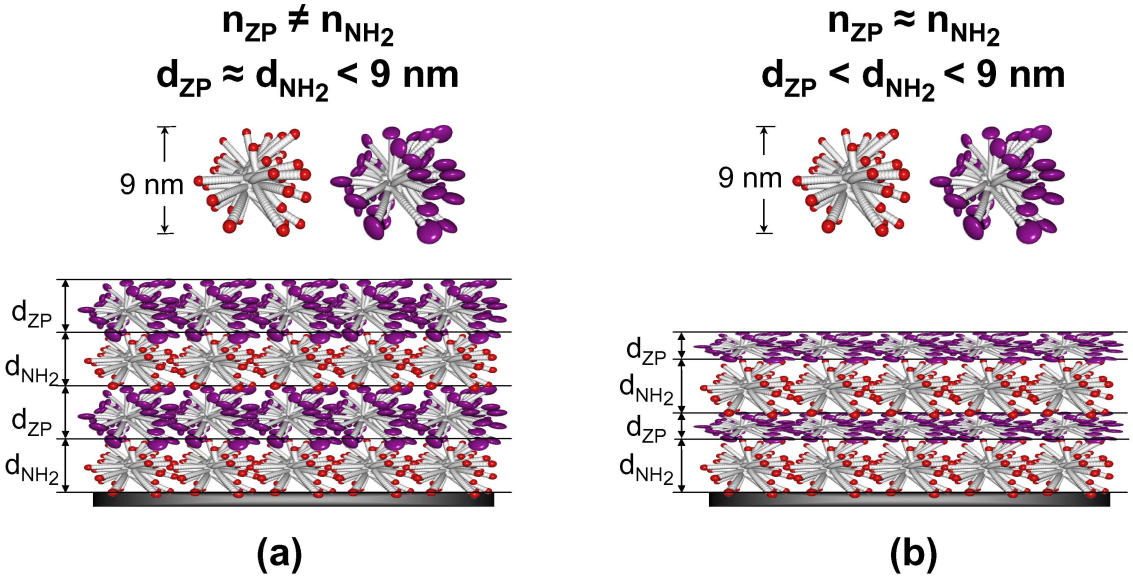

Figure 80. Probable multilayer structure with (a) the PS-NH_2 and PS-ZP layers having similar thicknesses but different refractive indices, or (b) the PS-NH_2 and PS-ZP having different thicknesses but similar refractive indices.

QCM results for a multilayer polymer film of alternating PS-NH_2/PS-ZP, with the initial PS-NH_2 layer deposited using CH_2Cl_2/THF and subsequent polymer layers deposited in THF/THF suggest that uniform amounts of PS-NH_2 and PS-ZP star polymer molecules were deposited during the LBL self-assembly process. This eliminates the model shown in Figure 80(b). Increases in compression of the PS-ZP polymer molecules should reduce the amount of PS-ZP polymer that can be deposited on the PS-NH_2 layers and the expected change in frequency for the PS-ZP layers should be less than the change in frequency for the PS-NH_2 layers in order to be consistent with the structure suggested in Figure 80(b). The model shown in Figure 80(a) more accurately reflects the structure of the PS-NH_2/PS-ZP multilayer. In order for PS-NH_2/PS-ZP multilayer to have the

same uniform thickness and still be consistent with SPR results (*i.e.*, ΔθSPR of PS-ZP layers < ΔθSPR PS-NH_2 layers) the PS-ZP layers must have different optical properties compared to the PS-NH_2 layers. The difference in optical properties of the PS-NH_2 and PS-ZP layers may be due to difference in layer salvation, *i.e.*, the amount of solvent trapped within a PS-NH_2 layer is different from the amount of solvent trapped within a PS-ZP layer.

5.4 UV-Vis Spectroscopy

The aim of this section is to confirm the role of coordination chemistry in the formation of alternating PS-NH_2/PZ-ZP polymeric layers. The zinc-porphyrin group on the periphery of the PS-ZP molecule is a dye material that strongly absorbs light in the visible region. The maximum absorption of this dye material changes upon coordination of the Zn (II) center with ligands such as amines as shown in Figure 81. Since different degrees of zinc-porphyrin-amino interaction will result in absorption of radiation of different wavelength, the degree of arm interaction can be determined from the absorption spectra obtained through the UV-Vis Spectrophotometer.

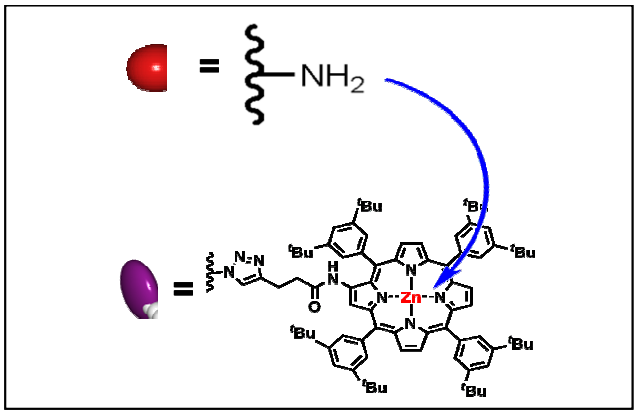

Figure 81. Organometallic Coordination of amino group on the star polymers with the Zn (II) center in the zinc-porphyrin group on the star polymers.

The substrates used in this study were optically transparent quartz wafers. The quartz wafers were conditioned as mentioned in the materials and methods section to ensure that an active silanol surface was present for polymer deposition. The polymer layers were deposited using the dipping method.

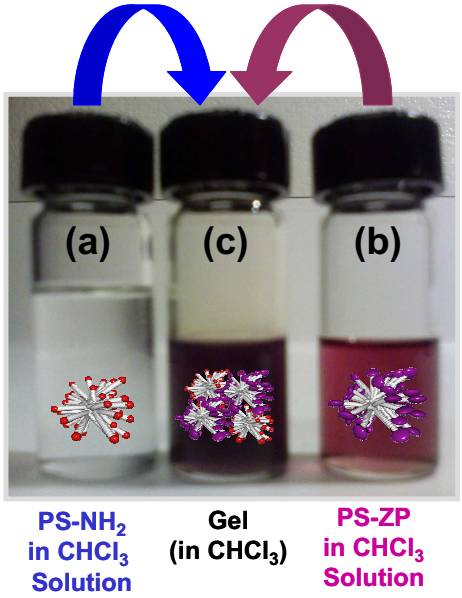

Figure 82. Photo of the addition of (a) PS-NH_2 solution in chloroform, and (b) PS-ZP solution in chloroform to form (c) PS-NH_2/PS-ZP gel in chloroform.

Bulk interaction between the clear PS-NH_2 solution (in chloroform) shown in Figure 82(a) and the clear crimson PS-ZP solution (in chloroform) shown in Figure 82(b) caused gelation to form shown in Figure 82(c). The resultant gel is not optically transparent; hence a UV-Vis analysis cannot be performed on the PS-NH_2/PS-ZP gel. A titration experiment was carried out to investigate the absorbance peak wavelength for non-reacted PS-ZP and for fully coordinated PS-ZP molecules. Absorbance spectrum for a solution of free, uncoordinated PS-ZP in THF was recorded. Amine ligands were added into the PS-ZP solution in tiny amounts at regular intervals and the absorbance

spectrum was recorded after every addition. The peak wavelength for free unbound PS-ZP in solution was recorded as 427 nm while the peak wavelength for fully coordinated PS-ZP in solution was recorded as 436 nm as shown by the spectral overlay in Figure 83. The difference in peak absorbance wavelength between the free, uncoordinated PS-ZP polymer and fully coordinated PS-ZP polymer is ~ 9 nm.

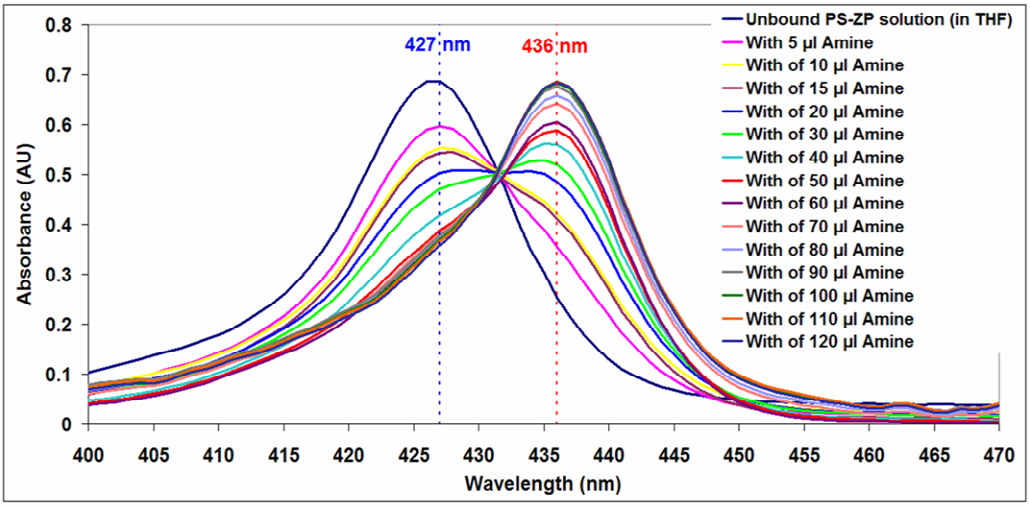

Figure 83. Overlay of absorbance spectra collected for free, uncoordinated PS-ZP in THF solution and for each subsequent addition of amine ligands in the titration experiment.

The LBL deposition of alternating layers of PS-NH_2 and PS-ZP were followed by UV-Vis analysis. Absorbance spectra were recorded after deposition and wash of each polymer layer using the established solvent system THF/THF. The partial UV-Vis spectra showing the maximum absorbance for the porphyrin dye (~ 440 nm) were plotted together as shown in Figure 84 and the changes in absorbance between PS-ZP layers were recorded as shown in the inset of the figure. The difference between the UV-Vis analysis done in solution and the UV-Vis analysis done on film was the orientation of the star polymer molecule containing zinc-porphyrin group: random orientation in solution

versus ordered orientation within a film. As only the layers containing PS-ZP contribute to the absorption spectrum in this spectral region (*i.e.*, PS-NH_2 is optically transparent in the visible region), only PS-ZP layer deposition results in an increase in peak absorbance. Since the dipping method was used, both sides of the quartz wafer were coated with the functionalized polymers, hence, the peak absorbance shown after the PS-ZP deposition was for 4 polymeric layers, *i.e.*, every quad layer (PS-NH_2/PS-ZP bilayer on each side of the wafer). As the polymer layers are being deposited, the absorbance should increase uniformly for every PS-ZP deposition. The incremental increase of peak absorbance intensity for the PS-ZP layers appeared to be uniform as shown by the linear relationship in the inset of Figure 84. This indicates that the amount of PS-ZP deposited is constant for each PS-ZP layer. Some slight variation may be due to the use of dipping method for film preparation as opposed to a flow system which has been shown in the AFM analysis (Section 5.1) to produce better quality films. The dipping method was used even though the flow cell method was found to produce polymer films that were superior in quality because the surface area exposed to polymers using the flow cell was insufficient for UV-Vis analysis. Another reason for the variability in the absorbance change could be due to the amount of solvent trapped within the film since the quartz wafer sample was exposed to the environment when spectra were recorded on the UV-Vis instrument.

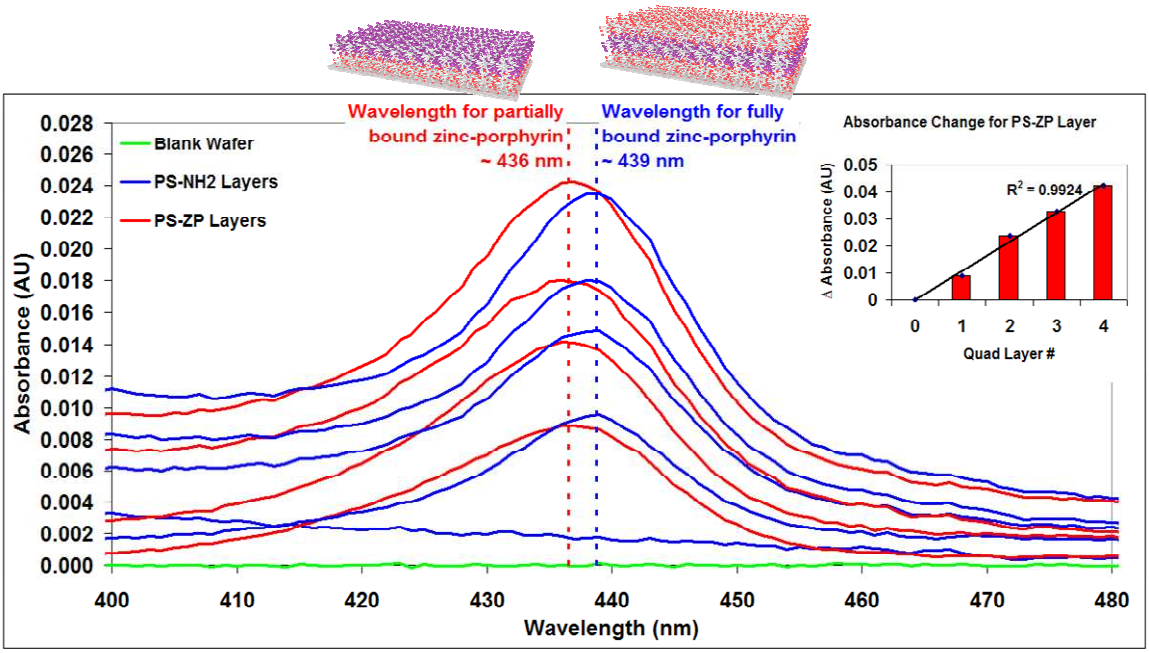

Figure 84. UV-Vis spectra for nine successive deposition of alternating PS-NH_2/PS-ZP polymeric layers and the change in absorbance for the PS-ZP layer (inset).

The typical change in maximum absorption wavelength between a solution of free, non-coordinated PS-ZP and a solution of PS-ZP that is fully coordinated with amine ligands is approximately 9 nm (Figure 83). When the PS-NH_2 layer was deposited on the quartz wafer (on both sides of the wafer), the UV-Vis spectrum did not show any absorption (400-480 nm). When a PS-ZP layer was deposited onto the amine layer, maximum absorption was detected at 436nm as shown in Figure 84. When the next amine polymer layer (PS-NH_2) was deposited onto the PS-ZP layer, the absorption maxima shifted to 439 nm while the absorption intensity remained constant. This shift confirms an interaction between the amino group on the PS-NH_2 molecule and the zinc-porphyrin group in the PS-ZP molecule. Interestingly, the maximum absorption at 439 nm after the deposition of the 3rd layer (PS-NH_2) on both sides of the quartz wafer should

represent the fully bound zinc-porphyrin state where the maximum number of amines is bound since the PS-ZP layer is sandwiched between two PS-NH_2 layers as shown in Figure 85(b). Hence if the wavelength difference for maximum absorption between unbound and fully bound zinc-porphyrin state was 9 nm, the detection of an absorption maxima for the first quad layer (PS-ZP layers on PS-NH_2 layers on both sides of the quartz wafer) at 436 nm indicates that ≥ 50% of zinc-porphyrin groups on the PS-ZP layer were unbound as shown in Figure 85(a). As the self-assembly process of alternating PS-NH_2 and PS-ZP progresses, the wavelength for maximum absorbance after every layer deposition should shift towards 439 nm. This is the result of the increase in the percentage of coordinated zinc-porphyrin groups at the periphery as the preceding PS-ZP layers have been fully coordinated with PS-NH_2 layers.

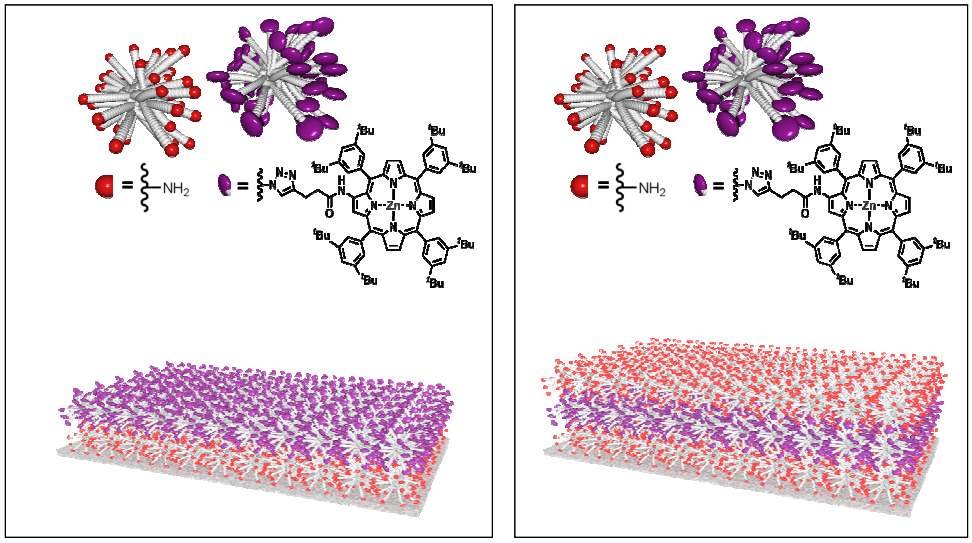

Figure 85. Illustration of self-assembled PS-NH_2/PS-ZP film with (a) 50% of the arms on the PS-ZP molecule interacting with the PS-NH_2 film and (b) 100% of the arms on the PS-NH_2 molecule interacting with PS-NH_2 films.

The characterization of the self-assembled film using UV-Vis is important to pave the way for further studies on the photoactive properties of the PS-NH_2/PS-ZP multilayers produced through the LBL self-assembly process. The ability to obtain information regarding the percentage of interacting arms on the PS-ZP molecule provides a foundation for future polymer design to enhance and optimize the self-assembly process. From the result from the UV-Vis analysis, it can be concluded with a high level of confidence that the interaction between the PS-NH_2 layer and the PS-ZP layer is organometallic ligand coordination bonding and the shift towards increasing wavelength in the absorbance peak after coordination of PS-ZP molecules to the PS-NH_2 layer indicates that most arms are involved in interactions within the polymer film. The UV-Vis spectra also confirm that the zinc-porphyrin group acts as individual non-aggregated dye within the PS-ZP film.

CHAPTER SIX
CONCLUSIONS

Multilayer thin polymer films that alternate between amino-functionalized star polymers (PS-NH_2) and zinc-functionalized star polymers (PS-ZP) were successfully generated via layer-by-layer (LBL) self-assembly on silicon dioxide surfaces using coordination chemistry. The polymeric films were effectively characterized using AFM, SPR, QCM and UV-Vis. The resultant multilayer film from self-assembly was verified to be stable and had homogeneous uniform polymer coverage. Each polymer layer is a monolayer (*i.e.*, one star polymer molecule thick).

Deposition of PS-NH_2 onto a silicon dioxide (SiO_2) surface in dichloromethane (CH_2Cl_2) followed by a tetrahydrofuran (THF) wash was found to be the best solvent system for the formation of a smooth base PS-NH_2 layer, however using THF as the solvent for PS-NH_2 deposition and as the wash solvent was shown not to impede the LBL self-assembly process. Subsequent layer deposition can be done in THF with THF wash without compromising film quality. The formation of the PS-NH_2 and the PS-ZP layers were shown to be rapid (approximately 10 seconds for PS-NH_2 layer formation and approximately 40 seconds for PS-ZP layer formation).

Comparison of the QCM and SPR data showed that the PS-NH_2 layer and the PS-ZP layer have equal mass but different optical properties. AFM analysis verified that the resultant self-assembled polymer multilayer film was stable over two weeks with complete and homogeneous polymer coverage while UV-Vis confirmed the organometallic coordination bond between a PS-NH_2 layer and a PS-ZP layer.

The research succeeded in producing multilayers of ordered pigment arrays within molecularly thin polymer layers using self-assembly. SPR was found to be a valuable and sensitive tool for measuring thin film depositions. Combined analysis of AFM, SPR, QCM, and UV-Vis results provided a thorough and comprehensive evaluation and established some fundamental attributes of the PS-NH_2/PS-ZP self-assembly process and the resultant multilayer assembly.

CHAPTER SEVEN
CURRENT AND FUTURE WORK

The successes highlighted in this thesis confirm the feasibility of the self-assembly process in making ensembles of functional nanostructure with precise ordering of pigment-arrays within thin film structures. The layer-by-layer self-assembly method presents a simple and low-cost approach to generate energy-cascade material for application in photovoltaic. The primary challenge of emulating structure and function observed in natural photosynthetic device has been partially overcome in this preliminary research work with the use of novel materials and the specificity of the chemical interactions. However, natural photosynthetic assemblies remain a complicated system that incorporates carefully arranged pigment molecules to support energy and electron transport events. Hence, further investigation is required to understand the resultant multilayer polymeric thin film structures through mathematical modeling and reconciliation of data obtained through the various characterization methods. Investigation into film robustness and formation kinetics is currently in progress to optimize process conditions for the formation of the PS-NH_2/PS-ZP polymeric thin film.

At present, efforts are devoted to combine the information gathered from the characterization methods used in this research work to obtain a descriptive assessment of the self-assembled polymeric layers. Analysis of the QCM data beyond the cursory estimates discussed in the thesis is still ongoing as a more complicated mathematical model may be required to quantify the frequency and resistance versus layer behavior. A detailed analysis of the QCM data can provide information such as the shear modulus of

the film and the interaction of the film with the solvent. Combined with SPR analysis, thicknesses of the individual polymer layer can be calculated.

Initial results using gold surfaces show that the self-assembly of the PS-NH_2/PS-ZP multilayer is feasible through coordination of the PS-NH_2 polymer to gold on the surface of the substrate. This broadens the choice of substrate for generation of the polymeric thin films. Further investigation into the reproducibility of the self-assembled multilayer structure on gold surfaces remains to be carried out.

The feasibility of energy transfer between the zinc-porphyrin layers is still under study. Preliminary fluorescence experiments reveal that the separation of the PS-ZP layers (achieved by the PS-NH_2 layers) may not be optimized for energy to transfer from one PS-ZP layer to subsequent PS-ZP layer. Future experiments will involve the formation of multilayer of pigment-arrays with chromophores of different absorbing wavelength to detect the movement of energy through the layers.

REFERENCES

1. M. Boncheva and G.M. Whitesides, "*Making things by self-assembly,"* MRS Bull., **30(10)**, 736-742 (2005).

2. J.W. Steed and J.L. Atwood, in Supramolecular Chemistry, 1st ed. (John Wiley & Sons, Ltd., 2000), pp. 2-33.

3. V.V. Borovkov, G.A. Hembury, and Y. Inoue, "*Origin, Control, and Application of Supramolecular Chirogenesis in Bisporphyrin-Based Systems,"* Acc. Chem. Res., **37(7)**, 449-459 (2004).

4. V. Uskokovic, "*Nanotechnologies: What we do not know,"* Technol. Soc., **29**, 43-61 (2007).

5. G.M. Whitesides and B. Grzybowski, "*Self-assembly at all scales,"* Science, **295(5564)**, 2418-2421 (2002).

6. G. Decher, "*Fuzzy nanoassemblies: Toward layered polymeric multicomposites,"* Science, **277(5330)**, 1232-1237 (1997).

7. O.N. Oliveira, J.A. He, V. Zucolotto, S. Balasubramanian, L. Li, H.S. Nalwa, J. Kumar, and S.K. Tripathy, "*Layer-by-Layer Polyelectrolyte-Based Thin Films for Electronic and Photonic Applications,"* in Handbook of Polyelectrolytes and Their Applications Volume 1,edited by S.K. Tripathy, J. Kumar, and H.S. Nalwa, 1st ed. (American Scientific Publishers, 2002), pp. 1-37.

8. J. Tien, A. Terfort, and G.M. Whitesides, "*Microfabrication through Electrostatic Self-Assembly,"* Langmuir, **13(20)**, 5349-5355 (1997).

9. J.S. Ahn, P.T. Hammond, M.F. Rubner, and I. Lee, "*Self-assembled particle monolayers on polyelectrolyte multilayers: particle size effects on formation, structure, and optical properties,"* Colloids Surf. A Physicochem. Eng. Asp., **259(1-3)**, 45-53 (2005).

10. D. Yoo, S.S. Shiratori, and M.F. Rubner, "*Controlling Bilayer Composition and Surface Wettability of Sequentially Adsorbed Multilayers of Weak Polyelectrolytes,"* Macromolecules, **31(13)**, 4309-4318 (1998).

11. J.J. Ramsden, Y.M. Lvov, and G. Decher, "*Determination of optical constants of molecular films assembled via alternate polyion adsorption,"* Thin Solid Films, **254**, 246-251 (1995).

12. R.v. Klitzing, J.E. Wong, W. Jaeger, and R. Steitz, "*Short range interactions in polyelectrolyte multilayers,"* Curr. Opin. Colloid Interface Sci., **9(1-2)**, 158-162 (2004).

13. L. Tang, T. Qiu, X. Tuo, H. You, D. Liu, and X. Tang, "*Influence of solution conditions on formation of amphiphilic hyperbranced polyanion/linear polycation multilayer films,"* Colloid. Polym. Sci., **284(9)**, 957-964 (2006).

14. M. Losche, J. Schmitt, G. Decher, W.G. Bouwman, and K. Kjaer, "*Detailed Structure of Molecularly Thin Polyelectrolyte Multilayer Films on Solid Substrates as Revealed by Neutron Reflectometry,"* Macromolecules, **31(25)**, 8893-8906 (1998).

15. J. Schmitt, T. Gruenewald, G. Decher, P.S. Pershan, K. Kjaer, and M. Loesche, "*Internal structure of layer-by-layer adsorbed polyelectrolyte films: a neutron and x-ray reflectivity study,"* Macromolecules, **26(25)**, 7058-7063 (1993).

16. B.J. Cha, Y.S. Kang, and J. Won, "*Preparation and Characterization of Dendrimer Layers on Poly(dimethylsiloxane) Films,"* Macromolecules, **34(19)**, 6631-6636 (2001).

17. V.V. Tsukruk, F. Rinderspacher, and V.N. Bliznyuk, "*Self-Assembled Multilayer Films from Dendrimers,"* Langmuir, **13(8)**, 2171-2176 (1997).

18. W.B. Stockton and M.F. Rubner. *Molecular layer processing of polyaniline via the use of hydrogen bonding interactions*. in *Proceedings of the 1994 MRS Fall Meeting, Nov 28-Dec 1 1994*. 1995. Boston, MA, USA: Materials Research Society, Pittsburgh, PA, USA.

19. Z. Liang, O.M. Cabarcos, D.L. Allara, and Q. Wang, "*Hydrogen-bonding-directed layer-by-layer assembly of conjugated polymers,"* Adv. Mater., **16(9-10)**, 823-827 (2004).

20. V. Kozlovskaya, S. Ok, A. Sousa, M. Libera, and S.A. Sukhishvili, "*Hydrogen-bonded polymer capsules formed by layer-by-layer self-assembly,"* Macromolecules, **36(23)**, 8590-8592 (2003).

21. M. Mammen, S.-K. Choi, and G.M. Whitesides, "*Polyvalent Interactions in Biological Systems: Implications for Design and Use of Multivalent Ligands and Inhibitors,"* Angew. Chem. Int. Ed., **37(20)**, 2754-2794 (1998).

22. A. Mulder, J. Huskens, and D.N. Reinhoudt, "*Multivalency in supramolecular chemistry and nanofabrication,"* Org. Biomol. Chem., **2(23)**, 3409-3424 (2004).

23. B. Halford, "*Dendrimers branch out,"* Chem. Eng. News, **83(24)**, 30-36 (2005).

24. D.C. Tully and J.M.J. Frechet, "*Dendrimers at surfaces and interfaces: chemistry and applications,"* Chem. Commun. (Feature Article), 1229-1239 (2001).

25. J. Sly, V.Y. Lee, and R.D. Miller, "*Versatile Polyvalent Support Architectures for Nano-scale Constructs,"* Unpublished Results, (2007).

26. O.A. Matthews, A.N. Shipway, and J. Fraser Stoddart, "*Dendrimers - branching out from curiosities into new technologies,"* Prog. Polym. Sci. (Oxford), **23(1)**, 1-56 (1998).

27. M. Wanunu, A. Vaskevich, S.R. Cohen, H. Cohen, R. Arad-Yellin, A. Shanzer, and I. Rubinstein, "*Branched coordination multilayers on gold,"* J. Am. Chem. Soc., **127(50)**, 17877-17887 (2005).

28. K.M. Smith and J.E. Falk, "*Porphyrins and metalloporphyrins : a new edition based on the original volume by J.E. Falk."* (Elsevier Scientific Pub. Co., 1975), pp.

29. E.I. Zenkevich and C.v. Borczyskowski, "*Multiporphyrin Self-Assembled Arrays in Solutions and Films: Thermodynamics, Spectroscopy, and Photochemistry,"* in Handbook of Polyelectrolytes and Their Applications Volume 2,edited by J.K. S.K. Tripathy, and H.S. Nalwa, 1st ed. (American Scientific Publishers, 2002), pp. 285-332.

30. Bullis K. (2006). *Solar Cells for Cheap* [Online]. Available at http://www.technologyreview.com/Energy/17490/page1/ (accessed 29 March 2007).

31. T. Hasobe, Y. Kashiwagi, M.A. Absalom, J. Sly, K. Hosomizu, M.J. Crossley, H. Imahori, P.V. Kamat, and S. Fukuzumi. *Supramolecular photovoltaic cells composed of clusterized fullerenes with porphyrin dendrimers and porphyrin-alkanethiolate protected-gold nanoparticles*. in *ECS Annual Spring Meeting - Fullerenes and Nanotubes: Materials for the New Chemical Frontier - International Symposium on Fullerenes, Nanotubes, and Carbon Nanoclusters, May 9-13 2004*. 2004. San Antonio, TX, United States: Electrochemical Society Inc., Pennington, NJ 08534-2896, United States.

32. M. Jaschke, H.-J. Butt, S. Manne, H.E. Gaub, O. Hasemann, F. Krimphove, and E.K. Wolff, "*Atomic force microscope as a tool to study and manipulate local surface properties,"* Proceedings of the 1995 Conference on Artificial Biosensing Interfaces, Jun 17-20 1995, **11(6-7)**, 601-612 (1996).

33. A. Brajter-Toth and J.Q. Chambers, in Electroanalytical Methods of Biological Materials, 1st ed. (Marcel Dekker Incorporated, 2002), pp. 49.

34. Marquart A., SPR Pages (2007). *SPR Theory* [Online]. Available at http://www.sprpages.nl/SPRtheory/SprTheory01.htm (accessed 30 March 2007).

35. P. Englebienne, A. Van Hoonacker, and M. Verhas, "*Surface plasmon resonance: Principles, methods and applications in biomedical sciences,"* Spectroscopy, **17(2-3)**, 255-273 (2003).

36. K. Kurihara and K. Suzuki, "*Theoretical Understanding of an Absorption-Based Surface Plasmon Resonance Sensor Based on Kretchmann's Theory,"* Anal. Chem., **74(3)**, 696-701 (2002).

37. K. Kurihara, K. Nakamura, and K. Suzuki, "*Asymmetric SPR sensor response curve-fitting equation for the accurate determination of SPR resonance angle,"* Sens. Actuators B Chem., **86**, 49-57 (2002).

38. G. McDermott, S.M. Prince, A.A. Freer, A.M. Hawthornthwaite-Lawless, M.Z. Papiz, R.J. Cogdell, and N.W. Isaacs, "*Crystal structure of an integral membrane light-harvesting complex from photosynthetic bacteria,"* Nature, **374(6522)**, 517-521 (1995).

39. A. Jager-Waldau, "*Status of thin film solar cells in research, production and the market,"* Thin Film PV, **77(6)**, 667-678 (2004).

40. Skinner L., Renewable Energy Access (2005). *Solar Silicon Market a Seller's Paradise* [Online]. Available at http://www.renewableenergyaccess.com/rea/news/story?id=22425 (accessed 29 March 2007).

41. Hasan R. (2006). *Solar Silicon Shortage and Its Impact on Solar Power Stocks* [Online]. Available at http://www.renewableenergystocks.com/Articles/080906a.asp (accessed 1 April 2007).

42. O. Crespo-Biel, B. Dordi, D.N. Reinhoudt, and J. Huskens, "*Supramolecular Layer-by-Layer Assembly: Alternating Adsorptions of Guest- and Host-Functionalized Molecules and Particles Using Multivalent Supramolecular Interactions,"* J. Am. Chem. Soc., **127(20)**, 7594-7600 (2005).

43. M. Wanunu, R. Popovitz-Biro, H. Cohen, A. Vaskevich, and I. Rubinstein, "*Coordination-based gold nanoparticle layers,"* J. Am. Chem. Soc., **127(25)**, 9207-9215 (2005).

44. P. Kohli and G.J. Blanchard, "*Design and demonstration of hybrid multilayer structures: Layer-by-layer mixed covalent and ionic interlayer linking chemistry,"* Langmuir, **16(22)**, 8518-8524 (2000).

45. D.R. Blasini, S. Flores-Torres, D.-M. Smilgies, and H.D. Abruna, "*Stepwise self-assembly of ordered supramolecular assemblies based on coordination chemistry,"* Langmuir, **22(5)**, 2082-2089 (2006).

46. F. Da Cruz, K. Driaf, C. Berthier, J.-M. Lameille, and F. Armand, "*Study of a self-assembled porphyrin monomolecular layer obtained by metal complexation,"* Thin Solid Films, **349(1-2)**, 155-161 (1999).

47. I. Doron-Mor, H. Cohen, S.R. Cohen, R. Popovitz-Biro, A. Shanzer, A. Vaskevich, and I. Rubinstein, "*Layer-by-layer assembly of ordinary and composite coordination multilayers,"* Langmuir, **20(24)**, 10727-10733 (2004).

48. M.S. Baptista, "*Supramolecular Assemblies of Natural and Synthetic Polyelectrolytes,"* in Handbook of Polyelectrolytes and Their Applications Volume 1,edited by J.K. S.K. Tripathy, and H.S. Nalwa, 1sst ed. (American Scientific Publishers, 2002), pp. 99-148.

49. H.-J. Kim, K. Lee, S. Kumar, and J. Kim, "*Dynamic sequential layer-by-layer deposition method for fast and region-selective multilayer thin film fabrication,"* Langmuir, **21(18)**, 8532-8538 (2005).

50. S. Dante, R. Advincula, C.W. Frank, and P. Stroeve, "*Photoisomerization of polyionic layer-by-layer films containing azobenzene,"* Langmuir, **15(1)**, 193-201 (1999).

51. D.A. Tomalia and J.M.J. Frechet, "*Discovery of dendrimers and dendritic polymers: A brief historical perspective,"* J. Polym. Sci., Part A: Polym. Chem., **40(16)**, 2719-2728 (2002).

52. N. Hadjichristidis, M. Pitsikalis, S. Pispas, and H. Iatrou, "*Polymers with complex architecture by living anionic polymerization,"* Chem. Rev., **101(12)**, 3747-3792 (2001).

53. J.B. Beil and S.C. Zimmerman, "*Synthesis of nanosized 'cored' star polymers,"* Macromolecules, **37(3)**, 778-787 (2004).

54. B. O'Regan and M. Gratzel, "*A low-cost, high-efficiency solar cell based on dye-sensitized colloidal TiO2 films,"* Letters to Nature, **353**, 737-740 (1991).

55. M. Gratzel, "*Perspectives for dye-sensitized nanocrystalline solar cells,"* Progress in Photovoltaics: Research and Applications, **8(1)**, 171-185 (2000).

56. E.M. Harth, S. Hecht, B. Helms, E.E. Malmstrom, J.M.J. Frechet, and C.J. Hawker, "*The effect of macromolecular architecture in nanomaterials: A comparison of site isolation in porphyrin core dendrimers and their isomeric linear analogues,"* J. Am. Chem. Soc., **124(15)**, 3926-3938 (2002).

57. J. Larsen, B. Bruggemann, T. Polivka, V. Sundstrom, E. Akesson, J. Sly, and M.J. Crossley, "*Energy transfer within Zn-porphyrin dendrimers: Study of the singlet-singlet annihilation kinetics,"* J. Phys. Chem. A, **109(47)**, 10654-10662 (2005).

58. J. Larsen, J. Andersson, T. Polivka, J. Sly, M.J. Crossley, V. Sundstrom, and E. Akesson, "*Energy transfer and conformational dynamics in Zn-porphyrin dendrimers,"* Chem. Phys. Lett., **403(1-3)**, 205-210 (2005).

59. D.S. Hecht, R.J.A. Ramirez, M. Briman, E. Artukovic, K.S. Chichak, J.F. Stoddart, and G. Gruner, "*Bioinspired detection of light using a porphyrin-sensitized single-wall nanotube field effect transistor,"* Nano Lett., **6(9)**, 2031-2036 (2006).

60. H.-J. Van Manen, R.H. Fokkens, N.M.M. Nibbering, F.C.J.M. Van Veggel, and D.N. Reinhoudt, "*Convergent synthesis of noncovalent metallodendrimers containing hydrophobic dendrons at the periphery,"* J. Org. Chem., **66(13)**, 4643-4650 (2001).

61. D.M. Kaschak, J.T. Lean, C.C. Waraksa, G.B. Saupe, H. Usami, and T.E. Mallouk, "*Photoinduced energy and electron transfer reactions in lamellar polyanion/polycation thin films: Toward an inorganic `leaf',"* J. Am. Chem. Soc., **121(14)**, 3435-3445 (1999).

62. S.S. Shiratori and M.F. Rubner, "*pH-Dependent Thickness Behavior of Sequentially Adsorbed Layers of Weak Polyelectrolytes,"* Macromolecules, **33(11)**, 4213-4219 (2000).

63. T. Mizutani, K. Wada, and S. Kitagawa, "*Molecular Recognition of Amines and Amino Esters by Zinc Porphyrin Receptors: Binding Mechanisms and Solvent Effects,"* J. Org. Chem., **65(19)**, 6097-6106 (2000).

64. S. Stechemesser and W. Eimer, "*Solvent-Dependent Swelling of Poly(amido amine) Starburst Dendrimers,"* Macromolecules, **30(7)**, 2204-2206 (1997).

65. M. Murat and G.S. Grest, "*Molecular Dynamics Study of Dendrimer Molecules in Solvents of Varying Quality,"* Macromolecules, **29(4)**, 1278-1285 (1996).

66. M. Ginzburg, J. Galloro, F. Jakle, K.N. Power-Billard, S. Yang, I. Sokolov, C.N.C. Lam, A.W. Neumann, I. Manners, and G.A. Ozin, "*Layer-by-layer self-assembly of organic-organometallic polymer electrostatic superlattices using poly(ferrocenylsilanes),"* Langmuir, **16(24)**, 9609-9614 (2000).

67. X. Tuo, D. Chen, H. Cheng, and X. Wang, "*Fabricating Water-Insoluble Polyelectrolyte into Multilayers with Layer-by-layer Self-assembly,"* Polym. Bull., **54(6)**, 427-433 (2005).

68. X. Tuo, D. Chen, and X. Wang, "*Preparation of azo polyelectrolyte self-assembled multilayers by using N,N-dimethylformamide/H2O mixtures as solvents,"* Front. Chem. China, **1(3)**, 329-333 (2006).

69. X.H. Xu, B. Han, Y.S. Fu, J. Han, H.B. Shi, B. Wu, S. Han, and Q. Chen, "*Preparation of chitosan/glucose oxidase nanolayered films for electrode modification by the technique of layer-by-layer self-assembly,"* J. Mater. Sci. Lett., **22(9)**, 695-697 (2003).

70. D.G.M. Rebecca L. Rich, "*Survey of the year 2005 commercial optical biosensor literature,"* J. Mol. Recognit., **19(6)**, 478-534 (2006).

71. A.K. Ray and A.V. Nabok, "*Composite Polyelectrolyte Self-Assembled Films for Sensor Applications,"* in Handbook of Polyelectrolytes and Their Applications Volume 3,edited by J.K. S.K. Tripathy, and H.S. Nalwa, 1st ed. (American Scientific Publishers, 2002), pp. 69-97.

72. N. Zhang, R. Schweiss, and W. Knoll, "*Layer-by-layer self-assembled conducting polymer films at elevated pressure investigated by surface plasmon spectroscopy with electrochemistry,"* J. Solid State Electrochem., **11(4)**, 451-456 (2007).

73. M. Palumbo, C. Pearson, J. Nagel, and M.C. Petty, "*Surface plasmon resonance sensing of liquids using polyelectrolyte thin films,"* Sens. Actuators B Chem., **91(1-3)**, 291-297 (2003).

74. A. Baba, M.-K. Park, R.C. Advincula, and W. Knoll, "*Simultaneous surface plasmon optical and electrochemical investigation of layer-by-layer self-assembled conducting ultrathin polymer films,"* Langmuir, **18(12)**, 4648-4652 (2002).

75. M. Szekeres, A. Szechenyi, K. Stepan, T. Haraszti, and I. Dekany, "*Layer-by-layer self-assembly preparation of layered double hydroxide/ polyelectrolyte nanofilms monitored by surface plasmon resonance spectroscopy,"* Colloid. Polym. Sci., **283(9)**, 937-945 (2005).

76. O. Prucker and J. Ruehe, "*Polymer layers through self-assembled monolayers of initiators,"* Langmuir, **14(24)**, 6893-6898 (1998).

77. J. Sly, L. Chang, C.S. Bonifacio, V.Y. Lee, M. McNeil, W.P. Risk, M.C. Jefferson, and R.D. Miller, "*Reaching for the Stars: layered polyvalent self-assembly of hyperbranched pigment arrays,"* Unpublished Results, (2007).

78. J. Sly, K.L. Glab, V.Y. Lee, and R.D. Miller, IBM Corporation, *Unpublished results* (2006).

79. G. Boisset (2007). *Thin Film and Bulk Index of Refractio and Photonics Calculations* [Online]. Available at www.luxpop.com (accessed 22 June 2007).

80. M. Commandre, P. Roche, J.-P. Borgogno, and G. Albrand, "*Absorption mapping for characterization of glass surfaces,"* Appl. Opt., **34(13)**, 2372 (1995).

81. W.P. Risk, IBM Corporation, *private communication* (17 January 2008).

82. R.F. Conley and M.K. Lloyd, "*Adsorption Studies on Kaolinites-II Adsorption of Amines,"* Clays Clay Miner., **19**, 273-282 (1970).

83. D. Barrón, S. Butí, M. Ruiz, and J. Barbosa, "*Preferential solvation in the THF-water mixtures. Dissociation constants of acid components of pH reference materials,"* Phys. Chem. Chem. Phys., **1**, 295-298 (1999).

84. E.M. Vartiainen, J.J. Saarinen, and K.-E. Peiponen, "*Method for extracting the complex dielectric function of nanospheres in a water matrix from surface-plasmon resonance data,"* J. Opt. Soc. Am. B, **22(6)**, 1173-1178 (2005).

85. W. Hinsberg, F.A. Houle, S.-W. Lee, H. Ito, and K. Kanazawa, "*Characterization of Reactive Dissolution and Swelling of Polymer Films Using a Quartz Crystal Microbalance and Visible and Infrared Reflectance Spectroscopy,"* Macromolecules, **38(5)**, 1882-1898 (2005).

86. B.D. Vogt, E.K. Lin, W.-l. Wu, and C.C. White, "*Effect of Film Thickness on the Validity of the Sauerbrey Equation for Hydrated Polyelectrolyte Films,"* J. Phys. Chem. B, **108(34)**, 12685-12690 (2004).

APPENDIX A

Mathematical Modeling of SPR Data by Dr. William Risk [81]

Assumption of refractive indices:
nSF11 = 1.76196
nPS = 1.577
nTHF = 1.3992
nCr = 3.0318-2.5642*i*
nAu = 0.1644-5.3512*i*
$nSiO_2$ = 1.4575

SF11 Substrate stack: 3 nm Cr / 50 nm Au / 4 nm SiO_2

The following SPR angular shifts were determined for different thicknesses of PS:
3 nm: 0.17 degrees
6 nm: 0.34 degrees
9 nm: 0.51 degrees

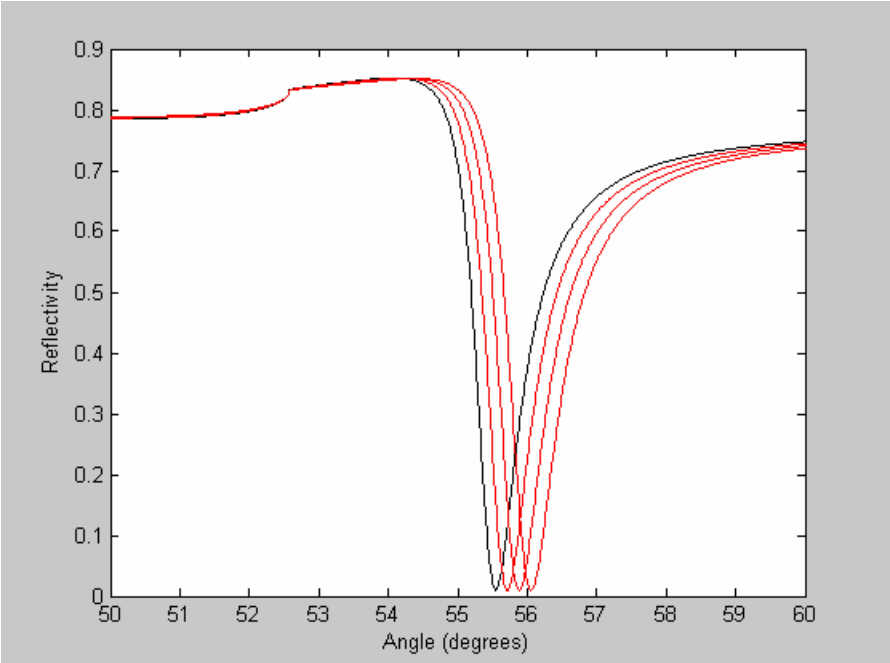

Hence a shift of 0.15 degrees would correspond to a thickness of about 2.6 nm.

It was then assumed that the layer looks like a monolayer of hexagonally-packed hard PS spheres with THF interpenetrating (so that the PS occupies 60.5% of the volume of the monolayer) as shown below.

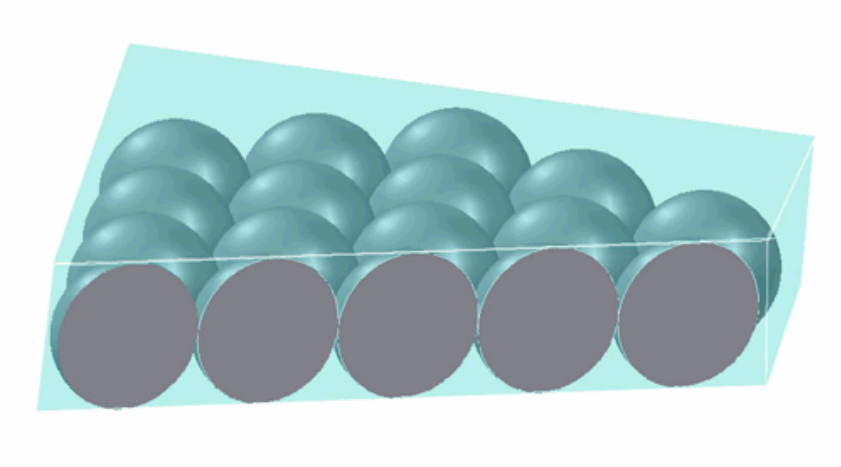

Maxwell-Garnet theory was used to calculate the effective refractive index of the layer with regards to SPR angular shift as shown below:
3 nm thick: 0.1 degrees
6 nm thick: 0.2 degrees
9 nm thick: 0.3 degrees

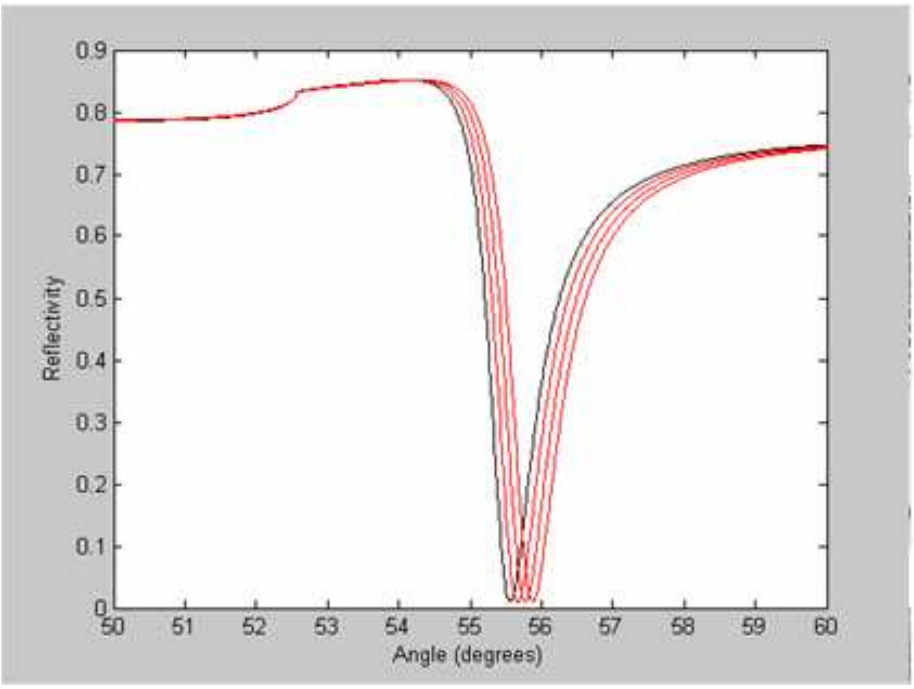

So a shift of 1.5 degrees would correspond to a thickness of about 4.5 nm

APPENDIX B

Experimental Error for SPR Experiments using THF Baselines

Run #	THF Resonance Angle (°)
1	55.0636
2	55.1636
3	54.7261
4	55.0606
5	54.6841
6	55.1093
7	54.715
8	54.7236
9	54.7227
10	55.2399

Statistical Analysis	
Mean	54.92085
Standard Error	0.070763
Median	54.89335
Mode	#N/A
Standard Deviation	0.223772
Sample Variance	0.050074
Kurtosis	-2.13504
Skewness	0.176987
Range	0.5558
Minimum	54.6841
Maximum	55.2399
Sum	549.2085
Count	10
Largest(1)	55.2399
Smallest(1)	54.6841
Confidence Level(95.0%)	0.160077